UARI Research Report No. 66

INVISCID HYPERSONIC FLOW OF CHEMICALLY RELAXING AIR ABOUT POINTED CIRCULAR CONES

by

Jürgen Thoenes

This work was partially supported by the National Aeronautics and Space Administration under research grant NGL-01-002-001

University of Alabama Research Institute
Huntsville, Alabama
May 1969

UARI Research Report No. 66

INVISCID HYPERSONIC FLOW OF CHEMICALLY RELAXING AIR ABOUT POINTED CIRCULAR CONES

by

Jürgen Thoenes

This work was partially supported by the
National Aeronautics and Space Administration
under research grant NGL-01-002-001

University of Alabama Research Institute
Huntsville, Alabama
May 1969

FOREWORD

The material contained in this report formed the author's dissertation for the degree of Doctor of Philosophy in Engineering Mechanics at the University of Alabama.

The author wishes to express his deep appreciation to Dr. Rudolf Hermann for his guidance and advice during the course of this investigation. Likewise, the author is indebted to Dr. Jerome J. Brainerd for many stimulating discussions concerning all phases of this work.

Sincere appreciation is also expressed to Dr. James D. Matheny, Dr. Howard B. Wilson, Jr., Dr. Harold R. Henry, and Dr. Fran Bosnjakovic from whose criticism the author has benefited.

The author feels much obliged to Mrs. Sylvia Heard who skillfully programmed the nonequilibrium, as well as the equilibrium flow solutions; to Dr. Kenneth O. Thompson who kindly furnished a subroutine for the equilibrium composition; and to Mr. Robert A. McGraw for programming the frozen flow solutions.

The efforts of Mrs. Ann White who typed the manuscript are gratefully acknowledged.

The author is indebted to the National Aeronautics and Space Administration for partial support of this work under research grant NGL-01-002-001.

ABSTRACT

Inviscid hypersonic flow of chemically relaxing air about pointed circular cones has been calculated using Dorodnitsyn's one-strip integral method. The air model used consists of O_2, N_2, O, N, and NO, of which the relative amounts are controlled by six reaction equations which actually represent eighteen chemical reactions. Also considered are the limiting cases of nonequilibrium flow, namely, chemically frozen flow, and the flow with chemical equilibrium. Vibrational equilibrium has been assumed throughout.

The principal contribution of this work lies in the method of solution. Specifically, it is demonstrated that the replacement of the approximate tangential momentum equation, and of all approximate species continuity equations by their exact forms along the body surface leads to a system of equations which, first, can be stably integrated, and second, yields results which compare quite well with those obtained by the method of characteristics. A detailed discussion of the polynomial approximations employed in the integral method, the introduction of a characteristic relaxation length defined in terms of the initial species mass fraction gradients, as well as many new results for hypersonic flow of air with finite rate nonequilibrium dissociation about circular cones are further contributions of the work reported herein.

The discussion of results includes two cases which show the very good agreement of the results from the integral method with those from the method of characteristics. Various other cases serve to illustrate the influence of free stream velocity ($5400 \leq V_\infty$ [m/sec] ≤ 11186), cone semi-vertex angle ($20^\circ \leq \theta \leq 45^\circ$), and altitude (31 km to 80 km) on the variation of all flow field variables. The analysis of a cone with constant semi-vertex angle and free stream velocity at three different altitudes is used to demonstrate the validity, and its range, of the nonequilibrium scaling law $\rho_\infty \cdot L =$ constant.

For one case, the asymptotic equilibrium state of the nonequilibrium flow is compared with the results of a conical equilibrium flow calculation. According to theoretical considerations an agreement between the two cannot be expected, and this is confirmed by the comparison. Although the cone surface pressures agree very closely, it is found that the values for the asymptotic body surface temperature are higher than those for conical equilibrium. Both, the asymptotic surface density and the surface velocity stay below their values for conical equilibrium.

TABLE OF CONTENTS

LIST OF TABLES

LIST OF FIGURES

LIST OF APPENDICES

NOMENCLATURE

a_f	Frozen speed of sound
b	Expression defined by Eq. (3.41)
C_i	Mass fraction of species i
c_p	Specific heat (frozen chemistry)
E	Total specific internal energy
E_i	Internal energy of species i
e_i	Specific internal energy of species i
F_1, F_2, F_3	Dimensionless functions defined by Eq. (4.21) through (4.23)
g_j	Degeneracy factor
H	Total enthalpy
h	Planck's constant, also static enthalpy
h_1, h_2, h_3	Metric coefficients
K	Longitudinal body curvature
K_c	Concentration equilibrium constant
k	Boltzmann's constant
$k_{d,M}$	Dissociation rate constant
$k_{r,M}$	Recombination rate constant
j	Indicator for plane or axisymmetric flow, defined in Eq. (3.11)
L	Dimensionless function defined in Appendix A
M	Molecular weight of undissociated air, also Mach number
M_i	Molecular weight of species i
m	Particle mass

$\bar{m}_o$	Total oxygen mass fraction
N^*	Avogadro's number
n_i	Number of particles of species i
p	Static pressure
Q	Partition function
$\vec{q}$	Velocity vector
R	Gas constant of undissociated air, also radius of curvature
R^*	Universal gas constant
r	Radial coordinate
S	Dimensionless function defined in Appendix A
T	Temperature
t	Time
u	Velocity component in x-direction
v	Velocity component in y-direction
V	Volume, velocity when subscripted
$\dot{W}_i$	Mass rate of formation of species i per unit volume
X_i	Concentration of species i
x_1, x_2, x_3	Generalized coordinates
x, y	Coordinate directions
Y_i	Molar concentration of species i
$\bar{Y}_i \equiv Y_i / \Sigma Y_i$	Mol fraction of species i
Z	Compressibility factor

α	Indicator, used in species continuity equations
β	$= \sigma - \theta$
δ	Defined by Eq. (4.45)
$\bar{\delta}$	Defined by Eq. (4.16)
ϵ	Indicator, used in x-momentum equation
ϵ_j	Excitation energy
θ	Body surface inclination angle
θ_i^*	Characteristic temperature of dissociation of species i
θ_j^e	Characteristic temperature of electronic excitation, state j
θ_i^v	Characteristic temperature of vibration of species i
$\varkappa$	Symmetry number
λ	Characteristic relaxation length, defined by Eq. (4.68)
ν_i, ν_i'	Stoichiometric coefficients
ξ	Dimensionless x-coordinate
ρ	Density
σ	Shock wave inclination angle
τ_i^d	Chemical relaxation time of species i
τ_i^v	Vibrational relaxation time of species i
ϕ	Circumferential coordinate
Ω_i	Dimensionless functions, defined in Appendix B

Superscripts

t	Translation
v	Vibration
r	Rotation
e	Electronic excitation
d	Dissociation
I → VI	Refers to reactions I → VI

Subscripts

b	Body surface
∞	Free stream
s	Behind the shock wave
n	Normal component
t	Tangential component
i	Species, i = O_2, N_2, O, N, NO
o	Undissociated state
tot	Total
M	Third body species
O2	Molecular oxygen
N2	Molecular nitrogen
O	Atomic oxygen
N	Atomic nitrogen
NO	Nitric oxyde

CHAPTER I

INTRODUCTION

Over the past few years considerable effort has been devoted to the understanding and the theoretical prediction of the nonequilibrium flow field conditions encountered in hypersonic flight. Present technology dictated the use of blunted body shapes for reentry vehicles in order to minimize the convective heating rate to the body surface. Quite naturally, calculations of flow fields surrounding hypersonic blunt bodies were of prime importance. For a survey of calculation techniques for this class of problems the reader is referred to Hayes and Probstein (Ref. 1). In particular, the general method of integral relations, proposed by Dorodnitsyn (Ref. 2), proved to be quite successful in predicting shock wave shapes and other flow field variables for certain simple blunt bodies. Also, this method is readily adaptable to machine calculations. The investigations of Shih, Baron, Krupp and Towle (Ref. 3), Hermann and Thoenes (Ref. 4), and most recently, Thompson (Ref. 5), are some examples of inviscid real gas flow field calculations using the integral method.

Comparatively less attention has been paid to the high temperature real gas flow past pointed bodies, which appear to be of growing interest and importance. Certainly the time will come when it is desirable to land on the Earth's surface some space probes returning from far distant planets. These probes will reenter the

atmosphere at a speed far above earth parabolic speed. Both, convective and radiative heating will occur, but because of the high speed, radiation is expected to be the dominant source of heating. It was therefore pointed out by Allen (Ref.6) that the shock wave sweepback provided by pointed conical entry bodies could be used to reduce the gas luminosity grossly, and thus the total heating rate. Therefore, besides being of fundamental interest, the calculation of high temperature nonequilibrium flow past pointed cones may be of very practical importance in the near future.

It is interesting to note that one of the first approximate theories for nonequilibrium cone flow was developed by Chapman (reported by Stephenson, Ref.7) in order to determine relaxation times of oxygen and nitrogen vibrations. Using essentially a stream tube method, Chapman derived equations which related the coordinates of the curved shock wave to an effective relaxation time of the flow in the shock layer. Having obtained shock wave coordinates from experiments, Stephenson (Ref. 7) evaluated relaxation times which agreed reasonably well with data obtained from shock tube experiments.

If the flow field is entirely supersonic then the method of characteristics is available for its calculation, provided that some initial data are available. Calculations using the method of characteristics were first reported by Sedney, South and Gerber (Ref. 8) for the case of vibrationally relaxing flow of pure nitrogen over a wedge. These calculations were later extended to include flows past

circular cones (Ref. 9). The authors also reported the necessity of introducing modifications in the method of characteristics in order to increase the accuracy of the results. This work was followed by Capiaux and Washington (Ref. 10) who treated nonequilibrium flow of an "ideal dissociating gas" (so-called Lighthill gas) past a wedge, also using the method of characteristics.

In Ref. 11, Wood, Springfield and Pallone investigated the flow over axisymmetric bodies by using the method of characteristics. They employed a multicomponent gas model and included a simple model for vibration-dissociation coupling. Results were given for flows over blunted cones and ogival bodies.

The first application of Dorodnitsyn's integral method to the real gas flow over pointed bodies was given by South (Ref. 12). He considered vibrationally relaxing flow of a pure diatomic gas past a circular cone, using the one strip approximation, and constant relaxation time. He also reported that a system of equations containing the tangential momentum equation and the vibrational rate equation in their exact forms could not be integrated successfully. He found it necessary to use linear approximations in all the conservation equations. The pressure distribution obtained from this set, together with a set of corrected equations then served to obtain a corrected solution. The application of the two and three strip integral method to the same problem is discussed in Ref. 13.

South and Newman (Ref. 14), and Newman (Ref. 15) discussed a modification to the one strip integral method as applied to wedge flow. Instead of using

first order polynomials to approximate certain integrands, the integrals themselves were replaced by weighted averages of the integrands. According to the authors, this procedure resulted in a better description of the flow within the shock layer, but again, it was found necessary to integrate a set of corrected equations after obtaining an approximate solution.

Thoenes (Ref. 16) used the one strip integral method and a simplified three component air model, applicable in the oxygen dissociation regime, to calculate chemically relaxing flow past cones. In particular, these calculations successfully employed the exact tangential momentum and species continuity equation, a method which the author labelled as the "semi-exact procedure". Results from the two strip integral method for dissociating flow were discussed in Ref. 17.

There are other methods which have been used for the calculation of non-equilibrium flow fields around pointed bodies. Lee (Ref. 18) evaluated vibrationally relaxing flow over wedges by a perturbation method, while DeJarnette (Ref. 19) presented an "artificial viscosity" method to evaluate wedge flows with simple relaxation processes, including various schemes of vibration-dissociation coupling. All these calculations with simple rate processes are of basic interest and valuable for determining suitable numerical techniques. However, with the exception of Ref. 11, they cannot describe adequately a flow field involving several simultaneous relaxation processes as they occur, in air for example. Presumably, this prompted Spurk, Gerber and Sedney (Ref. 20) to calculate hypersonic flow of air

past wedges and cones by the method of characteristics, considering a five component air model involving numerous chemical reactions. Unfortunately, the application of the method of characteristics to nonequilibrium flow is complicated and computation times can be very long, even on modern computers.

No calculations, comparable to the work of Spurk, Gerber and Sedney, but using procedures other than the method of characteristics, could be found in the literature at the present time. It is expected that the work herein will fill this gap by presenting a formulation of Dorodnitsyn's integral method for hypersonic flow of a multicomponent chemically reacting gas about pointed bodies. The principal advantage of the integral method is that it reduces the governing partial differential equations to ordinary differential equations for which highly efficient numerical integration techniques have been developed.

A detailed description of the multicomponent gas model for high temperature air, and its thermodynamic properties, is given in Chapter II. In Chapter III, the basic partial differential equations are presented. They are cast in a suitable coordinate system, and the discussion of applicable boundary conditions concludes the formulation of the problem. The solution is discussed in Chapter IV. After reviewing the method of integral relations in general, its application to the problem at hand is described in detail. A final section on the numerical techniques used leads to Chapter V, which is devoted to the discussion of the results.

CHAPTER II

GAS MODEL AND THERMODYNAMICS

2.1 Gas Model

To determine the values of the flow variables within the shock layer about a body moving in the atmosphere at hypersonic speeds, it is necessary to account for the effects of chemical reactions that take place within the layer. Such reactions proceed at a finite rate, but for flow about infinite cones, the gas will eventually reach a state of thermal and chemical equilibrium. Figure 1 presents lines of constant compressibility factor and temperature at the surface of a cone for equilibrium flow, using data given in Ref. 21. Although this is a purely hypothetical case, the figure shows approximately the conditions which have to be met by the air model to be chosen. For example, if a conical vehicle with a semi-vertex angle of thirty degrees enters the Earth's atmosphere at an altitude of 80 km at earth parabolic speed it is to be expected that, once equilibrium is reached on the streamline that wets the body, the surface temperature is around five thousand degrees Kelvin, and that a sizable fraction of the nitrogen molecules must have dissociated ($Z \approx 1.4$). This example shows that, in order to calculate such flow conditions, the gas model representing high temperature air must be assumed to consist at least of a mixture of O_2, N_2, NO, O, and N. It is furthermore

assumed that all species are in translational, rotational and vibrational equilibrium in every flow region, which implies a single temperature for all the degrees of freedom. Assuming weakly interacting particles (i.e. particles which exchange energy only by collisions, and the collision times are small compared with the time between collisions) partition functions may be used to calculate all thermodynamic properties. Thus ionization, vibrational nonequilibrium, as well as vibration-dissociation coupling are neglected. The latter two assumptions will be critically examined at the end of this chapter.

The composition of air along with other physical constants as used in the present investigation are summarized in Table I.

2.2 Partition Functions

Under the assumptions stated in the previous section, all of the thermodynamic properties of a gas may be derived from its partition function. Details on the partition function may be found in any text on statistical thermodynamics (Ref. 22, 23, 24). In this section only those relations will be summarized which are needed for subsequent calculations.

The partition function may be defined as

$$Q = \sum_j g_j \exp\left(-\frac{\epsilon_j}{kT}\right) \tag{2.1}$$

where ϵ_j is the common energy of several states, and g_j is the degeneracy, that

is, the number of states of the particle which have this common energy level. In the present investigation, the energy may be due to the translational, rotational or vibrational motion of the particles and, in a limited way, due to the motion of the electrons within the particle. Assuming that no coupling exists between the different modes of excitation, the partition function may be written as the product

$$Q = Q^t \, Q^r \, Q^v \, Q^e \tag{2.2}$$

where the factors on the right hand side of Eq. (2.2) are the partition functions associated with the translational, rotational, vibrational and electronic energy levels of the particle. For diatomic molecules these factors are:

$$Q^t = V \left(\frac{2 \pi m k T}{h^2} \right)^{3/2} \tag{2.3}$$

$$Q^r \approx \frac{8 \pi^2 I k T}{\varkappa h^2} = \frac{T}{\varkappa \theta^r} \tag{2.4}$$

$$Q^v = \left[1 - \exp \left(- \theta^v / T \right) \right]^{-1} \tag{2.5}$$

$$Q^e = \sum_{j=0}^{n} g_j \exp \left(- \theta_j^e / T \right) \tag{2.6}$$

Here θ^r, θ^v, and θ_j^e are characteristic temperatures for rotation, vibration, and electronic excitation, respectively. Monatomic particles have no modes of rotational or vibrational excitation, therefore, the respective partition functions take the value unity. Table II presents the atomic and molecular constants which were used in the present calculations.

2.3 Thermodynamic Properties

2.3.1 Thermal Equation of State

According to statistical thermodynamics the partial pressure which a system of weakly interacting particles of species i exerts on its surroundings is given in terms of the partition function as

$$p_i = n_i \, k \, T \, \frac{\partial}{\partial V} (\ln Q) \tag{2.7}$$

where n_i denotes the number of particles of species i contained in the volume V, and k is Boltzmann's constant. Since, as seen from Eq. (2.3) through (2.6), only the translational partition function depends on the volume V, one obtains

$$\frac{\partial}{\partial V} (\ln Q) = \frac{\partial}{\partial V} (\ln Q^t) = \frac{1}{V} \tag{2.8}$$

Hence, the pressure becomes

$$p_i = \frac{n_i k T}{V} \tag{2.9}$$

Introducing the molecular weight M_i, and Avogadro's number N*, Eq. (2.9) can be rewritten as

$$p_i = \left(\frac{n_i}{V} \; \frac{M_i}{N^*} \right) \frac{N^* k}{M_i} \; T \tag{2.10}$$

which is at once recognized as the equation of state of a thermally perfect gas, viz.

$$p_i = \rho_i \, \frac{R^*}{M_i} \, T \tag{2.11}$$

Since it is assumed that each species of the gas mixture can be treated as a thermally perfect gas, the pressure of the mixture is, according to Dalton's law, the sum of its partial pressures, that is

$$p = \sum_i p_i = R^* T \sum_i \frac{\rho_i}{M_i} \tag{2.12}$$

Defining the mass fraction of the ith species as

$$C_i \equiv \frac{\rho_i}{\rho} \tag{2.13}$$

the equation of state can be expressed as

$$p = \rho R^* T \sum_i Y_i \tag{2.14}$$

where the Y_i are the molar concentrations defined as

$$Y_i \equiv \frac{C_i}{M_i} \tag{2.15}$$

It is often convenient to express the pressure of the dissociated gas mixture in terms of the gas constant of the undissociated gas. Eq. (2.14) can then be written as

$$p = \rho R Z T \tag{2.16}$$

where $R = R^* / M$ is the specific gas constant of the undissociated gas, and Z is the compressibility factor defined by

$$Z \equiv M \sum_i Y_i \tag{2.17}$$

A gas mixture consisting of i distinct species in the dissociated state, and of i_o species in the original undissociated state, requires i_o mass balance equations and $(i - i_o)$ relations between the species mass fractions. The former are, first, that the sum of all mass fractions is unity,

$$\sum_i C_i = 1 \tag{2.18}$$

and, second, that the mass fraction of one element is fixed. For example, for air

$$C_O + C_{O2} + \left(\frac{M_O}{M_{NO}}\right) C_{NO} = (C_{O2})_o \tag{2.19}$$

or, alternatively

$$C_N + C_{N2} + \left(\frac{M_N}{M_{NO}}\right) C_{NO} = (C_{N2})_o \tag{2.20}$$

which is a direct consequence of relations (2.18) and (2.19).

2.3.2 Internal Energy and Enthalpy

Again calling on statistical thermodynamics, the internal energy of a system of n_i weakly interacting particles is given in terms of the partition function as

$$E_i = n_i\, k\, T^2 \frac{\partial}{\partial T} (\ln Q) \tag{2.21}$$

Introducing the molecular weight and Avogadro's number, the internal energy becomes

$$E_i = \left(\frac{n_i\, M_i}{N^*}\right) \frac{N^* k}{M_i}\, T^2 \frac{\partial}{\partial T} (\ln Q) \tag{2.22}$$

Recognizing that the term $(n_i M_i / N^*)$ has the dimension of mass, the specific internal energy, that is internal energy per unit mass, can be expressed as

$$e_i = \frac{R^*}{M_i} T^2 \frac{\partial}{\partial T} (\ln Q) \tag{2.23}$$

Using Eq. (2.2) through (2.6), and (2.23), the specific internal energy for a pure monatomic gas is

$$e_i = \frac{R^*}{M_i} \left\{ \frac{3}{2} T + \frac{\sum_j g_j \theta_j^e \exp(-\theta_j^e / T)}{\sum_j g_j \exp(-\theta_j^e / T)} \right\} \tag{2.24}$$

and, for a pure diatomic gas,

$$e_i = \frac{R^*}{M_i} \left\{ \frac{5}{2} T + \frac{\theta_i^v}{\exp(\theta_i^v / T) - 1} + \frac{\sum_j g_j \theta_j^e \exp(-\theta_j^e / T)}{\sum_j g_j \exp(-\theta_j^e / T)} \right\} \tag{2.25}$$

The last terms in the above equations, representing the contribution of electronic excitation to the internal energy, become significant at extreme temperatures only, and can be neglected for the range of temperatures considered in the present investigation.

In the case of a dissociating gas mixture the dissociation energy for each molecular species must be included in the internal energy. This energy term may be expressed as

$$e_j^d = \frac{R^*}{M_j} \left[(C_j)_o - C_j \right] \theta_j^* \tag{2.26}$$

where, in the present case, $j = O_2, N_2, NO$, and the subscript o designates the undissociated state.

The total specific internal energy of a mixture of monatomic and diatomic gases can now be written as

$$E = \sum_i C_i \, e_i + \sum_j e_j^d \tag{2.27}$$

The specific enthalpy of the mixture is defined as

$$h = E + \frac{p}{\rho} \tag{2.28}$$

and substitution of the pertinent relations into Eq. (2.28) yields, for the five component gas mixture considered herein, the following expression for the enthalpy:

$$h = R^* \left\{ \frac{7}{2} T(Y_{O2} + Y_{N2} + Y_{NO}) + \frac{5}{2} T (Y_O + Y_N) \right.$$
$$+ \frac{Y_{O2} \theta^v_{O2}}{e^{\theta^v_{O2}/T} - 1} + \frac{Y_{N2} \theta^v_{N2}}{e^{\theta^v_{N2}/T} - 1} + \frac{Y_{NO} \theta^v_{NO}}{e^{\theta^v_{NO}/T} - 1}$$
$$\left. + \left[(Y_{O2})_o - Y_{O2}\right]\theta^*_{O2} + \left[(Y_{N2})_o - Y_{N2}\right]\theta^*_{N2} + \left[(Y_{NO})_o - Y_{NO}\right]\theta^*_{NO} \right\} \tag{2.29}$$

Utilizing the mass balance equations, Eq. (2.19) and (2.20), in order to eliminate the molar concentrations $(Y_{O2})_o$ and $(Y_{N2})_o$, and also considering that in the adopted air model $(Y_{NO})_o$ is zero, a more convenient expression for the enthalpy is easily derived from Eq. (2.29):

$$h = R^* \Bigg\{ Y_{O2} \left(\frac{7}{2} T + \frac{\theta^v_{O2}}{e^{\theta^v_{O2}/T} - 1} \right) + Y_{N2} \left(\frac{7}{2} T + \frac{\theta^v_{N2}}{e^{\theta^v_{N2}/T} - 1} \right)$$

$$+ Y_{NO} \left(\frac{7}{2} T + \frac{\theta^v_{NO}}{e^{\theta^v_{NO}/T} - 1} + \frac{\theta^*_{O2}}{2} + \frac{\theta^*_{N2}}{2} - \theta^*_{NO} \right)$$

$$+ Y_O \left(\frac{5}{2} T + \frac{\theta^*_{O2}}{2} \right) + Y_N \left(\frac{5}{2} T + \frac{\theta^*_{N2}}{2} \right) \Bigg\} \qquad (2.30)$$

It is recognized that the specific enthalpy now has the more general form

$$h = \sum_i C_i \, h_i (T) \qquad (2.31)$$

For the calculations in the following chapters it is convenient to define a frozen specific heat as the partial derivative of h with respect to T, that is

$$c_p \equiv \frac{\partial h}{\partial T} \qquad (2.32)$$

which, according to Eq. (2.31) may be expressed as

$$c_p = \sum_i C_i \frac{\partial h_i}{\partial T} = \sum_i C_i \, c_{p_i} \qquad (2.33)$$

Hence, like the specific enthalpy, the frozen specific heat of the gas mixture is simply the weighted sum of the individual specific heats. An explicit expression for c_p, as derived from Eq. (2.30), is given in Appendix A.

2.4 Rate Processes

2.4.1 Finite Rate Nonequilibrium

In general, a large number of collisions among the particles is required to equilibrate the molecular vibrations, dissociation and higher modes of excitation with the local translational temperature. This means that, once being in a state of nonequilibrium, a finite amount of time is needed for the gas properties to achieve thermodynamic equilibrium. The departure from equilibrium of a flowing gas is characterized by the magnitude of this relaxation time τ relative to some translational time t needed by the particles to change their state. The limiting values of the ratio of τ over t are a convenient means to characterize the equilibrium state ($\tau / t \to 0$) and the frozen state ($\tau / t \to \infty$).

The purpose of this section is to present the equations which are necessary to account for finite rate nonequilibrium effects in the calculations. Essentially this is equivalent to finding an expression for the relaxation time τ in terms of the variables of state.

2.4.2 Species Continuity Equation

Consider an arbitrary material volume containing particles of various species, each species forming the partial density ρ_i. Neglecting diffusion, the mass rate of change of the ith component in the mixture must equal the rate of production (which may be negative or positive) of the ith species, that is

$$\frac{D}{Dt}\int_V \rho_i \, dV = \int_V \dot{W}_i \, dV \tag{2.34}$$

where $\dot{W}_i$ is defined as the mass rate of formation of species i per unit volume due to chemical reactions. Using Reynolds' transport theorem, Eq. (2.34) may be rewritten

$$\int_V \left[\frac{\partial \rho_i}{\partial t} + \nabla \cdot (\rho_i \vec{q}) - \dot{W}_i \right] dV = 0 \tag{2.35}$$

Since the volume considered was arbitrary, this means that

$$\frac{\partial \rho_i}{\partial t} + \nabla \cdot (\rho_i \vec{q}) = \dot{W}_i \tag{2.36}$$

Summing over all species i, and considering that $\sum_i \rho_i = \rho$, also $\sum_i \dot{W}_i = 0$ since total mass must be conserved, one obtains the overall mass conservation equation

$$\frac{\partial \rho}{\partial t} + \nabla \cdot (\rho \vec{q}) = 0 \tag{2.37}$$

Replacing ρ_i by ρC_i in Eq. (2.36), and expanding differentials yields

$$C_i \left[\frac{\partial \rho}{\partial t} + \nabla \cdot (\rho \vec{q}) \right] + \rho \left[\frac{\partial C_i}{\partial t} + \vec{q} \cdot \nabla C_i \right] = \dot{W}_i \tag{2.38}$$

Since the first term on the left hand side vanishes according to Eq. (2.37), the species continuity equation finally assumes the form

$$\frac{\partial C_i}{\partial t} + \vec{q} \cdot \nabla C_i = (\dot{W}_i / \rho) \tag{2.39}$$

It is worth noting that the quantity $(\rho / \dot{W}_i)$ has the dimension of time, and

therefore may be interpreted as a relaxation time for the species i. In the following section an explicit expression for $\dot{W}_i$ will be derived.

2.4.3 Rate Equations

Following Vincenti and Kruger (Ref. 24), a chemical reaction is considered to have the following description:

$$\sum_i \nu_i A_i + \nu_M A_M \underset{k_{r,M}}{\overset{k_{d,M}}{\rightleftharpoons}} \sum_i \nu_i' A_i + \nu_M A_M \tag{2.40}$$

where the ν_i are the stoichiometric coefficients of the reactants, ν_i' those of the products. A_M is a so-called third body species which does not participate as a reactant. $k_{d,M}$ and $k_{r,M}$ are the respective reaction rate constants for dissociation and recombination.

Defining the concentration of the species A_i by X_i, that is

$$X_i \equiv \frac{C_i}{M_i} \rho = \rho Y_i \tag{2.41}$$

it is an experimentally observed fact that the rate of formation of any one of the products in a single step reaction can be expressed as

$$\left(\frac{d X_i}{d t}\right)_d = (\nu_i' - \nu_i) k_{d,M} \prod X_i^{\nu_i} X_M^{\nu_M} \tag{2.42}$$

where the product on the right hand side extends over all the reactants.

Similarly, the rate of disappearance of any species A_i can be expressed as

$$\left(\frac{d X_i}{d t}\right)_r = (\nu_i - \nu_i') k_{r,M} \prod_i X_i^{\nu_i'} X_M^{\nu_M} \tag{2.43}$$

where again the product is taken over all of the reactants.

The net rate of production of the species A_i is then the sum of its rate of formation and its rate of disappearance, vis.

$$\frac{d X_i}{d t} = \left(\frac{d X_i}{d t}\right)_d + \left(\frac{d X_i}{d t}\right)_r \tag{2.44}$$

or, with Eq. (2.42) and (2.43):

$$\frac{d X_i}{d t} = (\nu_i' - \nu_i)\left[k_{d,M} X_M^{\nu_M} \prod_i X_i^{\nu_i} - k_{r,M} X_M^{\nu_M} \prod_i X_i^{\nu_i'}\right] \tag{2.45}$$

For thermodynamic equilibrium, the net rate of production of each and all species must vanish ("principle of detailed balancing"), hence from Eq. (2.45):

$$k_{d,M} \prod_i X_i^{\nu_i} - k_{r,M} \prod_i X_i^{\nu_i'} = 0 \tag{2.46}$$

Eq. (2.46) can also be written in the more familiar form

$$\frac{k_{d,M}}{k_{r,M}} = \frac{\prod_i X_i^{\nu_i'}}{\prod_i X_i^{\nu_i}} \equiv K_c(T) \tag{2.47}$$

where $K_c(T)$ is called the concentration equilibrium constant, and expression (2.47) represents the law of mass action.

If it is assumed that, for given temperature and reactant concentrations, the rate at which a reaction proceeds in a given direction is the same whether the system is or is not in equilibrium, Eq. (2.47) may be used to replace either $k_{d,M}$ or $k_{r,M}$ in Eq. (2.45). Hence let

$$k_{d,M} = k_{r,M} K_c (T) \tag{2.48}$$

Using this expression, and also accounting for the possibility of several species acting as third bodies, the resulting rate of production is obtained from expression (2.45) as

$$\frac{d X_i}{d t} = (\nu_i' - \nu_i) \sum_M k_{r,M} X_M^{\nu_M} \left[K_c \prod_i X_i^{\nu_i} - \prod_i X_i^{\nu_i'} \right] \tag{2.49}$$

Considering also that there may be m different chemical reactions of the type represented by Eq. (2.40), the total rate of production of the element A_i is given by the sum over all reactions, that is

$$\left(\frac{d X_i}{d t} \right)_{tot} = \sum_m (\nu_i' - \nu_i) \sum_M k_{r,M} X_M^{\nu_M} \left[K_c \prod_i X_i^{\nu_i} - \prod_i X_i^{\nu_i'} \right] \tag{2.50}$$

It is obvious from Eq. (2.47) that K_c (T) is, for the mth reaction, independent of the third body species A_M. Naturally, for different reactions, the equilibrium constants are different functions of temperature. Their evaluation is discussed in section 2.5 of this chapter.

For the air model used in this investigation the following set of chemical reactions will be considered (Ref. 15):

$$m = I \quad O_2 + M + 5.1\ ev \underset{k^{I}_{r,M}}{\overset{k^{I}_{d,M}}{\rightleftharpoons}} 2O + M \tag{2.51}$$

$$II \quad N_2 + M + 9.8\ ev \rightleftharpoons 2N + M \tag{2.52}$$

$$III \quad NO + M + 6.5\ ev \rightleftharpoons O + N + M \tag{2.53}$$

$$IV \quad NO + O + 1.4\ ev \rightleftharpoons O_2 + N \tag{2.54}$$

$$V \quad N_2 + O + 3.3\ ev \rightleftharpoons NO + N \tag{2.55}$$

$$VI \quad O_2 + N_2 + 1.9\ ev \rightleftharpoons 2\ NO \tag{2.56}$$

Reactions I, II, and III are the principal dissociation reactions, and, considering the various third body species (see Table III), actually represent fifteen different reactions. The remaining equations represent the so called shuffle reactions. Altogether, eighteen chemical reactions are considered between the five components of the gas mixture.

The application of Eq. (2.50) to the above set of reactions yields the following expressions, already simplified by introducing the molar concentrations Y_i :

$$\left(\frac{dX_{O2}}{dt}\right)_{tot} = \rho^2 \Big\{ (\rho Y_O^2 - Y_{O2} K_c^I) \Big[Y_{O2}\, k_{r(O2)}^I + Y_O\, k_{r(O)}^I + (Y_{N2} + Y_{NO} + Y_N)\, k_{r(N2)}^I \Big] - (Y_{O2}\, Y_N - Y_{NO}\, Y_O\, K_c^{IV})\, k_r^{IV} + (Y_{NO}^2 - Y_{O2}\, Y_{N2}\, K_c^{VI})\, k_r^{VI} \Big\} \qquad (2.57)$$

$$\left(\frac{dX_{N2}}{dt}\right)_{tot} = \rho^2 \Big\{ (\rho Y_N^2 - Y_{N2} K_c^{II}) \Big[Y_{N2}\, k_{r(N2)}^{II} + Y_N\, k_{r(N)}^{II} + (Y_{O2} + Y_{NO} + Y_O)\, k_{r(O2)}^{II} \Big] + (Y_{NO}\, Y_N - Y_{N2}\, Y_O\, K_c^V)\, k_r^V + (Y_{NO}^2 - Y_{O2}\, Y_{N2}\, K_c^{VI})\, k_r^{VI} \Big\} \qquad (2.58)$$

$$\left(\frac{dX_{NO}}{dt}\right)_{tot} = \rho^2 \Big\{ (\rho Y_O\, Y_N - Y_{NO} K_c^{III})(Y_{O2} + Y_{N2} + Y_{NO} + Y_O + Y_N) k_r^{III} + (Y_{O2}\, Y_N - Y_{NO}\, Y_O\, K_c^{IV})\, k_r^{IV} - (Y_{NO}\, Y_N - Y_{N2}\, Y_O\, K_c^V)\, k_r^V - 2\,(Y_{NO}^2 - Y_{O2}\, Y_{N2}\, K_c^{VI})\, k_r^{VI} \Big\} \qquad (2.59)$$

Proper rearrangement of terms in the corresponding expressions for the monatomic species O and N shows that

$$\left(\frac{dX_O}{dt}\right)_{tot} = -2\left(\frac{dX_{O2}}{dt}\right)_{tot} - \left(\frac{dX_{NO}}{dt}\right)_{tot} \qquad (2.60)$$

$$\left(\frac{dX_N}{dt}\right)_{tot} = -2\left(\frac{dX_{N2}}{dt}\right)_{tot} - \left(\frac{dX_{NO}}{dt}\right)_{tot} \qquad (2.61)$$

These equations can be obtained, in a simpler way, directly from the mass balance equations, Eq. (2.19) and (2.20).

It is important to keep in mind that the expressions given by Eq. (2.57) through (2.61) are equations representing rates of production due to chemical reactions taking place in a closed system of fixed volume, assuming also a constant temperature. As pointed out by Vincenti and Kruger (Ref. 24), they are customarily extended to open systems of varying volume and temperature by identifying density and temperature as the instantaneous values for the system. This implies that the internal rate processes in a moving fluid are the same as those which occur at the same state in a static system. The $(dX_i/dt)_{tot}$ is related to the mass rate of formation of species i, as defined in the species continuity equation, by the relation

$$\dot{W}_i = M_i \left(\frac{dX_i}{dt}\right)_{tot} \qquad (2.62)$$

2.4.4 Reaction Rate Constants

In order to evaluate the reaction rates given in the previous section, expressions are needed for the rate constants. Although theories exist for the

calculation of dissociation and recombination rate constants (Ref. 24, 26), they are either too complex to be useful in practice, or too simplified to produce acceptable agreement with experimental data. However, it was recognized on experimental grounds that, for many reactions, a plot of the logarithm of the dissociation rate constant versus reciprocal temperature produces an essentially straight line of negative slope, which leads to the Arrhenius equation

$$k_d = A\ e^{-\frac{\epsilon_A}{kT}} \tag{2.63}$$

where ϵ_A is the activation energy and A some constant independent of temperature. A refinement of this expression is usually obtained by assuming

$$k_d = A\ T^n\ e^{-\frac{\theta^*}{T}} \tag{2.64}$$

where θ^* is the characteristic temperature of dissociation, and the constants A and n are determined by curve fits to the experimental data. Expressions of this type are numerous in the literature and can usually be traced to the papers by Wray (Ref. 25) and Lin and Teare (Ref. 26). Expressions used in the present calculations were taken from Spurk, Gerber and Sedney (Ref. 20), and are listed in Table III.

2.5 Equilibrium Constants

The equilibrium constants, defined in Eq. (2.47), are also needed for the evaluation of the reaction rates. Following again Vincenti and Kruger (Ref. 24),

it is found that, in terms of the partition functions, the equilibrium composition of a gas is given by

$$\frac{\prod_i n_i^{\nu_i'}}{\prod_i n_i^{\nu_i}} = \frac{\prod_i Q^{\nu_i'}}{\prod_i Q^{\nu_i}} \exp\left(-\frac{\Delta E}{R^* T}\right) \tag{2.65}$$

where ΔE is the difference in the bond energy of the reactants in Eq. (2.40), n_i are the numbers of particles involved, and ν_i and ν_i' are the stoichicmetric coefficients. The n_i are easily expressed in terms of the concentrations by noticing that, according to Eq. (2.41),

$$X_i = \frac{C_i}{M_i}\rho = \frac{\rho_i}{M_i} = \frac{n_i}{VN^*} \tag{2.66}$$

Therefore, expressing the left hand side of Eq. (2.65) in terms of the concentrations X_i, it can be shown that

$$\frac{\prod_i X_i^{\nu_i'}}{\prod_i X_i^{\nu_i}} = (N^*V)^{\sum\nu_i - \sum\nu_i'} \frac{\prod_i n_i^{\nu_i'}}{\prod_i n_i^{\nu_i}} \tag{2.67}$$

Combining this with Eq. (2.47) and (2.65) it is seen that

$$K_c(T) = (N^*V)^{\sum\nu_i - \sum\nu_i'} \frac{\prod_i Q^{\nu_i'}}{\prod_i Q^{\nu_i}} \exp\left(-\frac{\Delta E}{R^* T}\right) \tag{2.68}$$

which, when applied to the reactions given in Eq. (2.51) through (2.56), turns out to be a function of temperature only. Eq. (2.68) shows also why the contributions due to electronic excitation must not be neglected in the equilibrium constants.

Here, the ratio of the partition function is important, while in the internal energy their contribution is only additive.

It is clear that substitution of the proper expressions for the partition functions in Eq. (2.68) leads to complicated functions of the temperature. In particular, since use is often made of the equilibrium constants in comparing dissociation and recombination rate constants, it is convenient to have them in a simple analytic form. For this purpose Wray (Ref. 25) has fitted the equilibrium constants calculated from Eq. (2.68) for the reactions given by Eq. (2.51) through (2.56) with Arrhenius type expressions of the form

$$K_c(T) = A\, T^n \exp(-\theta^*/T) \tag{2.69}$$

These expressions, given in Table IV, are employed in the present calculations.

With respect to these curve fits a remark is in order at this time. As mentioned earlier, the principle of detailed balancing requires that, for a gas mixture to be in overall equilibrium, every molecular process and its inverse must be individually in balance. Thus it can be shown that, if the total reaction rates and their individual contributions are set to zero, the concentration equilibrium constants, for the reactions chosen herein, result as follows:

$$K_c^{I} = (X_O^2 / X_{O2})_{equil.} \tag{2.70}$$

$$K_c^{II} = (X_N^2 / X_{N2})_{equil.} \tag{2.71}$$

$$K_c^{III} = (X_O X_N / X_{NO})_{equil.} \tag{2.72}$$

and it can also be shown that

$$K_c^{IV} = \frac{K_c^{III}}{K_c^{I}} \tag{2.73}$$

$$K_c^{V} = \frac{K_c^{II}}{K_c^{III}} \tag{2.74}$$

$$K_c^{VI} = \frac{K_c^{I} K_c^{II}}{(K_c^{III})^2} = \frac{K_c^{V}}{K_c^{IV}} \tag{2.75}$$

Since Wray curve fitted all the K_c except for K_c^{VI}, which was determined from K_c^{IV} and K_c^{V} according to Eq. (2.75), it is not surprising that Wray's expressions for K_c^{IV} and K_c^{VI} differ from K_c^{IV} and K_c^{VI} as given in Table IV. For the sake of consistency, the latter expressions were obtained from K_c^{I} through K_c^{III} according to Eq. (2.73) through (2.75). Numerical calculations show that the disagreement between the K_c given by Wray and those obtained from equations (2.73) through (2.75) is negligible.

2.6 Equilibrium Composition

It was mentioned at the beginning of this chapter that is is of interest to calculate equilibrium flow even though it is, in the exact sense, a purely

hypothetical case. In order to do this, the equilibrium composition of the mixture has to be determined as a function of other flow variables.

For a five component mixture this means that five linearly independent equations are needed to solve for all the unknowns. Equations (2.18) and (2.19), together with Eq. (2.70) through (2.72), provide just such a set. Hence, from Eq. (2.18) and (2.19):

$$\sum_i c_i = 1 \tag{2.76}$$

$$c_O + c_{O2} + \left(\frac{M_O}{M_{NO}}\right) c_{NO} = \bar{m}_o \tag{2.77}$$

while from Eq. (2.70) through (2.72):

$$c_{O2} = \frac{2\rho c_O^2}{M_O K_c^{I}} \tag{2.78}$$

$$c_{N2} = \frac{2\rho c_N^2}{M_N K_c^{II}} \tag{2.79}$$

$$c_{NO} = \frac{\rho c_O c_N}{K_c^{III}} \left(\frac{M_{NO}}{M_O M_N}\right) \tag{2.80}$$

Substituting the expressions for the mass fractions c_{O2}, c_{N2} and c_{NO} into the mass balance equations yields

$$C_O + C_N + \frac{2\rho}{M_O K_c^{I}} C_O^2 + \frac{2\rho}{M_N K_c^{II}} C_N^2$$

$$+ \frac{\rho}{K_c^{III}} \left(\frac{M_{NO}}{M_O M_N} \right) C_O C_N = 1 \qquad (2.81)$$

and

$$C_O + \frac{2\rho}{M_O K_c^{I}} C_O^2 + \frac{\rho}{M_N K_c^{III}} C_O C_N = \bar{m}_o \qquad (2.82)$$

from which C_N is obtained in terms of C_O as

$$C_N = \frac{M_N K_c^{III}}{\rho C_O} \left[\bar{m}_o - C_O - \frac{2\rho}{M_O K_c^{I}} C_O^2 \right] \qquad (2.83)$$

Using this equation to eliminate C_N from Eq. (2.81) eventually results in a fourth order equation for C_O:

$$b_4 C_O^4 + b_3 C_O^3 + b_2 C_O^2 + b_1 C_O + b_0 = 0 \qquad (2.84)$$

where

$$b_0 = 2 (\bar{m}_o M_O)^2 K_c^{I} K_c^{III}$$

$$b_1 = \bar{m}_o M_O^2 K_c^{I} K_c^{III} K_c^{V} \left[1 - \frac{4}{K_c^{V}} \right]$$

$$b_2 = M_O^2 K_c^I \left\{ 2 K_c^{III} \left[1 - \frac{4 \bar{m}_o \rho}{M_O K_c^I} \right] - \rho K_c^V \left[\frac{1 - \bar{m}_o}{M_N} - \frac{\bar{m}_o}{M_O} \right] - K_c^{III} K_c^V \right\}$$

$$b_3 = \rho M_O K_c^I K_c^V \left[\frac{8}{K_c^{VI}} - 2 K_c^{IV} - 1 \right]$$

$$b_4 = 2 \rho^2 K_c^V \left[\frac{4}{K_c^{VI}} - 1 \right] \qquad (2.85)$$

Since the b's are functions of temperature and density only, Eq. (2.84) determines the equilibrium composition for given temperature and density. It is seen from Eq. (2.77) that the only possible solution can be selected by requiring the atomic oxygen mass fraction C_O found from Eq. (2.84) to satisfy

$$0 \leq C_O \leq \left[\bar{m}_o - C_{O2} - \left(\frac{M_O}{M_{NO}} \right) C_{NO} \right] \qquad (2.86)$$

2.7 Review of Assumptions

It is instructive to examine the validity of the assumption of vibrational equilibrium which was employed throughout this chapter. A measure for the validity of this assumption is given by the ratio of the chemical over the vibrational relaxation time of the respective species.

Using expressions given in Ref. 27, vibrational relaxation times for O_2 and N_2 are given by

$$\tau^{v}_{O2}\ p = 1.6212 \cdot 10^{-4} \exp\left(\frac{101.44}{T^{1/3}}\right) \tag{2.87}$$

$$\tau^{v}_{N2}\ p = 1.1146 \cdot 10^{-6}\ T^{1/2} \exp\left(\frac{154}{T^{1/3}}\right) \tag{2.88}$$

where τ^{v}_{i} is given in sec for the pressure in N/m^2 and the temperature in ^{o}K.

As previously indicated, the quantity $(\rho / \dot{W}_i)$ has the dimension of time. A chemical relaxation time can thus be defined as

$$\tau^{d}_{i} \equiv \frac{\rho}{\dot{W}_i} \tag{2.89}$$

where the mass rate of formation, $\dot{W}_i$, can be evaluated for O_2 and N_2 from Eq. (2.57), (2.58) and (2.62).

Ratios $(\tau^{d}/\tau^{v})_i$ for $i = O_2, N_2$ are shown in Fig. 2 as function of temperature, together with results for O_2 taken directly from Ref. (28). It should be noted that the values of τ^{d}/τ^{v} are independent of density.

It is seen from Fig. 2 that, at least for molecular oxygen and nitrogen, vibrational relaxation times are always shorter than chemical relaxation times for temperatures below 12,000 ^{o}K. Hence it is concluded that, for the temperature of interest in the present investigation, vibrational relaxation will in general proceed much faster than chemical relaxation. Therefore, the assumption of vibrational equilibrium is a justifiable simplification.

However, it is also recognized, that for temperatures above 8,000 ^{o}K vibrational and chemical relaxation times assume values of the same order of magnitude. Strictly speaking, vibrational relaxation and vibration-dissociation coupling should therefore be considered in this temperature range. The difficulty here is that, although vibrational relaxation rates are known, an accurate model for the coupling does not seem to be available. Conclusions drawn by investigators in this particular field, Ref. 19 for example, leave the question open as to the relative validity of the various models. Rather than to introduce equations of which the effect is not yet well understood, the vibrational excitation is assumed to be uncoupled to the dissociation, and in equilibrium at all times.

CHAPTER III

FORMULATION OF THE PROBLEM

3.1 Basic Equations

Neglecting body forces, viscosity, diffusion, heat conduction, and radiation, the basic equations for steady, adiabatic continuum flow are the following:

Conservation of mass:

$$\nabla \cdot (\rho \vec{q}) = 0 \tag{3.1}$$

Conservation of momentum:

$$\nabla \left(\frac{q^2}{2}\right) + (\nabla \times \vec{q}) \times \vec{q} + \frac{1}{\rho} \nabla p = 0 \tag{3.2}$$

Conservation of energy:

$$\vec{q} \cdot \nabla \left(h + \frac{q^2}{2}\right) = 0$$

or, assuming all streamlines to originate from the same reservoir,

$$h + \frac{q^2}{2} = H = \text{constant} \tag{3.3}$$

These equations are the common equations of motion which do not depend on any particular gas model. In order to solve these equations for the unknowns, they must be supplemented by a thermal and a caloric equation of state which do depend on the particular gas model and were derived in Chapter II as

$$p = \rho R Z T \tag{3.4}$$

and

$$h = \sum_i C_i \, h_i \, (T) \tag{3.5}$$

If the gas under consideration is chemically reacting, additional unknowns arise in form of the mass fractions, C_i, hence, additional equations for the conservation of species must be added to the system. For the air model used herein these are given by Eq. (2.39), which, for steady flow, reduces to

$$\vec{q} \cdot \nabla C_i = \frac{\dot{W}_i}{\rho} \tag{3.6}$$

where i = O, N, and NO, and the mass balance equations given by equations (2.18) and (2.19).

The choice of the coordinate system is largely a matter of experience. For the problem at hand, an orthogonal curvilinear coordinate system with coordinates tangential and normal to the body surface (see Fig. 3) seems to be the most suitable. From Ref. 29 one obtains for the gradient

$$\nabla F = \frac{\vec{e}_1}{h_1} \frac{\partial F}{\partial x_1} + \frac{\vec{e}_2}{h_2} \frac{\partial F}{\partial x_2} + \frac{\vec{e}_3}{h_3} \frac{\partial F}{\partial x_3} \tag{3.7}$$

where F is any scalar point function. For a vector point function $\vec{F}$ the divergence is given by

$$\nabla \cdot \vec{F} = \frac{1}{h_1 h_2 h_3} \left[\frac{\partial}{\partial x_1} (h_2 h_3 F_1) + \frac{\partial}{\partial x_2} (h_3 h_1 F_2) + \frac{\partial}{\partial x_3} (h_1 h_2 F_3) \right] \tag{3.8}$$

and the curl by

$$\nabla \times \vec{F} = \frac{1}{h_1 h_2 h_3} \begin{vmatrix} h_1 \vec{e}_1 & h_2 \vec{e}_2 & h_3 \vec{e}_3 \\ \frac{\partial}{\partial x_1} & \frac{\partial}{\partial x_2} & \frac{\partial}{\partial x_3} \\ h_1 F_1 & h_2 F_2 & h_3 F_3 \end{vmatrix} \qquad (3.9)$$

The metric coefficients h_1, h_2, h_3 follow from the differential arc length

$$(ds)^2 = (h_1 dx_1)^2 + (h_2 dx_2)^2 + (h_3 dx_3)^2 \qquad (3.10)$$

Using as coordinates x, y, and ϕ, where ϕ is the circumferential coordinate, one obtains from Fig. 4

$$h_1 dx_1 = (1 + Ky) dx$$

$$h_2 dx_2 = dy$$

$$h_3 dx_3 = r^j d\phi = (r_b + y \cos\theta)^j d\phi \qquad (3.11)$$

where $K = 1/R$ is the body surface curvature, and

$$j = \begin{cases} 0 & \text{for plane flow} \\ 1 & \text{for axisymmetric flow} \end{cases}$$

Applying equations (3.7) through (3.11) to equations (3.1), (3.2) and (3.6) and restricting to plane or axisymmetric flow, that is, zero angle of attack, the resulting equations are as follows.

Conservation of mass:

$$\frac{\partial}{\partial x}(\rho u r^j) + \frac{\partial}{\partial y}\left[(1+Ky)\ \rho v r^j\right] = 0 \qquad (3.12)$$

x - Momentum:

$$u \frac{\partial u}{\partial x} + (1+Ky)\, v \frac{\partial u}{\partial y} + u\, v\, K + \frac{1}{\rho} \frac{\partial p}{\partial x} = 0 \qquad (3.13)$$

y - Momentum:

$$u \frac{\partial v}{\partial x} + (1+Ky)\, v \frac{\partial v}{\partial y} - u^2 K + \frac{1+Ky}{\rho} \frac{\partial p}{\partial y} = 0 \qquad (3.14)$$

Conservation of species:

$$u \frac{\partial C_i}{\partial x} + (1+Ky)\, v \frac{\partial C_i}{\partial y} - (1+Ky) \frac{\dot{W}_i}{\rho} = 0 \qquad (3.15)$$

The above equations, together with the thermal equation of state, the energy equation, and two mass balance equations, form a set of ten equations for the unknowns u, v, p, ρ, T and five C_i.

Before discussing the details of the solution of the above system, it will be convenient to have equations (3.13) through (3.15) also available in the divergence form. After some algebraic manipulations the following equations can be obtained.

x - Momentum:

$$\frac{\partial}{\partial x}\left[(p+\rho u^2)\, r^j\right] + \frac{\partial}{\partial y}\left[(1+Ky)\, \rho u v\, r^j\right] + \rho u v K r^j - j p (1-Ky) \sin\theta = 0 \qquad (3.16)$$

y - Momentum:

$$\frac{\partial}{\partial x}(\rho u v r^j) + \frac{\partial}{\partial y}\left[(1+Ky)(p+\rho v^2) r^j\right] - (p+\rho u^2) K r^j - j p (1+Ky) \cos\theta = 0 \qquad (3.17)$$

Conservation of Species:

$$\frac{\partial}{\partial x}(\rho u C_i r^j) + \frac{\partial}{\partial y}\left[(1+Ky)\rho v C_i r^j\right] - (1+Ky) r^j \dot{W}_i = 0 \qquad (3.18)$$

The boundary conditions which are needed to solve the equations established here are given in the next section.

3.2 Boundary Conditions

3.2.1 Body Surface and Shock Conditions

The body surface is assumed to be chemically inert. The condition for flow tangency on the body surface is given by

$$v_b = 0 \qquad (3.19)$$

The conditions behind the shock wave are obtained from the conservation of mass, momentum and energy across the shock wave.

Conservation of mass:

$$\rho_\infty V_{n\infty} = \rho_s V_{ns} \qquad (3.20)$$

Conservation of momentum:

$$V_{t\infty} = V_{ts} \qquad (3.21)$$

$$\rho_\infty V_{n\infty}^2 + p_\infty = \rho_s V_{ns}^2 + p_s \qquad (3.22)$$

Conservation of energy:

$$h_\infty + \frac{1}{2} V_{n\infty}^2 = h_s + \frac{1}{2} V_{ns}^2 \qquad (3.23)$$

where the pressure and the enthalpy are given by the equation of state, Eq. (2.16), and the enthalpy equation, Eq. (2.30), respectively. It should be noted that the form of the enthalpy equation implies that the molecular vibrations are in equilibrium everywhere.

For the calculations to follow, the velocities behind the shock must be given in the present coordinate system. The following geometric relations are obtained from Fig. 5:

$$u_s = V_{ns} \sin\beta + V_{ts} \cos\beta \tag{3.24}$$

$$v_s = -V_{ns} \cos\beta + V_{ts} \sin\beta \tag{3.25}$$

where the velocity components as referred to the shock are given by

$$V_{ns} = \frac{\rho_\infty}{\rho_s} V_\infty \sin\sigma \tag{3.26}$$

$$V_{ts} = V_{t\infty} = V_\infty \cos\sigma \tag{3.27}$$

Fig. 4 also indicates that the relation between the shock coordinates and the shock wave angle σ is given by

$$\frac{dy_s}{dx} = (1 + Ky_s) \tan\beta \tag{3.28}$$

where, in general, β is a function of x.

3.2.2 Frozen Shock Conditions

For frozen and nonequilibrium flow it will be assumed that the composition of the air does not change across the shock, that is, $Z_\infty = Z_s$. Since, in the present calculations, the shock wave is assumed to be a discontinuity of zero thickness, and any possible chemical reaction would need some finite thickness in order to take place, the assumption is a logical one.

Combining the equation of state with equations (3.20) through (3.23), it can be shown that

$$T_s = \frac{V_{n\infty}}{R Z_s}\left(1+\frac{R Z_\infty T_\infty}{V_{n\infty}^2}\right)\sqrt{V_{n\infty}^2 - 2(h_s - h_\infty)} - \frac{V_{n\infty}^2 - 2(h_s - h_\infty)}{R Z_s} \tag{3.29}$$

For any given free stream conditions (i.e. T_∞, V_∞, $C_{i\infty}$) and the shock wave angle σ, the temperature behind the shock, T_s, can now be found from equations (3.29) and (2.30) by solving these equations numerically. Using the continuity equation, Eq. (3.20), and the energy equation, Eq. (3.23), the density ratio across the shock is obtained as

$$\frac{\rho_s}{\rho_\infty} = \frac{V_{n\infty}}{\sqrt{V_{n\infty}^2 - 2(h_s - h_\infty)}} \tag{3.30}$$

Knowing the temperature and the density behind the shock, the static pressure ratio across the shock becomes

$$\frac{p_s}{p_\infty} = \frac{\rho_s}{\rho_\infty} \cdot \frac{T_s}{T_\infty} \tag{3.31}$$

which completes the calculations of the static conditions on the downstream side of the shock wave.

Unfortunately, the solution described above involves an iterative calculation of the temperature T_s. Since iterations are normally time consuming, it is impractical to calculate the shock conditions by this process at each step in the course of a numerical calculation. Instead, the expressions for u_s, v_s, T_s, ρ_s, and p_s, presented in this and in the previous section, may be expressed in differential form in terms of the shock wave angle gradient. It is then possible to integrate for some selected key variables, say density ρ_s and temperature T_s, while the values of the remaining variables are determined from simple algebraic equations.

Differentiating the expressions for u_s, v_s, T_s, ρ_s and p_s with respect to x results in the following differential shock relations:

$$\frac{d T_s}{d x} = T_\infty \Omega_1 \frac{d\sigma}{d x} \tag{3.32}$$

$$\frac{d \rho_s}{d x} = \rho_\infty \Omega_2 \frac{d\sigma}{d x} \tag{3.33}$$

$$\frac{d p_s}{d x} = R Z_s (\rho_s T_\infty \Omega_1 + \rho_\infty T_s \Omega_2) \frac{d\sigma}{d x} \tag{3.34}$$

$$\frac{d u_s}{d x} = V_\infty \Omega_3 \frac{d \sigma}{d x} + v_s K \tag{3.35}$$

$$\frac{d v_s}{d x} = V_\infty \Omega_4 \frac{d \sigma}{d x} - u_s K \tag{3.36}$$

where Ω_1 through Ω_4 are dimensionless functions explicitly given in Appendix B.

From Fig. 3 it may be deduced that

$$r_s = r_b + y_s \cos \theta \tag{3.37}$$

which, upon differentiation, yields

$$\frac{d r_s}{d x} = (1 - K y_s) \sin \theta + (1 + K y_s) \cos \theta \tan \beta \tag{3.38}$$

where use was made of the relation

$$\frac{d r_b}{d x} = \sin \theta \tag{3.39}$$

which is obtainable from geometry.

3.2.3 Equilibrium Shock Conditions

In this case it will be assumed that the gas instantaneously reaches the state of thermodynamic, that is, thermal and chemical, equilibrium behind the shock, irrespective of the conditions in the free stream which may be arbitrary. While for frozen shock conditions the composition of the gas on the downstream side of the shock wave is prescribed by the free stream composition, it is unknown in the present problem. The necessary additional relations are furnished by the equations for chemical equilibrium, derived in section 2.6.

Using the equation of state to eliminate the pressures from the equations of conservation of mass and momentum across the shock, it can be shown that

$$\frac{\rho_\infty}{\rho_s} = \frac{b}{2} - \sqrt{\left(\frac{b}{2}\right)^2 - \frac{R Z_s T_s}{V_{n\infty}^2}} \tag{3.40}$$

where

$$b = 1 + \frac{R Z_\infty T_\infty}{V_{n\infty}^2} \tag{3.41}$$

The reciprocal of Eq. (3.30), which was derived from the conservation of energy, yields

$$\frac{\rho_\infty}{\rho_s} = \sqrt{1 - \frac{2(h_s - h_\infty)}{V_{n\infty}^2}} \tag{3.42}$$

For given shock wave angle σ, equations (3.40) and (3.42) are two independent relations for the density ratio across the shock as function of density ρ_s and temperature T_s. Hence, assuming some reasonable values for ρ_s and T_s, a solution is obtained (by iteration on ρ_s and T_s) when the difference between the right hand sides of equations (3.40) and (3.42) assumes a specified minimum value.

Having determined the density ρ_s and the temperature T_s, in the course of which the species mass fractions C_{is} have also been calculated, all other flow variables are readily evaluated from the available equations.

Although equilibrium shock data are available in the literature (Ref. 30, 31), these data are usually presented for selected atmospheric free stream conditions at

relatively low altitudes. The procedure described above, however, is applicable for arbitrary combinations of free stream pressure, temperature and composition, as they may occur at high altitudes or in a hypersonic wind tunnel.

CHAPTER IV

METHOD OF SOLUTION

4.1 The Method of Integral Relations

4.1.1 The Method in General

In order to apply the method of integral relations as described by Dorodnitsyn in Ref. 2, all the partial differential equations are cast into the divergence form, namely

$$\frac{\partial F_i}{\partial x} + \frac{\partial G_i}{\partial y} + H_i = 0$$

$$(i = 1, 2, \ldots, m) \qquad (4.1)$$

Here x and y are the independent variables, while F_i, G_i and H_i are the known functions of the dependent variables, and m denotes the number of equations.

Consider now the solution of the above system of m equations in the region which is bounded by the body surface and by the shock wave $y_s(x)$. Dividing this region into N curvilinear strips (see Fig. 6) bounded by lines

$$y = y_k = \frac{k}{N}\, y_s(x) \qquad (4.2)$$

where $k = 0, 1, 2, \ldots, N$, the system (4.1) can be integrated with respect to y across each strip. The result is a system of integral equations of the form

$$\int_{y_k}^{y_{k+1}} \frac{\partial F_i}{\partial x}\, dy + G_{i,\,k+1} - G_{i,k} + \int_{y_k}^{y_{k+1}} H_i\, dy = 0 \qquad (4.3)$$

where $k = 0, 1, 2, \ldots, N-1$. Using Leibniz's rule for differentiation under the integral sign (Ref. 32), the first integral may be rewritten and the above equations become

$$\frac{d}{dx} \int_{y_k}^{y_{k+1}} F_i\, dy - \left(\frac{k+1}{N} F_{i,k+1} - \frac{k}{N} F_{i,k} \right) \frac{dy_s}{dx}$$

$$+ G_{i,k+1} - G_{i,k} + \int_{y_k}^{y_{k+1}} H_i\, dy = 0 \qquad (4.4)$$

In order to evaluate the integrals, the integrands must be known functions of y. Unfortunately the integrands F_i and H_i contain precisely those dependent variables for which values are to be calculated, hence some approximations have to be made. Generally, as an approximation, any interpolation formula can be used which expresses the value of F_i or H_i at an arbitrary $0 \le y \le y_s$ through its values on the lines $y = y_k$. For example, one may use polynomials of the form

$$F_i = \sum_{n=0}^{N} a_{in}(x)\, y^n$$

$$H_i = \sum_{n=0}^{N} b_{in}(x)\, y^n \qquad (4.5)$$

where the $a_{in}(x)$ and $b_{in}(x)$ are to be evaluated in terms of the boundary values at the strip interfaces, say

$$\text{at } y = y_k : \quad F_i = F_{i,k}$$

$$H_i = H_{i,k} \tag{4.6}$$

Performing the necessary operations on these polynomial approximations yields a system of m. N ordinary differential equations of the following form:

$$\sum_{n=0}^{N} \frac{1}{n+1} \frac{d}{dx}\left[a_{in}(x) \left(y_{k+1}^{n+1} - y_k^{n+1} \right) \right]$$

$$- \left(\frac{k+1}{N} F_{i,k+1} - \frac{k}{N} F_{i,k} \right) \frac{dy_s}{dx} + G_{i,k+1} - G_{i,k} \tag{4.7}$$

$$+ \sum_{n=0}^{N} \frac{b_{in}(x)}{n+1} \left(y_{k+1}^{n+1} - y_k^{n+1} \right) = 0$$

where $k = 0, 1, \ldots, N-1$; $n = 0, 1, \ldots, N$ and $i = 1, 2, \ldots, m$.

The solution of the system (4.7), obtained when the region is divided into N strips, is called the Nth approximation. It is obvious from the above that with higher approximations the complexity of the problem increases considerably. Belotserkovskii (Ref. 37) demonstrated the convergence of the method by comparing one-, two-, and three-strip solutions for supersonic flow past a circular cylinder. He showed that, at least for that case, there is practically no difference between the three solutions. Moreover, since previous investigations with simple rate

processes (Ref. 12, 13) have shown that the first (linear) approximation also agrees well with results from other methods, the linear approximation is investigated herein.

4.1.2 The First Approximation

For the first approximation, according to the previous section, $N = 1$, $k = 0$, $n = 0, 1$. Hence from Eq. (4.5) the polynomial approximations have the general form

$$P_i = c_{i\,0}(x) + c_{i\,1}(x)\, y \tag{4.8}$$

According to (4.6), and the coordinate system, (Fig. 3), it is found that at

$$\begin{aligned} y = 0: \qquad & P_{i,b} = c_{i\,0}(x) \\ y = y_s: \qquad & P_{i,s} = c_{i\,0}(x) + c_{i\,1}(x)\, y_s \end{aligned} \tag{4.9}$$

From (4.9) the coefficient functions in general are

$$\begin{aligned} c_{i\,0}(x) &= P_{i,b} \\ c_{i\,1}(x) &= \frac{1}{y_s}\,(P_{i,s} - P_{i,b}) \end{aligned} \tag{4.10}$$

Applying this procedure to F_i and H_i, the coefficient functions are given by Eq. (4.10). Equation (4.7) may now be simplified and, for the first approximation, results in

$$\frac{d}{dx}\left(F_{i,s} + F_{i,b}\right) - \frac{1}{y_s}\left(F_{i,s} - F_{i,b}\right)\frac{dy_s}{dx}$$

$$+ \frac{2}{y_s}\left(G_{i,s} - G_{i,b}\right) + \left(H_{i,s} + H_{i,b}\right) = 0 \qquad (4.11)$$

The above equation might be called an operator equation, permitting the transformation of the given partial differential equations of the form (4.1) directly into ordinary differential equations for the dependent variables along the body surface and the shock wave boundary.

4.2 Nonequilibrium Flow

4.2.1 General Remarks

As early as 1929, Busemann (Ref. 33) showed that supersonic flow of an inviscid gas about circular cones is characterized by the fact that the pressure and the velocity vector are constant on coaxial conical surfaces having the same vertex as the conical body. A consequence of this is that the shock wave, forming one boundary of this flow field, must itself be a conical surface. It will be shown in the discussion of the results, that, in the case of nonequilibrium, chemically relaxing flow in this case, the time dependency of the chemical reactions destroy this self-similarity mentioned by Busemann, even though the flow is considered to be inviscid. Therefore, no definite statement can be made, a priori, about the shock shape or the behavior of other flow parameters. Values for all variables

must be calculated by integrating the conservation equations together with the equation of state and the boundary conditions in a step-by-step fashion along the length of the cone.

Two different sets of equations will be examined. The first set, later referred to as the standard approximation, contains all the conservation equations, equations (3.12) through (3.15), in approximate form. The second set, later referred to as the semi-exact procedure, uses only the continuity and the y-momentum equations in their approximate form, while the x-momentum and species continuity equations are used in the exact form.

For a supersonic flow field, which will be considered here, the equations are of quasi hyperbolic character and thus form an initial value problem. Initial values are given by the frozen flow solution to be discussed in section 4.3, where it will also be shown that initial gradients can be derived as functions of the initial values.

4.2.2 The Standard Approximation

The application of Eq. (4.11) to the conservation equations, Eq. (3.12) and equations (3.16) through (3.18), results in the following ordinary differential equations where use was made of the fact that $v_b = 0$, and $y = 0$, at the body surface.

Continuity:

$$\frac{d}{dx}\left(\rho_b u_b r_b^j\right) + \frac{d}{dx}\left(\rho_s u_s r_s^j\right)$$

$$= \frac{1}{y_s}\left(\rho_s u_s r_s^j - \rho_b u_b r_b^j\right)\frac{dy_s}{dx} - \frac{2}{y_s}\left(1+Ky_s\right)\rho_s v_s r_s^j \qquad (4.12)$$

x-Momentum:

$$\frac{d}{dx}\left[\left(p_b + \rho_b u_b^2\right) r_b^j\right] + \frac{d}{dx}\left[\left(p_s + \rho_s u_s^2\right) r_s^j\right]$$

$$= \frac{1}{y_s}\left[\left(p_s + \rho_s u_s^2\right) r_s^j - \left(p_b + \rho_b u_b^2\right) r_b^j\right]\frac{dy_s}{dx}$$

$$- \frac{2}{y_s}\left(1+Ky_s\right)\rho_s u_s v_s r_s^j - \rho_s u_s v_s K r_s^j$$

$$+ j \sin\theta\left[p_s\left(1-Ky_s\right) + p_b\right] \qquad (4.13)$$

y-Momentum:

$$\frac{d}{dx}\left(\rho_s u_s v_s r_s^j\right) = \frac{1}{y_s}\left(\rho_s u_s v_s r_s^j\right)\frac{dy_s}{dx}$$

$$- \frac{2}{y_s}\left[\left(1+Ky_s\right)\left(p_s + \rho_s v_s^2\right) r_s^j - p_b r_b^j\right]$$

$$+ K\left[\left(p_s + \rho_s u_s^2\right) r_s^j + \left(p_b + \rho_b u_b^2\right) r_b^j\right]$$

$$+ j \cos\theta\left[p_s\left(1+Ky_s\right) + p_b\right] \qquad (4.14)$$

Species continuity:

$$\frac{d}{dx}\left(\rho_b u_b C_{ib} r_b^j\right) + \frac{d}{dx}\left(\rho_s u_s C_{is} r_s^j\right)$$

$$= \frac{1}{y_s}\left(\rho_s u_s C_{is} r_s^j - \rho_b u_b C_{ib} r_b^j\right) \frac{dy_s}{dx}$$

$$- \frac{2}{y_s}(1+Ky_s)\rho_s v_s C_{is} r_s^j + (1+Ky_s) r_s^j \dot{W}_{is} + r_b^j \dot{W}_{ib} \quad (4.15)$$

Expanding the differentials and introducing the differential shock relations given in section 3.22, the above equations assume the following form, where $\bar{\delta}$ is defined as

$$\bar{\delta} \equiv \frac{y_s(x)}{r_b(x)} \quad (4.16)$$

Continuity:

$$u_b \frac{d\rho_b}{dx} + \rho_b \frac{du_b}{dx} + (1+j\bar{\delta}\cos\theta)(\rho_\infty u_s \Omega_2 + \rho_s V_\infty \Omega_3) \frac{d\sigma}{dx}$$

$$= \frac{1}{y_s}(\rho_s u_s F_1 - \rho_b u_b F_2 - \rho_s v_s F_3) \quad (4.17)$$

x-Momentum:

$$\frac{dp_b}{dx} + u_b^2 \frac{d\rho_b}{dx} + 2\rho_b u_b \frac{du_b}{dx} + (1+j\bar{\delta}\cos\theta)\Big[RZ_s(\rho_s T_\infty \Omega_1$$

$$+ \rho_\infty T_s \Omega_2) + \rho_\infty u_s^2 \Omega_2 + 2\rho_s V_\infty u_s \Omega_3\Big] \frac{d\sigma}{dx}$$

$$= \frac{1}{y_s}\Big\{(p_s + \rho_s u_s^2) F_1 - (p_b + \rho_b u_b^2) F_2$$

$$- \rho_s u_s v_s (1+j\bar{\delta}\cos\theta)(2+5Ky_s)$$

$$+ \left[p_b + p_s(1+Ky_s)\right] j\bar{\delta}\sin\theta\Big\} \quad (4.18)$$

y-Momentum:

$$(1+j\,\bar{\delta}\cos\theta)\,(\rho_\infty\, u_s\, v_s\, \Omega_2+\rho_s\, V_\infty\, v_s\, \Omega_3+\rho_s\, V_\infty\, u_s\, \Omega_4)\,\frac{d\sigma}{dx}$$

$$=\frac{1}{y_s}\Big\{\rho_s\, v_s\,(u_s F_1 - v_s F_3)+(p_b-p_s)\,(2+j\,\bar{\delta}\cos\theta+Ky_s)$$

$$+\Big[\rho_b\, u_b^2+2\,\rho_s\, u_s^2\,(1+j\,\bar{\delta}\cos\theta)\Big]\,Ky_s\Big\} \qquad (4.19)$$

Species continuity:

$$\rho_b\, u_b\,\frac{dC_{ib}}{dx}=(C_{ib}-C_{is})\,(1+j\,\bar{\delta}\cos\theta)\,(\rho_\infty\, u_s\,\Omega_2$$

$$+\rho_s\, V_\infty\,\Omega_3)\,\frac{d\sigma}{dx}$$

$$=\dot{W}_{ib}+(1+Ky_s)\,(1+j\,\bar{\delta}\cos\theta)\,\dot{W}_{is}$$

$$-\frac{1}{y_s}\,(C_{ib}-C_{is})\,(\rho_s\, u_s\, F_1-\rho_s\, v_s\, F_3) \qquad (4.20)$$

where F_1, F_2, and F_3 are dimensionless functions defined as

$$F_1=(1+Ky_s)\tan\beta-(1-Ky_s)\,j\,\bar{\delta}\sin\theta \qquad (4.21)$$

$$F_2=(1+Ky_s)\tan\beta+j\,\bar{\delta}\sin\theta \qquad (4.22)$$

$$F_3=(2+3\,Ky_s)\,(1+j\,\bar{\delta}\cos\theta) \qquad (4.23)$$

The equations given above must be supplemented by the energy equation and the equation of state in differential form.

Energy:

$$u_b \frac{du_b}{dx} + c_{pb} \frac{dT_b}{dx} + \sum_i h_{ib} \frac{dC_{ib}}{dx} = 0 \qquad (4.24)$$

State:

$$\frac{dp_b}{dx} - RZ_b T_b \frac{d\rho_b}{dx} - RZ_b \rho_b \frac{dT_b}{dx}$$

$$- \rho_b R^* T_b \sum_i \frac{1}{M_i} \frac{dC_{ib}}{dx} = 0 \qquad (4.25)$$

Since the mass fractions C_i are linearly related to each other by the two mass balance equations, only three of the five C_i are independent. Therefore, equations (4.17) through (4.25) constitute a system of eight simultaneous differential equations for the gradients of ρ_b, u_b, p_b, T_b, σ, and three of the five C_{ib}.

It may be seen from the conservation equations in the divergence form, and from the discussion of the integral method, that the equations presented in this section contain linear approximations for the following terms:

Continuity: $\rho u r^j$

x-Momentum: $(p + \rho u^2) r^j$,

$$\rho u v K r^j - j p (1 - Ky) \sin \theta$$

y-Momentum: $\rho u v r^j$,

$$(p + \rho u^2) K r^j + j p (1 + Ky) \cos \theta$$

Species continuity:

$$(\rho u C_i r^j), (1 + Ky) \dot{W}_i r^j$$

It is of interest to examine these approximations in some detail. First, it is noted that it has no effect on the x-Momentum equation, Eq. (4.13), whether one approximates the terms $\rho u v K r^j$ and $j p (1 - Ky) \sin \theta$ separately, or combined. The situation is analogous for the y-Momentum equation. Second, the body surface curvature $K(x)$, and the surface inclination angle $\theta(x)$ are constants as far as the linear approximations in y-direction are concerned. It is then noted that both of the momentum equations contain linear approximations for $(p + \rho u^2) r^j$ and $\rho u v r^j$. However, while the term $p (1 - Ky)$ is linearized in the x-Momentum equation, it is $p (1 + Ky)$ in the y-Momentum equation. This is an obvious discrepancy which requires particular attention.

Application of equations (4.8) through (4.10) to these terms leads to the following relations for $p(y)$:

$$p_1(y) = \frac{1}{1-Ky}\left[p_b + \frac{p_s(1-Ky_s) - p_b}{y_s}\, y\right]$$

$$p_2(y) = \frac{1}{1+Ky}\left[p_b + \frac{p_s(1+Ky_s) - p_b}{y_s}\, y\right]$$

Since two different values for the pressure at any one point in the flow field are unacceptable, $p_1(y)$ and $p_2(y)$ must be required to be the same. It can be seen at once that this condition is satisfied for $K = 0$. On the other hand, for $K \neq 0$, it can be shown that this not only requires p_b and p_s to be the same, but also that

$$p(y) = p_b = p_s = \text{constant}$$

Fortunately this discrepancy is the only one, since the application of equations (4.8) through (4.10) to the remaining terms generally leads to only one nonlinear function of y, each, for ρu, $\rho u v$, $p + \rho u^2$, $\rho u C_i$, and $\dot{W}_i$. A procedure to avoid the discrepancy altogether, and simultaneously reduce the number of functions for which approximations have to be introduced, is discussed in the next section.

Apart from this it should be noted that certain terms disappear in the conservation equations when either j or K, or both, are zero. In this case, no linearizations are introduced for the respective terms. Thus, for example, when the equations are applied to wedge flow ($K = 0$, $j = 0$), the linearized terms which are actually used reduce to (ρu), p, (ρu^2), $(\rho u v)$, $(\rho u C_i)$, and $\dot{W}_i$.

4.2.3 The Semi-exact Procedure

The general form of the conservation equations for the one-strip approximation, Eq. (4.11), already indicated that the equations are formulated in terms of the variables along the shock wave and along the body surface, only. This situation suggests the use of the flow tangency condition, Eq. (3.19), in order to simplify some of the partial differential equations before they are integrated in y-direction, and thereby converted to ordinary differential equations. As a matter of fact, it is seen from equations (3.12) through (3.15) that the x-Momentum

equation and the species continuity equation reduce to ordinary differential equations in terms of the variables along the body surface when v is set to zero. Therefore, only the overall continuity equation and the y-Momentum equation need to be used in approximate form, which results in a much simpler set of equations for the semi-exact procedure. This set then consists of equations (4.17), (4.19), and (4.21) through (4.25), while the x-Momentum and the species continuity equations are replaced by

$$\rho_b \, u_b \, \frac{d u_b}{d x} + \frac{d p_b}{d x} = 0 \tag{4.26}$$

and

$$\rho_b \, u_b \, \frac{d C_{ib}}{d x} - \dot{W}_{ib} = 0 \tag{4.27}$$

respectively. Thus, the introduction of the above exact equations eliminates the need to approximate the terms $\rho u \, C_i \, r^j$, $(1+Ky)\dot{W}_i \, r^j$, and $p\,(1-Ky)$. In particular, the discrepancy discussed in the previous section is removed by not using an approximation for $p\,(1-Ky)$.

A careful comparison of equations (4.26) and (4.27) with their approximate counterparts reveals that they may be expressed in a combined form by introducing certain indicators, say ϵ and α. Setting the indicators to zero results in the exact equations, while assigning the value unity yields the approximate equations. Hence,

x-Momentum:

$$\frac{dp_b}{dx} + \epsilon u_b^2 \frac{d\rho_b}{dx} + (1+\epsilon)\,\rho_b\, u_b \frac{du_b}{dx}$$

$$+\epsilon\,(1+j\,\bar{\delta}\cos\theta)\Big[KZ_s(\rho_s T_\infty \Omega_1 + \rho_\infty T_s \Omega_2)$$

$$+u_s(\rho_\infty u_s \Omega_2 + 2\rho_s V_\infty \Omega_3)\Big]\frac{d\sigma}{dx} \qquad (4.28)$$

$$= \frac{\epsilon}{y_s}\Big\{(p_s + \rho_s u_s^2)F_1 - (p_b + \rho_b u_b^2)F_2$$

$$-\rho_s u_s v_s (1+j\,\bar{\delta}\cos\theta)(2+5Ky_s)$$

$$+\Big[p_b + p_s(1+Ky_s)\Big]\,j\,\bar{\delta}\sin\theta\Big\}$$

Species continuity:

$$\rho_b u_b \frac{dC_{ib}}{dx} - \alpha(C_{ib} - C_{is})(1+j\,\bar{\delta}\cos\theta)(\rho_\infty u_s \Omega_2 + \rho_s V_\infty \Omega_3)\frac{d\sigma}{dx}$$

$$= \dot{W}_{ib} + \alpha\Big[(1+Ky_s)(1+j\,\bar{\delta}\cos\theta)\,\dot{W}_{is} \qquad (4.29)$$

$$-\frac{1}{y_s}(C_{ib} - C_{is})(\rho_s u_s F_1 - \rho_s v_s F_3)\Big]$$

Equations (4.17), (4.19), (4.24), (4.25), (4.28), and (4.29) now represent a system of six simultaneous equations for the gradients of u_b, ρ_b, p_b, T_b, C_{ib} and σ. Noticing that the y-Momentum equation and the species continuity equations yield the derivatives of the shock wave angle σ and the mass fractions C_{ib} directly, the above set is easily solved for the remaining gradients. Using

the energy equation, Eq. (4.24), and the equation of state, Eq. (4.25), to eliminate the derivatives of u_b and p_b, the following equations are obtained:

$$\frac{d\rho_b}{dx} = \frac{a_{22} A_1 - a_{12} A_2}{a_{11} a_{22} - a_{12} a_{21}} \tag{4.30}$$

$$\frac{d T_b}{dx} = \frac{a_{11} A_2 - a_{21} A_1}{a_{11} a_{22} - a_{12} a_{21}} \tag{4.31}$$

$$\frac{d\sigma}{dx} = \frac{A_3}{a_{33}} \tag{4.32}$$

$$\frac{dC_{ib}}{dx} = \frac{A_4}{a_{44}} \qquad (i = O, N, NO) \tag{4.33}$$

The coefficients a_{ij} and the terms A_i are functions of the variables along the body and the shock wave. They are explicitly given in Appendix C in their most general form, valid for any combination of the appropriate values for j, K, α, and ϵ. For the present investigation which is primarily concerned with the application of the semi-exact procedure ($\alpha = 0$, $\epsilon = 0$) to the flow about circular cones ($j = 1$, $K = 0$), this implies the use of nonlinear approximations for ρu and $\rho u v$,

$$\rho u = \frac{\rho_b u_b r_b + (\rho_s u_s r_s - \rho_b u_b r_b)(y/y_s)}{r_b + y \cos\theta} \tag{4.34}$$

$$\rho u v = \frac{\rho_s u_s v_s r_s}{r_b + y \cos\theta} \left(\frac{y}{y_s}\right) \tag{4.35}$$

and a linear approximation for p,

$$p(y) = p_b + \frac{p_s - p_b}{y_s} y \qquad (4.36)$$

Since it can be shown that the right hand sides of equations (4.34) and (4.35) are the sums of infinite alternating series in powers of y/y_s, where $0 \leq y/y_s \leq 1$, the error of the method is determined by the linear approximation, Eq. (4.36), for the pressure $p(y)$ across the shock layer.

Having determined the density ρ_b, temperature T_b, shock wave angle σ, and the mass fractions C_{ib} ($i = O, N, NO$) by numerical integration of equations (4.30) through (4.33), the remaining C_{ib} ($i = O_2, N_2$) are calculated from the mass balance equations. Knowing the temperature T_b and all of the mass fractions C_{ib}, the static enthalpy can be evaluated, whereupon the velocity u_b can be computed from the energy equation. Similarly, with density ρ_b, temperature T_b, and the mass fractions C_{ib} known, the pressure p_b is given by the equation of state.

As far as the variables along the shock wave are concerned, it suffices to integrate equations (3.28), (3.32) and (3.33) in addition to (4.32). Once the shock wave angle σ, density ρ_s, and temperature T_s are known, all other variables behind the shock can be computed algebraicly from the expressions given in Chapter III.

The advantage of the semi-exact procedure over the standard approximation appears not only in its relative simplicity, but also in the fact that no

approximations are involved which contain the rate equations or the species mass fractions. This is important because, for chemically relaxing flow, the C_i are key variables of particular interest.

4.3 Initial Solution

4.3.1 Frozen Flow

In order to start the numerical integration of the equations presented in section 4.2, the values of all variables must be known at $x = 0$. The calculation of these values will be based on the assumptions that, first, the flow is chemically frozen and, second, that, in case of a body with non-zero curvature ($K \neq 0$) there is a small region including the tip where the body may be considered to be a circular cone or a wedge ($K = 0$). Since the use of frozen shock conditions implies that the flow is frozen at the tip, this assumption is not a new one.

With the molecular vibrations in equilibrium, and the gas composition frozen, there exists no mechanism to destroy the self-similar character of the flow field, and therefore the classical result of a straight shock wave and constant properties along the body streamline may be applied. Mathematically expressed, this means that in equations (4.17) through (4.19), the gradients of all flow variables along the body and that of the shock wave angle σ can be set to zero. This implies that also the right hand sides of these equations must vanish. Hence, with $\bar{\delta}$, defined by Eq. (4.16), taking the form

$$\bar{\delta} = \frac{y_s}{x \sin \theta} = \frac{\tan\beta}{\sin\theta} \tag{4.37}$$

and F_1, F_2, F_3 reducing to

$$F_1 = (1 - j) \tan \beta \tag{4.38}$$

$$F_2 = (1 + j) \tan \beta \tag{4.39}$$

$$F_3 = 2 (1 + j \cot \theta \tan \beta) \tag{4.40}$$

the following algebraic equations, valid for chemically frozen flow about wedges ($j = 0$) or circular cones ($j = 1$), are obtained from equations (4.17) through (4.19).

Continuity:

$$\rho_s u_s (1 - j) \tan \beta - \rho_b u_b (1 + j) \tan \beta$$

$$- 2 \rho_s v_s (1 + j \cot \theta \tan \beta) = 0 \tag{4.41}$$

x-Momentum:

$$(p_s + \rho_s u_s^2) (1 - j) \tan \beta - (p_b + \rho_b u_b^2) (1 + j) \tan \beta$$

$$- 2 \rho_s u_s v_s (1 + j \cot \theta \tan \beta) + j (p_b + p_s) \tan \beta = 0 \tag{4.42}$$

y-Momentum:

$$\rho_s u_s v_s (1 - j) \tan \beta - 2 \rho_s v_s^2 (1 + j \cot \theta \tan \beta)$$

$$+ (p_b - p_s) (2 + j \cot \theta \tan \beta) = 0 \tag{4.43}$$

Equations (4.41) through (4.43), together with the energy equation and the equation of state, then represent five equations for five unknowns: u_b, ρ_b, T_b, p_b, and σ.

For a given flight configuration, that is given semi-vertex angle θ and free stream conditions, the calculation is started with an assumed value for the shock wave angle σ, and calculating the temperature T_s, the density ρ_s, and the pressure p_s from the frozen shock conditions, that is, from equations (3.29) through (3.31), respectively. With the velocity components u_s and v_s, which are to be computed from equations (3.24) and (3.25), the velocity at the body surface, u_b, is given by

$$u_b = u_s + \frac{v_s}{2 \cot \beta + j \cot \theta} \tag{4.44}$$

This relation can be derived by first eliminating $(p_b - p_s)$ from the two momentum equations, and then replacing the term $(\rho_b u_b)$ from the continuity equation.

Knowing the velocity u_b, the continuity equation yields the density ρ_b. With u_b and ρ_b available, the surface pressure can be calculated from one of the momentum equations. Finally, the equation of state serves to obtain the temperature T_b. The energy equation, not needed so far, is now used to check the value of u_b. If the velocity u_b so calculated does not agree with the value obtained from Eq. (4.44), a new value for the shock wave angle σ must be chosen; and the procedure is repeated.

4.3.2 Initial Derivatives

The necessity for determining the derivatives of all variables at $x = 0$ arises from the fact that the equations for the initial values were obtained by equating

the numerators of the right hand sides of equations (4.17) through (4.19) to zero. Since, for an attached shock wave, also $y_s(0) = 0$, the right hand sides of these equations become indeterminate at the tip of the body. The condition of frozen flow (C_i = constant) leads to the same difficulty in Eq. (4.20).

A set of linear equations for the initial derivatives can be derived from the governing equations by evaluating their limiting expressions as $x \to 0$. For this purpose let the right hand sides of equations (4.17), (4.28), (4.19), and (4.29) be denoted by B_1, B_2, B_3, and B_4, respectively. Specializing them for the case of zero curvature ($K = 0$, $r_b = x \sin\theta$), and introducing

$$\delta = \frac{y_s}{x} \tag{4.45}$$

they may be written as follows:

$$B_1 = \frac{1}{y_s}\Big[\rho_s u_s (\tan\beta - j\delta) - \rho_b u_b (\tan\beta + j\delta) - 2\rho_s v_s (1 + j\delta\cot\theta)\Big] \tag{4.46}$$

$$B_2 = \frac{\epsilon}{y_s}\Big[\rho_s u_s^2 (\tan\beta - j\delta) - \rho_b u_b^2 (\tan\beta + j\delta) - 2\rho_s v_s u_s (1 + j\delta\cot\theta) + (p_s - p_b)\tan\beta\Big] \tag{4.47}$$

$$B_3 = \frac{1}{y_s}\Big[\rho_s u_s v_s (\tan\beta - j\delta) - 2\rho_s v_s^2 (1 + j\delta\cot\theta) - (p_s - p_b)(2 + j\delta\cot\theta)\Big] \tag{4.48}$$

$$B_4 = \dot{W}_{ib} + \alpha \left\{ (1 + j\,\delta \cot\theta)\,\dot{W}_{is} - \frac{1}{y_s}(C_{ib} - C_{is})\left[\rho_s u_s (\tan\beta - j\,\delta) - 2\rho_s v_s (1 + \delta j \cot\theta)\right]\right\} \quad (4.49)$$

Then applying L'Hospital's rule in order to resolve the indeterminacy, the following limiting expressions can be obtained:

$$\lim_{x\to 0} B_1 = \left\{ \frac{\rho_s u_s - \rho_b u_b}{\sin 2\beta} + \frac{\rho_s v_s}{\sin^2\beta} + (1 - j)(\rho_\infty u_s \Omega_2 + \rho_s V_\infty \Omega_3) - 2(\cot\beta + j \cot\theta)(\rho_\infty v_s \Omega_2 + \rho_s V_\infty \Omega_4)\right\} \frac{d\sigma}{dx} - (1 + j)\frac{d}{dx}(\rho_b u_b) \quad (4.50)$$

$$\lim_{x\to 0} B_2 = \epsilon\left\{\frac{(p_s + \rho_s u_s^2) - (p_b + \rho_b u_b^2)}{\sin 2\beta} + \frac{\rho_s u_s v_s}{\sin^2\beta} + (1 - j)(\rho_\infty u_s^2 \Omega_2 + 2\rho_s V_\infty u_s \Omega_3) + RZ_s(\rho_s T_\infty \Omega_1 + \rho_\infty T_s \Omega_2) - 2(\cot\beta + j\cot\theta)(\rho_\infty u_s v_s \Omega_2 + \rho_s V_\infty v_s \Omega_3 + \rho_s V_\infty u_s \Omega_4)\right\} \frac{d\sigma}{dx} - \epsilon(1 + j)\frac{d}{dx}(\rho_b u_b^2) - \epsilon\frac{dp_b}{dx} \quad (4.51)$$

$$\lim_{x\to 0} B_3 = \left\{ \frac{\rho_s u_s v_s}{\sin 2\beta} + \frac{p_s + \rho_s v_s^2 - p_b}{\sin^2 \beta} \right.$$

$$+ (1 - j)(\rho_\infty u_s v_s \Omega_2 + \rho_s V_\infty v_s \Omega_3 + \rho_s V_\infty u_s \Omega_4)$$

$$- 2(\cot\beta + j \cot\theta)(\rho_\infty v_s \Omega_2 + 2 \rho_s V_\infty \Omega_4) v_s$$

$$\left. - R Z_s (2 \cot\beta + j \cot\theta)(\rho_s T_\infty \Omega_1 + \rho_\infty T_s \Omega_2) \right\} \frac{d\sigma}{dx}$$

$$+ (2 \cot\beta + j \cot\theta) \frac{dp_b}{dx} \qquad (4.52)$$

and, finally,

$$\lim_{x\to 0} B_4 = \dot{W}_{ib} + \alpha \left[(1 + j \tan\beta \cot\theta) \dot{W}_{is} \right.$$

$$\left. - (1 + j) \rho_b u_b \frac{dC_{ib}}{dx} \right] \qquad (4.53)$$

where it is noted that the above expressions are to be evaluated at $x = 0$ only.

If the limiting process is now applied to equations (4.17), (4.28), (4.19), and (4.29), and if the expressions given above are inserted on their right hand sides, the following equations for the initial derivatives in terms of the initial values result.

Continuity:

$$u_b \frac{d\rho_b}{dx} + \rho_b \frac{du_b}{dx} + \rho_\infty V_\infty \Omega_5 \frac{d\sigma}{dx} = 0 \qquad (4.54)$$

x-Momentum:

$$(1 + \epsilon) \frac{dp_b}{dx} + \epsilon(2 + j) u_b^2 \frac{d\rho_b}{dx}$$

$$+ \left[1 + \epsilon (3 + 2j)\right] \rho_b u_b \frac{du_b}{dx} + \epsilon \rho_\infty V_\infty^2 \Omega_6 \frac{d\sigma}{dx} = 0 \qquad (4.55)$$

y-Momentum:

$$\frac{dp_b}{dx} + \rho_\infty V_\infty^2 \Omega_7 \frac{d\sigma}{dx} = 0 \qquad (4.56)$$

Species continuity:

$$\left[1+\alpha(1+j)\right]\rho_b u_b \frac{dC_{ib}}{dx}$$

$$= \dot{W}_{ib} + \alpha(1+j\tan\beta\cot\theta)\dot{W}_{is} \qquad (4.57)$$

where Ω_5, Ω_6, and Ω_7 are dimensionless functions listed in Appendix B.

Supplementing equations (4.54) through (4.57) by the energy equation and the equation of state,

$$\rho_b u_b \frac{du_b}{dx} + \rho_b c_{pb} \frac{dT_b}{dx} + \frac{\rho_b V_\infty^2}{\lambda} L_b = 0 \qquad (4\ 58)$$

$$\frac{dp_b}{dx} - RZ_b T_b \frac{d\rho_b}{dx} - \rho_b R Z_b \frac{dT_b}{dx} - \frac{\rho_b T_b V_\infty^2}{\lambda T_\infty} S_b = 0 \qquad (4.59)$$

where λ is a characteristic length, and L and S are dimensionless functions defined in Appendix A, this set can be solved for the initial gradients. The resulting expressions are:

$$\left(\frac{d\sigma}{dx}\right)_{x=0} = \left[1+\epsilon(1+j)\right]\frac{\rho_b}{\rho_\infty}\frac{u_b^2}{\lambda F}\left(RZ_b L_b - \frac{c_{pb}T_b}{T_\infty} S_b\right) \qquad (4.60)$$

where

$$F = u_b^2 \left\{ \left[1+\epsilon(1+j)\right] c_{pb} - (1+\epsilon) R Z_b \right\} \Omega_7$$

$$- R Z_b c_{pb} T_b \left\{ \left[1+\epsilon(3+2j)\right] \frac{u_b}{V_\infty} \Omega_5 - \epsilon \Omega_6 + (1+\epsilon)\Omega_7 \right\}$$

$$- \epsilon R Z_b u_b^2 \left[(2+j) \frac{u_b}{V_\infty} \Omega_5 - \Omega_6 \right] \qquad (4.61)$$

$$\left(\frac{d\rho_b}{dx}\right)_{x=0} = - \frac{\rho_\infty V_\infty^2}{\left[1+\epsilon(1+j)\right] u_b^2} \left\{ \left[1+\epsilon(3+2j)\right] \frac{u_b}{V_\infty} \Omega_5 \right.$$

$$\left. - \epsilon \Omega_6 + (1+\epsilon)\Omega_7 \right\} \left(\frac{d\sigma}{dx}\right)_{x=0} \qquad (4.62)$$

$$\left(\frac{dT_b}{dx}\right)_{x=0} = - \frac{\rho_\infty V_\infty^2}{\rho_b c_{pb}} \left\{ \left(\frac{\rho_b}{\rho_\infty}\right) \frac{L_b}{\lambda} \right.$$

$$\left. + \frac{\epsilon(2+j)\frac{u_b}{V_\infty} \Omega_5 - \epsilon\Omega_6 + (1+\epsilon)\Omega_7}{1+\epsilon(1+j)} \left(\frac{d\sigma}{dx}\right)_{x=0} \right\} \qquad (4.63)$$

$$\left(\frac{dC_{ib}}{dx}\right)_{x=0} = \frac{\dot{W}_{ib} + \alpha(1+j\tan\beta\cot\theta)\dot{W}_{is}}{\rho_b u_b \left[1+\alpha(1+j)\right]} \qquad (4.64)$$

It should be noted that, since no assumptions or approximations were used in deriving the initial gradients from the governing equations, the compatibility of equations (4.60) through (4.64) with equations (4.30) through (4.33) is assured. Again, for $\alpha = 0$ and $\epsilon = 0$, the expressions given above reduce to the initial gradients to be used for the semi-exact procedure. Letting $\alpha = 1$ and $\epsilon = 1$ results in the initial gradients for the standard approximation.

4.4 Equilibrium Flow

As mentioned earlier, an equilibrium flow solution in connection with nonequilibrium flow about wedges or circular cones is useful because it provides a check, in an approximate way, for the values which should be approached asymptotically by the nonequilibrium solution. There are two reasons for the approximation. It will be shown in the discussion of the results that, for nonequilibrium flow about cones, the shock wave is curved. By assumption, the shock wave angle σ at the apex is the same as that for frozen flow, while further downstream, σ approaches the equilibrium shock wave angle which is always found to be smaller than the shock wave angle σ for frozen flow. Consequently, those streamlines which have passed through the stronger portion of the shock wave form a region close to the body surface which must have a higher entropy than the stream lines farther away from the surface. This region is sometimes called an entropy layer. Furthermore, it is known from theory that, in contrast to equilibrium, nonequilibrium dissociation and recombination are nonisentropic processes. Thus, the chemical relaxation in the flow provides another mechanism by which entropy is increased. It is therefore concluded that the equilibrium state which is reached after complete relaxation has a higher entropy than an equilibrium flow, originating from the same free stream conditions, would have. Since, by assumption, the two flows have the same total enthalpy, but their entropy is different, they cannot reach the same final state.

Assuming that the air is in thermodynamic equilibrium everywhere in the flow field, the same considerations as for frozen flow apply, namely, that the flow field is similar. Again, this implies that all flow field parameters are constant on planes, or coaxial cones intersecting at the tip of the body.

Newman (Ref. 36) has used equations (4.41) through (4.43), in connection with thermodynamic data from tables, to calculate conical flow parameters for air in equilibrium. He found that these algebraic equations yield results which are in excellent agreement with the results from the numerical integration of the Taylor-Maccoll differential equation by Romig (Ref. 21). Similar calculations by Thoenes (Ref. 16, 17) for a simple air model, but using equations analogous to those presented in Chapter II for the thermodynamic properties, confirmed this agreement. The more sophisticated air model employed in the present investigation requires a method of calculation which differs slightly from that used previously, and is therefore outlined below.

For an assumed shock wave angle σ the equilibrium conditions behind the shock wave can be calculated as described in Section 3.2.3, whereupon the body surface velocity, u_b, is computed from Eq. (4.44). Substituting this expression into the continuity equation, Eq. (4.41), yields

$$\rho_b = \frac{\left[\rho_s u_s (1-j) - 2\rho_s v_s (\cot\beta + j\cot\theta)\right](2\cot\beta + j\cot\theta)}{(1+j)\left[u_s (2\cot\beta + j\cot\theta) + v_s\right]} \qquad (4.65)$$

Solving the y-Momentum equation, Eq. (4.43), for the body surface pressure results in

$$p_b = p_s + \frac{2\rho_s v_s^2 (1 + j \cot\theta \tan\beta) - \rho_s u_s v_s (1 - j) \tan\beta}{2 + j \cot\theta \tan\beta} \qquad (4.66)$$

Starting from a first guess for the body surface temperature, T_b, together with the density at the body surface, ρ_b, from Eq. (4.65), the equilibrium species mass fractions must now be calculated by an iteration, using the equations provided in Section 2.6. This iteration can be terminated when the mass fractions C_{ib} and the temperature T_b thus obtained, together with density ρ_b and pressure p_b from equations (4.65) and (4.66), satisfy the equation of state.

The energy equation, not used so far, again provides the closing link in the loop. If the value for the velocity at the body surface, u_b, obtained from the energy equation does not agree with the one calculated from Eq. (4.44), the procedure has to be repeated by selecting a new value for the shock wave angle σ.

4.5 Numerical Techniques

For the numerical evaluation all equations were converted to dimensionless form by introducing the following dimensionless variables:

$$u' = \frac{u}{V_\infty} ; \quad v' = \frac{v}{V_\infty} ; \quad \rho' = \frac{\rho}{\rho_\infty} ; \quad T' = \frac{T}{T_\infty} ;$$

$$p' = \frac{p}{\rho_\infty V_\infty^2} ; \quad h' = \frac{h}{V_\infty^2} ; \quad c_p' = \frac{c_p T_\infty}{V_\infty^2} ; \tag{4.67}$$

$$\xi, \eta = \frac{x, y}{\lambda}$$

Since infinite long cones have no typical dimension, the characteristic length λ was defined as a dissociation relaxation length by

$$\lambda = \frac{1}{\left(\frac{dZ}{dx}\right)_{x=0}} \tag{4.68}$$

where Z is the compressibility factor defined by Eq. (2.17). The equations were then programmed in FORTRAN V, suitable for the UNIVAC 1108 located at the University of Alabama Research Institute. For simplicity of program check-out and debugging the problem was programmed in three separate parts for frozen, equilibrium, and nonequilibrium flow.

The frozen flow program consists essentially of a double loop iteration, following the process of solution as described in Section 4.3.1. The process is started with an assumed value for the shock wave angle σ in the main program, which then calls a subroutine for the iterative calculation of the temperature behind the shock, T_s, from Eq. (3.29). If the difference in the body surface velocity, u_b, which is computed from two independent equations, is larger

than a specified minimum, the computation returns to the main program and resumes with an adjusted value of the shock wave angle σ. The built-in limit of ten iterations was in no case exceeded. Running times, including compilation of the program, are in the order of 5 to 10 seconds, even with double precision.

The structure of the equilibrium flow program is analogous to the one for frozen flow, however, with additional loops for the calculation of the equilibrium compositions as function of density and temperature.

The nonequilibrium flow program is set up in terms of some eighteen subroutines for the various thermodynamic and other functions discussed in Chapters II through IV. Its core consists of the standard fourth order variable step Runga-Kutta integration routine RKVS, which is described in detail in Ref. 38. Using the initial gradients and a simple Euler integration to calculate values for all variables at an incremental distance away from $x = 0$, the computation switches over to the Runga-Kutta integration of equations (4.30) through (4.33). Numerical problems and running times depend on the case and will be discussed in Chapter V.

CHAPTER V

DISCUSSION OF RESULTS

5.1 Frozen Flow

The success of the one-strip integral method when applied to the computation of supersonic flow of a perfect gas ($\gamma = 1.4$) about circular cones was previously demonstrated by South (Ref. 12). He showed that, particularly for higher free stream Mach numbers ($M_\infty > 3$), the results from the integral method are in excellent agreement with the charts in Ref. 39. In the present investigation, chemically frozen flow was therefore studied only to obtain proper initial conditions for the calculation of chemically relaxing flow, as pointed out in section 4.3.

Figures 7 through 12 show the variation of some typical flow field variables with cone semi-vertex angle and free stream Mach number, for undissociated air in vibrational equilibrium. In Figures 7, 8, 11, and 12, the perfect gas results are also given for comparison. In view of previous findings (Ref. 12), the difference between the perfect gas results and those of the present investigation can be attributed to vibrational equilibrium. It can be observed that for those combinations of free stream velocity and cone angle where the temperature in the shock layer becomes high enough to cause significant molecular vibration, the shock wave tends to be closer to the body than for the perfect gas case.

Simultaneously, there is a slight increase in the surface velocity, while the surface pressure is hardly affected at all.

5.2 Equilibrium Flow

Rather than to duplicate the work of Newman (Ref. 36), conical flow parameters for air in thermodynamic equilibrium are presented here in order to demonstrate the validity of the five component air model for the range of cone semi-vertex angles and free stream conditions considered in this work. The usefulness of an equilibrium flow solution in connection with calculations of non-equilibrium flow was already discussed in section 4.4.

Figures 13 through 16 present a comparison of equilibrium flow results obtained from the one-strip integral method, used in this investigation, with results obtained by integrating the Taylor-Maccoll equation (Ref. 21). In addition, these figures represent a comparison of the thermodynamic properties of the air model used in the present investigation with the thermodynamic tables of Blackwell et al., which were used in Romig's work (Ref. 21).

Thirteen cases for a variety of cone semi-vertex angles ($30 \leq \theta \leq 45$) and free stream Mach numbers ($10 \leq M_\infty \leq 30$) were selected to cover a wide range of values of the hypersonic similarity parameter ($5 \leq M_\infty \sin \theta \leq 18$) at two different free stream pressures. In all cases, the results from the two calculations, each using a different air model and a different method of solution, agree quite well.

Additional cases for conical equilibrium flow were calculated for the purpose of comparison with chemically relaxing flow. In particular, it will be shown at the end of this chapter, how the state of equilibrium, which is approached asymptotically by the nonequilibrium flow, compares with the state of equilibrium found when thermodynamic equilibrium is assumed throughout the flow field. In the next section, these equilibrium states are, for simplicity, labelled "asymptotic equilibrium" and "conical equilibrium", respectively.

5.3 Nonequilibrium Flow

Nonequilibrium flow calculations have been carried out for various purposes, and the free stream conditions were chosen accordingly. Table V gives a detailed summary of all cases which were investigated, while Fig. 17 displays, for each case, the three independent characteristic parameters (semi-vertex angle θ, free stream velocity, and altitude) in a velocity-altitude diagram.

Cases 1 and 2 were selected principally for the purpose of comparing the results from the integral method used in the present investigation, with those of the method of characteristics (Ref. 20). Case 3 was computed to check previous calculations using a much simpler air model (Ref. 16). Cases 4 through 8 are for similar cones at constant altitude but at different free stream velocities. Cases 9 and 10, together with case 5, were selected to study the effect of different altitudes on all flow variables at the same cone angle and flight velocity. The

influence of the semi-vertex angle θ on the flow parameters is studied by comparing cases 10 through 13, in which both altitude and free stream velocity are kept constant.

Figures 18 and 19 show the species mass fractions on the cone surface for cases 1 and 2, respectively. The slight difference in the results near the tip of the cone might be due to one or more of the differences in the calculation procedures. A small difference in the initial values, for example, which is undetectable from the graphs shown in Ref. 20, together with different expressions of the equilibrium constants used for the reactions IV and VI (see section 2.5), may be one reason for the discrepancy. Another cause may be the fact that, in order to use the method of characteristics, a certain small but finite area of frozen flow has to be assumed near the tip, while no such assumption is needed for the integral method. In any case, the results for the gas composition from the two methods are almost identical for $x > 4$ mm. The temperature and density along the cone surface, plotted in figures 20 and 21, show the same excellent agreement.

The variation of the shock wave angle along the length of the cone is shown in Fig. 22. The results from the two methods agree insofar as both methods predict that the shock wave angle σ should decrease. While the characteristics solution from Ref. 20 seems to indicate that the shock wave angle σ should approach its value for conical equilibrium flow monotomically from above, the

integral method solution indicates a limiting value for σ which is slightly higher than that. As a matter of fact, when the integration was carried out to a distance of about 70 cm away from the tip for case 2, it was found that the shock wave angle has a minimum value ($\sigma = 44.39$) between $x = 25$ mm and $x = 75$ mm, then approaches its asymptotic equilibrium value ($\sigma = 44.41$) from below. From $x = 23$ cm onward none of the variables show any change in the first four significant figures. Apart from this, it is noted that the difference in shock wave angle between frozen flow and equilibrium flow is relatively small (only about 1.5 degrees in case 1, and even less than that in case 2).

Cone surface pressures for cases 1 and 2 may be compared in Fig. 23. In both cases, the difference between the values for frozen flow and those for equilibrium flow is less than 2%. The method of characteristics is seen to predict a slightly lower surface pressure (lower by about 0.5%) than the integral method.

Case 1 also was the only case that presented numerical problems. The density, the shock wave angle, the pressure and the surface velocity exhibited small damped oscillations, of which an example is given in Fig. 23a. It was found that a systematic removal of all possible sources for numerical inconsistencies in the program reduced the amplitude of these oscillations considerably. A further reduction was achieved by finding an optimum size for the initial step which was then taken to be $\Delta\xi = 10^{-5}$ for all remaining cases. The fact that case 1 has the lowest body surface Mach number, in connection with other

fir. lings, indicates that the probable cause for these oscillations lies in a violation of the stability criterion for hyperbolic equations. No definite conclusions have been reached at the present time since it is felt that this problem requires a more detailed analysis.

The body surface velocity and the surface Mach number for cases 1 and 2 are shown in figures 24 and 25, respectively. No results from the method of characteristics were available for these variables. However, the fact that the authors of Ref. 20 present results for wedge flow where u_b was considered to be constant, permit the conclusion that they also found that the change in surface velocity along the body surface is negligible.

For both, case 1 and case 2, the flow field has been calculated up to a dimensionless distance of $\xi = 10.0$ from the tip of the cone. This corresponds to a physical distance of about 10 mm in case 1, and about 70 mm for case 2. Computation times were 146 sec for case 1, and 93 sec for case 2. This contrasts with computation times of about 1 hour per case on the BRLESC computer (Ref. 20) for the method of characteristics calculations. For the integration of case 2 up to $\xi = 100.0$, the running time was only 252 seconds in this work.

Figure 26 shows the influence of the free stream velocity on the surface species mass fractions for constant altitude and cone semi-vertex angle. Including the nitric oxyde mass fractions, which show the lowest values for the highest velocity, all variations are as expected. The large difference in the characteristic relaxation lengths is particularly noteworthy. The surface temperatures,

shown in Fig. 27, again display the drastic drop near the cone tip, which is caused by the strong dissociation gradients in this region. Surface density, shock wave angle, and surface pressure are shown in figures 28 through 30. Their limiting values for large ξ show only a slight dependence on the free stream velocity, in contrast to the gas composition and the surface temperatures.

Figures 31 through 33, representing a 30° cone at constant free stream velocity but at three different altitudes, clearly demonstrate the validity of the nonequilibrium scaling law

$$\rho_{\infty} \cdot L = \text{constant}$$

which is discussed in detail in Ref. 40. Here L is some characteristic dimension of the flow field or the body. According to the theory, nonequilibrium scaling is applicable for that region of the relaxation zone where the reactions are predominantly dissociation reactions. As seen from the production rate equations given in Chapter II, the dissociation rates are proportional to the density. Once the state of equilibrium is approached, the rate of recombination, being proportional to the square of the density, becomes of equal importance, and therefore the nonequilibrium scaling law should cease to be valid. Figures 31 through 33 show that this is precisely so.

The length scale in these figures is somewhat arbitrary because the reference density was chosen for convenience such that the characteristic length

$$\bar{\lambda} = \left(\frac{\rho_\infty}{\rho_{ref}}\right) \lambda$$

which should theoretically be the same constant for all cases, was equal to one meter for case 10. This means that the $\bar{x}$ scale is practically identical with the ξ scale, which permits an easy conversion to the actual physical length in each case.

The reason for the close agreement in all variables shown, in spite of differences in the free stream temperature, lies in the fact that, for hypersonic conditions, the total enthalpy of the free stream is given mainly in terms of the velocity, while the free stream temperature contributes only a negligible amount. On the downstream side of the shock wave the situation is almost opposite, and therefore the absolute temperature, which controls the reactions, is practically the same in the three cases.

Figures 31 through 33 show that the results, plotted versus $\bar{x}$, are identical, or at least in very close agreement, up to $\bar{x} = 10$. For $\bar{x} > 10$, case 10 rapidly approaches equilibrium, which is reached near $\bar{x} = 80$. In fact, for $\bar{x} > 80$, no changes in the first four significant figures for the density ρ and the temperature T at the body surface could be observed. The curves for case 9 show a tendency towards equilibrium at $\bar{x} = 100$, but no such trend can be recognized for case 5. It is also noted from figures 32 and 33 that the asymptotic equilibrium values of

the surface temperature and the surface density do not agree with the respective values for conical equilibrium.

It is concluded that, under otherwise identical conditions, the altitude has a decisive influence on the flow field variables. While, for practical purposes, the state of equilibrium is reached at a distance of about 50 cm away from the tip in case 10 (40 km altitude), this equilibrium state is not yet reached at 150 m from the tip in case 5 (80 km altitude).

The influence of the cone semi-vertex angle θ on the flow field is shown in figures 34 through 37. It is found that, qualitatively, an increase in θ has the same effect as an increase in free stream velocity. Actually, the effect of a change in θ depends very much on the other parameters, namely altitude and free stream velocity. It is shown in Fig. 35, for example, that for a variation of θ from 20° to 35°, the temperature at the cone tip changes by roughly $8000^\circ K$. The values for conical equilibrium indicate that, once equilibrium is reached, the temperatures at the body surface still differ by $3000^\circ K$, approximately.

Figures 38 through 40 display the strong dependency of the characteristic relaxation length λ on free stream velocity, altitude and semi-vertex angle. For the examples discussed herein, λ varies approximately between 10^{-3} and 10^2 meters, that is, by five orders of magnitude.

Finally, Fig. 41 shows a comparison of conical and asymptotic equilibrium in a Mollier chart for air in thermodynamic equilibrium. The three equilibrium

states shown were fixed by their respective values for the enthalpy and the density. First, the figure demonstrates that conical equilibrium flow is characterized by an isentropic compression from the shock wave to the body, since the two equilibrium states are located on the same vertical line. Second, it is shown that the value of the entropy of the equilibrium state, which is asymptotically approached by the nonequilibrium flow, differs from the entropy value for conical equilibrium, as discussed in section 4.4. Whether the entropy increase shown is mainly due to the difference in the shock wave angle for the two situations, or due to the relaxation process cannot be explained unless more detailed calculations are carried out. Finally, the close agreement of all variables calculated for conical equilibrium at the body (e.g. $T_b = 5527\,^{\circ}K$, $Z_b = 1.255$) with the corresponding values indicated in the Mollier chart ($T_b \approx 5500\,^{\circ}K$, $Z_b \approx 1.253$) provides another demonstration for the accuracy of the air model and its thermodynamic properties as used in this investigation.

5.4 Conclusions

A semi-exact procedure, which uses exact forms of the x-Momentum and species continuity equations along the body surface, was shown to yield results which are in excellent agreement with those obtained by the method of characteristics. Although this procedure was also successfully used in the investigation of nonequilibrium blunt body flows (Ref. 3,4,5), it was reported to be always

unsuccessful for the case of vibrational equilibrium flow past pointed bodies (Ref. 12, 13).

The amplitude of some bounded oscillations, which were encountered in one case with a relatively low surface Mach number near the cone tip ($M_b < 2.5$), could be reduced to a negligible amount by carefully removing all possible sources for inconsistencies in the program. The rapid increase of the surface Mach number near the cone tip apparently caused the oscillations to stabilize quickly, and no further problems were encountered.

Although it is recognized that the method of characteristics furnishes information about the variables within the shock layer which cannot be obtained by the one-strip integral method without additional calculation schemes, it appears that running times for the semi-exact procedure used in this investigation are drastically shorter than those reported for the method of characteristics.

The definition of a characteristic relaxation length for dissociation, $\lambda = (d\,Z/\,dx)^{-1}$, was found to be extremely useful. Its principal advantage is that it transforms all problems to the same length scale, thereby avoiding the need to specify integration ranges for each problem individually. The latter process could be very time consuming because of the strong variation of λ from case to case ($10^{-3} < \lambda\,[m] < 10^{2}$, in the examples discussed).

The application of the nonequilibrium scaling law, $\rho_\infty \cdot L = \text{constant}$, to cases covering a wide range in altitude clearly demonstrated its validity for the type of flow considered in this investigation.

It was also demonstrated that, the three parameters, cone semi-vertex angle, free stream velocity, and altitude, exert a strong influence on the variation of most flow field variables. It is therefore concluded that, for cases where the characteristic length is of the same order of magnitude as the length of the conical body, large variations of the gas composition, the temperature and the density along the streamlines have to be expected in the entire shock layer.

REFERENCES

1. Hayes, W. D., Probstein, R. F., Hypersonic Flow Theory, I, Inviscid Flows, Academic Press, New York and London, 1966.

2. Dorodnitsyn, A.A., "A Contribution to the Solution of Mixed Problems of Transonic Aerodynamics", Advances in Aeronautical Sciences, Vol. 2, Pergamon Press, New York, 1959.

3. Shih, W. C. L., Baron, J. R., Krupp, R. S., and Towle, W. J., "Nonequilibrium Blunt Body Flow Using the Method of Integral Relations", MIT Aerophysics Laboratory, Technical Report 66, May 1963; also cataloged by DDC as AD No. 415 934.

4. Hermann, R., Thoenes, J., "Hypersonic Flow of Air Past a Circular Cylinder With Non-equilibrium Oxygen Dissociation Including Dissociation of the Free Stream", paper presented at the VIth European Aeronautical Congress, Munich, Sept. 1-4, 1965; also UARI Research Report No. 28, University of Alabama Research Institute, Huntsville, Alabama, September 1965.

5. Thompson, K. O., "Hypersonic Flow of Air Around Blunt Bodies With Finite Chemical Reaction Rate", Dissertation, University of Alabama, University, Alabama, 1967; also UARI Research Report No. 48, University of Alabama Research Institute, Huntsville, Alabama, September 1967.

6. Allen, H. J., "Hypersonic Aerodynamic Problems of the Future", The High Temperature Aspects of Hypersonic Flow, AGARDograph 68, edited by W. C. Nelson, The Macmillan Company, New York, 1964.

7. Stephenson, J. D., "A Technique for Determining Relaxation Times by Free-Flight Test of Low-Fineness-Ratio Cones; With Experimental Results for Air at Equilibrium Temperatures up to 3440°K", NASA TN D-327, September 1960.

8. Sedney, R., South, J. C., and Gerber, N., "Characteristic Calculation of Non-Equilibrium Flows", The High Temperature Aspects of Hypersonic Flow, AGARDograph 68, edited by W. C. Nelson, The Macmillan Company, New York, 1964.

9. Sedney, R., Gerber, N., "Non-Equilibrium Flow Over a Cone", IAS Paper No. 63-71, also AIAA J., Vol. 1, No. 11, November 1963.

10. Capiaux, R., Washington, M., "Non-Equilibrium Flow Past a Wedge", AIAA J., Vol. 1, No. 3, March 1963.

11. Wood, A. D., Springfield, J. F., and Pallone, A. J., "Chemical and Vibrational Relaxation of an Inviscid Hypersonic Flow", AIAA Paper 63-441, also AIAA J., Vol. 2, No. 10, October 1964.

12. South, J. C., "Application of Dorodnitsyn's Integral Method to Nonequilibrium Flows Over Pointed Bodies", NASA TN D-1942, August 1963.

13. South, J. C., "Application of the Method of Integral Relations to Supersonic Nonequilibrium Flow Past Wedges and Cones", NASA TR R-205, August 1964.

14. South, J. C., Newman, P. A., "Application of the Method of Integral Relations to Real-Gas Flows Past Pointed Bodies", AIAA Paper No. 65-27, January 1965.

15. Newman, P. A., "A Modified Method of Integral Relations for Supersonic Nonequilibrium Flow Over a Wedge", NASA TN D-2654, February 1965.

16. Thoenes, J., "Nonequilibrium Flow Past a Circular Cone Including Freestream Dissociation", AIAA J., Vol. 4, No. 8, August 1966; also UARI Research Report No. 25, University of Alabama Research Institute, Huntsville, Alabama, May 1965.

17. Thoenes, J., "Hypersonic Flow of Dissociating Air Past a Circular Cone", UARI Research Report No. 26, University of Alabama Research Institute, Huntsville, Alabama, January 1966.

18. Lee, R. S., "A Unified Analysis of Supersonic Nonequilibrium Flow over a Wedge: I. Vibrational Nonequilibrium", IAS Paper 63-40; also AIAA J., Vol. 2, No. 4, April 1964.

19. DeJarnette, F. R., "Numerical Solution of Inviscid Hypersonic Flows for Nonequilibrium Vibration and Dissociation Using an "Artificial Viscosity" Method", Ph.D. Thesis, Virginia Polytechnic Institute, March 1965.

20. Spurk, J. H., Gerber, N., and Sedney, R., "Characteristic Calculation of Flowfields with Chemical Reactions", AIAA J., Vol. 4, No. 1, January 1966.

21. Romig, Mary F., "Conical Flow Parameters For Air in Dissociation Equilibrium", Convair Scientific Research Laboratory, Research Report 7, May 1960.

22. Herzfeld, K. F., Griffing, V., Hirschfelder, J. O., Curtiss, C. F., Bird, R. B., and Spotz, E. L., Fundamental Physics of Gases, Princeton Aeronautical Paperbacks, Vol. 7, Princeton University Press, 1961.

23. Lee, J. F., Sears, F. W., Turcotte, D. L., Statistical Thermodynamics, Addison-Wesley Publishing Co., Inc., Reading, Mass., 1963.

24. Vincenti, W. G., Kruger, C. H., Introduction To Physical Gas Dynamics, John Wiley and Sons, Inc., New York, 1965.

25. Wray, K. L., "Chemical Kinetics of High Temperature Air", Hypersonic Flow Research, Progress in Astronautics and Rocketry - Vol. 7, edited by F. R. Riddell; Academic Press, New York, 1962.

26. Lin, S. C., Teare, J. D., "A Streamtube Approximation for Calculation of Reaction Rates in the Inviscid Flow Field of Hypersonic Objects", Proceedings of the Sixth Symposium on Ballistic Missile and Aerospace Technology: Reentry, Vol. 4, Academic Press, New York, 1961.

27. Treanor, C. E., Marrone, P. V., "Effect of Dissociation on the Rate of Vibrational Relaxation", Cornell Aeronautical Laboratory Report No. QM-1626-A-4, Feb. 1962.

28. Rose, P. H., Teare, D. J., "On Chemical Effects and Radiation in Hypersonic Aerodynamics", The High Temperature Aspects of Hypersonic Flow, AGARDograph 68, edited by W. C. Nelson, The Macmillan Co., New York, 1964.

29. Schwartz, M., Green, J., and Rutledge, N. A., "Vector Analysis", Harper and Brothers, New York, 1960.

30. Wittliff, C. E., Curtis, J. T., "Normal Shock Wave Parameters in Equilibrium Air", Cornell Aeronautical Laboratory Report No. CAL-111, November 1961.

31. Marrone, P. V., "Normal Shock Waves in Air: Equilibrium Composition and Flow Parameters for Velocities from 26,000 to 50,000 ft/sec," Cornell Aeronautical Laboratory Report No. AG - 1729 - A - 2, August 1962.

32. Sokolnikoff, I. S., Redheffer, R. M., Mathematics of Physics and Modern Engineering, McGraw-Hill Book Company, Inc., New York, 1958.

33. Busemann, A., "Drücke auf kegelförmige Spitzen bei Bewegung mit Überschallgeschwindigkeit", ZAMM, Vol. 9, pp. 496-498, 1929.

34. Hansen, C. F., "Approximations for the Thermodynamic and Transport Properties of High Temperature Air", NASA TR R-50, 1959.

35. U. S. Standard Atmosphere, 1962, Prepared under sponsorship of NASA, U.S. Air Force, U. S. Weather Bureau, U. S. Government Printing Office, Washington, D. C., December 1962.

36. Newman, P. A., "Approximate Calculation of Hypersonic Conical Flow Parameters for Air in Thermodynamic Equilibrium", NASA TN D-2058, January 1964.

37. Belotserkovskii, O. M., "Flow With a Detached Shock Wave About a Symmetrical Profile", PMM, Vol. 22, No. 2, 1958, pp. 206-219.

38. UNIVAC 1107 BEEF MATH ROUTINES, Manual No. UP-3984, published by the UNIVAC Division of the SPERRY RAND Corporation.

39. Ames Research Staff, "Equations, Tables and Charts for Compressible Flow", NACA Report 1135, 1953.

40. Hall, J. G., Eschenroeder, A. Q., and Marrone, P. V., "Inviscid Hypersonic Air-Flows With Coupled Nonequilibrium Processes", IAS Paper, No. 62-67, 1962.

41. Feldman, S., "Hypersonic Gas Dynamic Charts for Equilibrium Air", Avco Research Laboratory, Research Report 40, January 1957.

TABLE I

GAS MODEL DATA

Adopted Primary Quantities		
$(\bar{Y}_{O2})_o$	0.21	
$(\bar{Y}_{N2})_o$	0.79	
$Z_o = p_o/\rho_o R T_o$	1.0	
p_o	$1.01325 \cdot 10^5$	N/m^2
T_o	288.15	^oK
R^*	8314.32	$J / kmol\ ^oK$
N^*	$6.02257 \cdot 10^{26}$	$kmol^{-1}$
h	$6.6237 \cdot 10^{-34}$	$J \cdot sec$
Derived Quantities		
$(C_{O2})_o \equiv \bar{m}_o$	0.232 918	
$(C_{N2})_o$	0.767 082	
M	28.850 335	$kg/kmol$
R	288.187 988	$J/kg\ ^oK$
ρ_o	1.220 174	kg / m^3

TABLE II

ATOMIC AND MOLECULAR CONSTANTS

Species	Molecular Weight M_i 1)	Rotational Temperature $\varkappa\ \theta_i^r$ 2)	Vibrational Temperature θ_i^v 3)	Char. Temp. of Dissoc. θ_i^* 3)	Electronic Degeneracy g_j 4)	Electronic Temperature θ_j^e 4)
	kg / kmol	°K	°K	°K		°K
O_2	31.9988	4.20	2256	59 380	3 2 1	0 11 390 18 990
N_2	28.0134	5.80	3374	113 260	1	0
O^2	15.9994				5 3 1	0 228 326
N	14.0067				4 10	0 27 700
NO	30.0061	2.50	2719	75 490	2 2	0 174

1) Ref. 35; 2) Ref. 24; 3) Ref. 20; 4) Ref. 34, Values for NO from Ref. 23.

TABLE III

DISSOCIATION RATE CONSTANTS

#	Reaction	Third Body M	k_d [m^3 / kmol · sec], Ref. 20
I	$O_2 + M \rightleftarrows 2O + M$	N_2, N, NO	$k_{d(N2)}^{I} = 1.2 \cdot 10^{18} T^{-1.5} \exp(-\theta^*_{O2}/T)$
		O_2	$k_{d(O2)}^{I} = 3.0\ k_{d(N2)}^{I}$
		O	$k_{d(O)}^{I} = 1.75 \cdot 10^{-3}\ T\ k_{d(N2)}^{I}$
II	$N_2 + M \rightleftarrows 2N + M$	O_2, O, NO	$k_{d(O2)}^{II} = 9.9 \cdot 10^{17} T^{-1.5} \exp(-\theta^*_{N2}/T)$
		N_2	$k_{d(N2)}^{II} = 3.03\ k_{d(O2)}^{II}$
		N	$k_{d(N)}^{II} = 15.15\ k_{d(O2)}^{II}$
III	$NO + M \rightleftarrows N + O + M$	O_2, N_2, O, N, NO	$k_d^{III} = 5.2 \cdot 10^{18} T^{-1.5} \exp(-\theta^*_{NO}/T)$
IV	$NO + O \rightleftarrows O_2 + N$		$k_d^{IV} = 2.4 \cdot 10^{8} T^{0.5} \exp(-19230/T)$
V	$N_2 + O \rightleftarrows NO + N$		$k_d^{V} = 5.0 \cdot 10^{10} \exp(-38000/T)$
VI	$O_2 + N_2 \rightleftarrows 2\,NO$		$k_d^{VI} = 9.1 \cdot 10^{21} T^{-2.5} \exp(-65000/T)$

TABLE IV

EQUILIBRIUM AND RECOMBINATION RATE CONSTANTS

#	Equilibrium Constant K_c	M	$k_r = k_d / K_c$
I	$K_c^I = 1.2 \cdot 10^6 T^{-0.5} \exp(-\theta^*_{O2}/T)$ [kmol / m^3]	N_2, N, NO	$k^I_{r(N2)} = 10^{12} T^{-1}$
		O_2	$k^I_{r(O2)} = 3.0\, k^I_{r(N2)}$
		O	$k^I_{r(O)} = 1.75 \cdot 10^9$
II	$K_c^{II} = 1.8 \cdot 10^4 \exp(-\theta^*_{N2}/T)$ [kmol / m^3]	O_2, O, NO	$k^{II}_{r(O2)} = 5.5 \cdot 10^{13} T^{-1.5}$
		N_2	$k^{II}_{r(N2)} = 3.03\, k^{II}_{r(O2)}$
		N	$k^{II}_{r(N)} = 15.15\, k^{II}_{r(O2)}$
III	$K_c^{III} = 4.0 \cdot 10^3 \exp(-\theta^*_{NO}/T)$ [kmol / m^3]	O_2, N_2, O, N, NO	$k^{III}_r = 1.3 \cdot 10^{15} T^{-1.5}$
IV	$K_c^{IV} = 3.333 \cdot 10^{-3} T^{0.5} \exp(-16\,110/T)$		$k^{IV}_r = 7.2 \cdot 10^{10} \exp(-3120/T)$
V	$K_c^V = 4.5 \exp(-37\,770/T)$		$k^V_r = 1.111 \cdot 10^{10} \exp(-230/T)$
VI	$K_c^{VI} = 1.35\ 10^3 T^{-0.5} \exp(-21660/T)$		$k^{VI}_r = 6.741\ 10^{18} \exp(-43340/T)$

K_c^I through K_c^{III} from Ref. 25, K_c^{IV} through K_c^{VI} calculated.

TABLE V

TABULATION OF CASES FOR CHEMICALLY RELAXING FLOW

#	θ *)	alt.*) km	V_∞ *) m/sec	ρ_∞ kg/m^3	T_∞ ^oK	M_∞	Comments
1	45.43	31	6638.0	$1.287 \cdot 10^{-2}$	273.16	20	For comparison with method of characteristics (Ref. 20)
2	41.07	"	5974.0	"	"	18	
3	25	40	6390.0	$3.996 \cdot 10^{-3}$	250.35	20	For comparison with Ref. 16
4	30	80	11186.0	$1.999 \cdot 10^{-5}$	180.65	41.4	To study influence of free stream velocity on flow field parameters
5	"	"	9350.0	"	"	34.6	
6	"	"	7909.6	"	"	29.3	
7	"	"	6750.0	"	"	25	
8	"	"	5400.0	"	"	20	
9	"	60	9350.0	$3.059 \cdot 10^{-4}$	255.77	29.1	To study influence of altitude (incl. # 5)
10	"	40	"	$3.996 \cdot 10^{-3}$	250.35	29.4	
11	35	"	"	"	"	"	To study influence of semivertex angle (incl. # 10)
12	25	"	"	"	"	"	
13	20	"	"	"	"	"	

*) Parameters which are considered as independent.

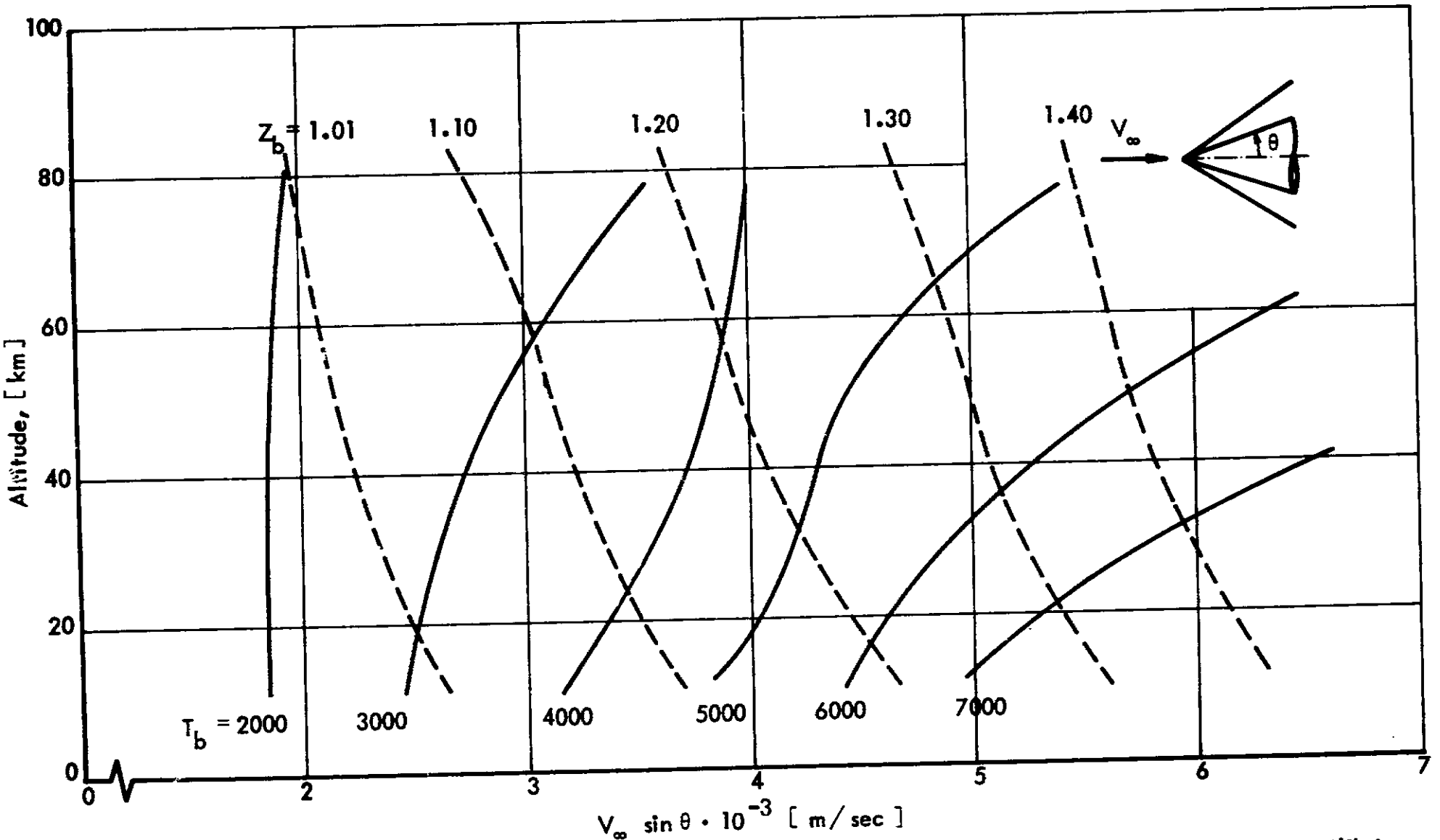

Fig. 1 Temperature [°K] and compressibility factor at the surface of a circular cone for air in thermodynamic equilibrium (Data from Ref. 21).

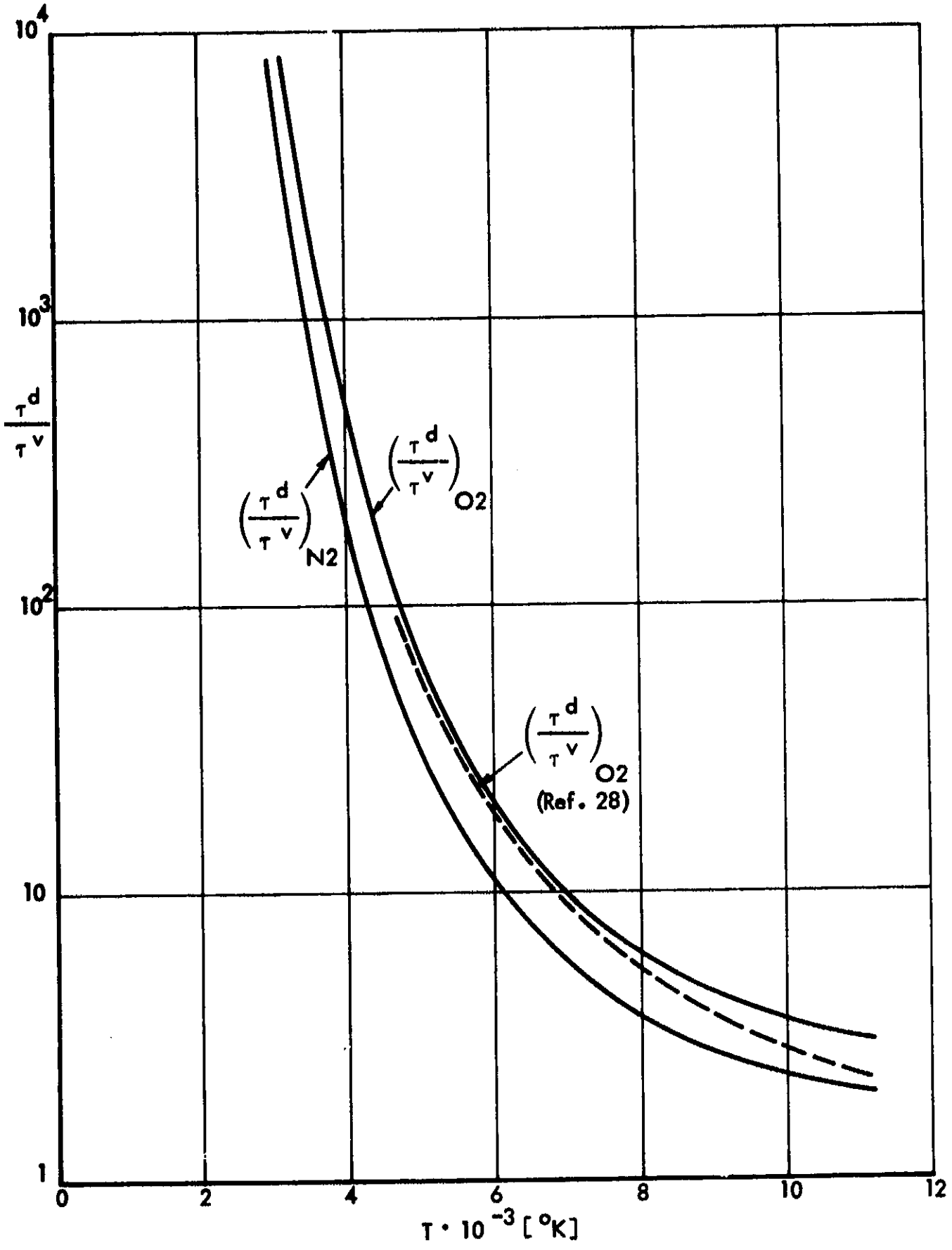

Fig. 2 Ratio of chemical to vibrational relaxation time for molecular oxygen and nitrogen ($C_O = C_N = C_{NO} = 0$).

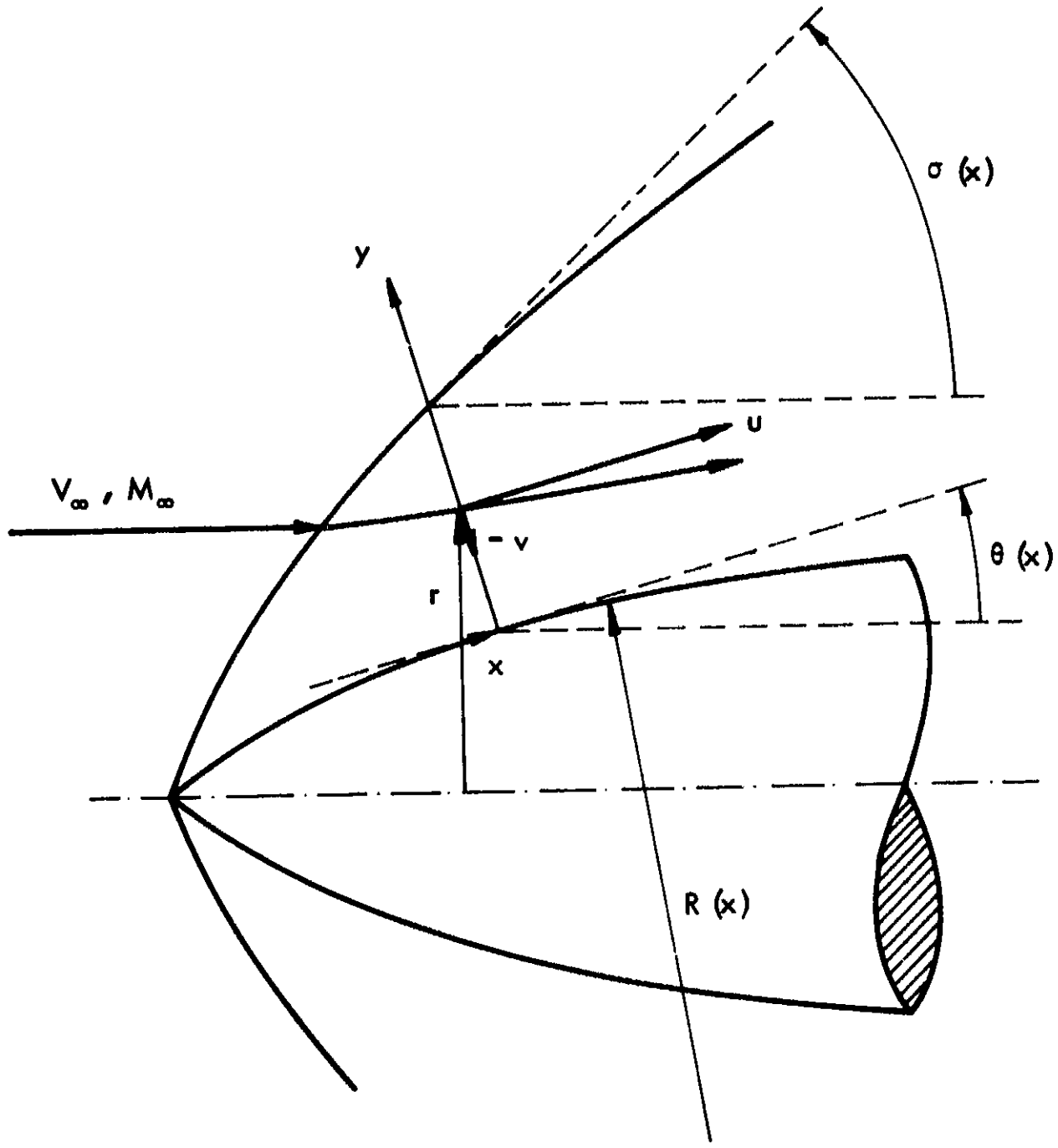

Fig. 3 Coordinate system on a pointed body with convex longitudinal curvature.

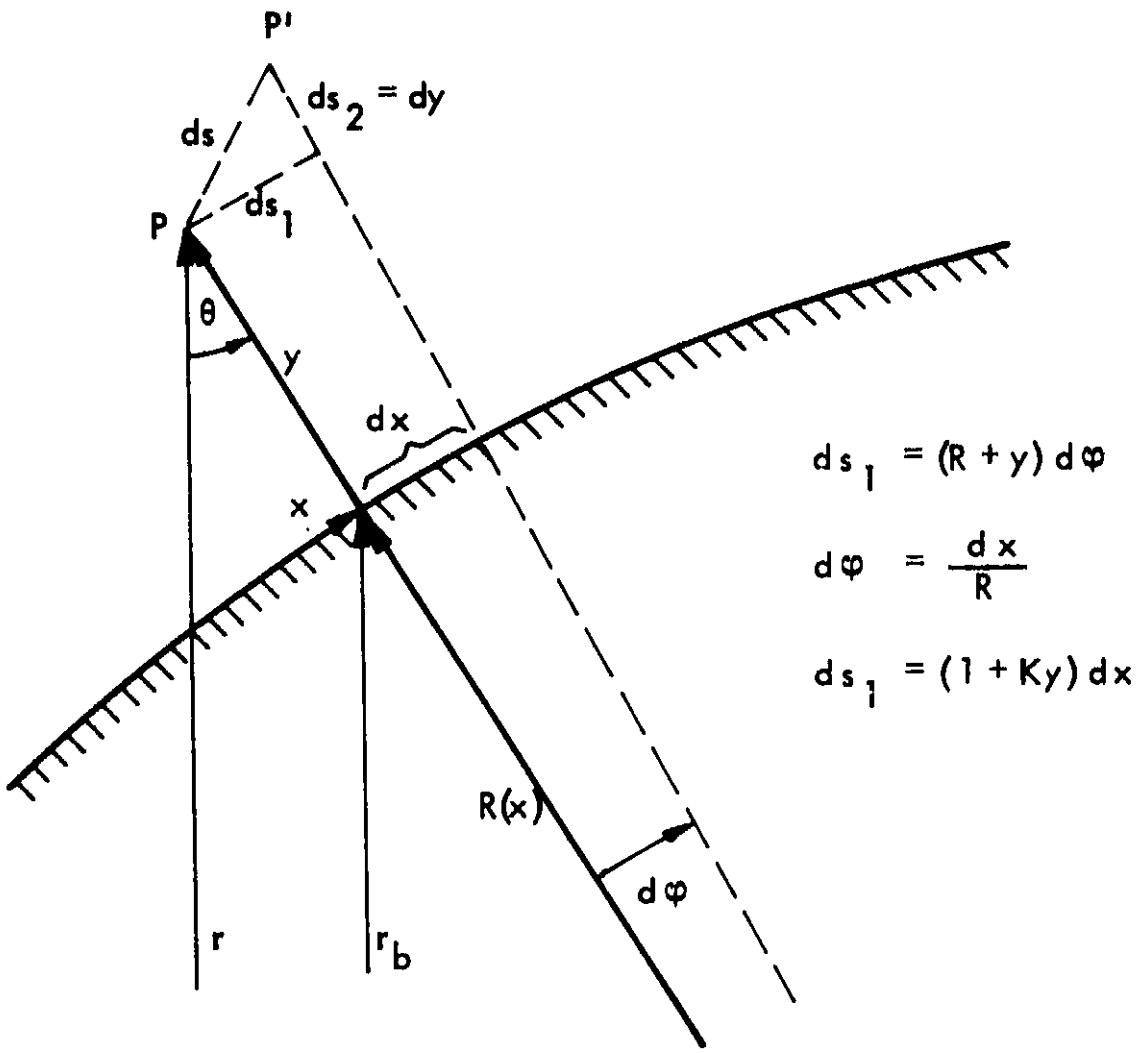

$$ds_1 = (R + y)\, d\varphi$$

$$d\varphi = \frac{dx}{R}$$

$$ds_1 = (1 + Ky)\, dx$$

Fig. 4 Differential flow field geometry for the determination of the metric coefficients.

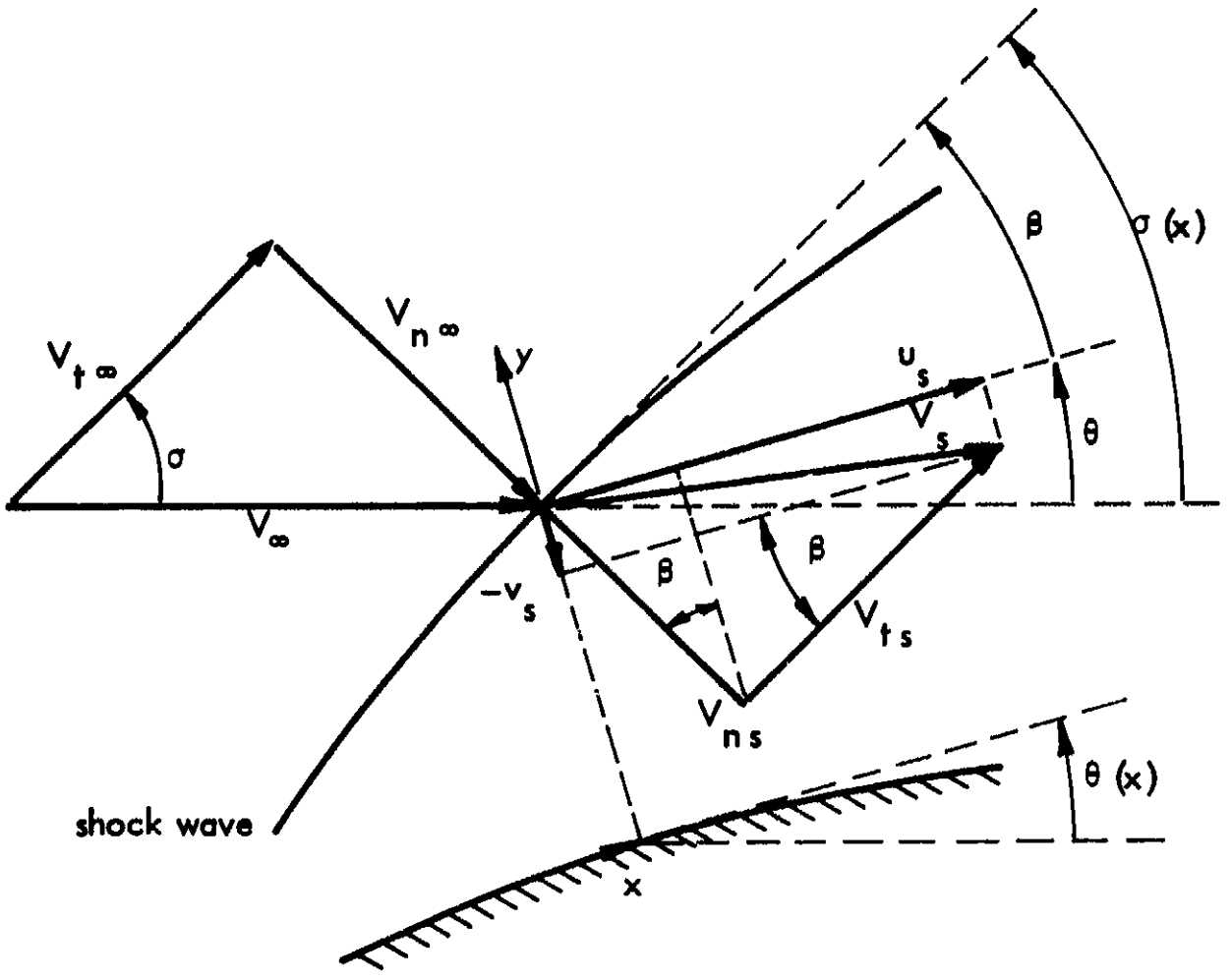

Fig. 5 Velocity diagram for locally oblique shock waves.

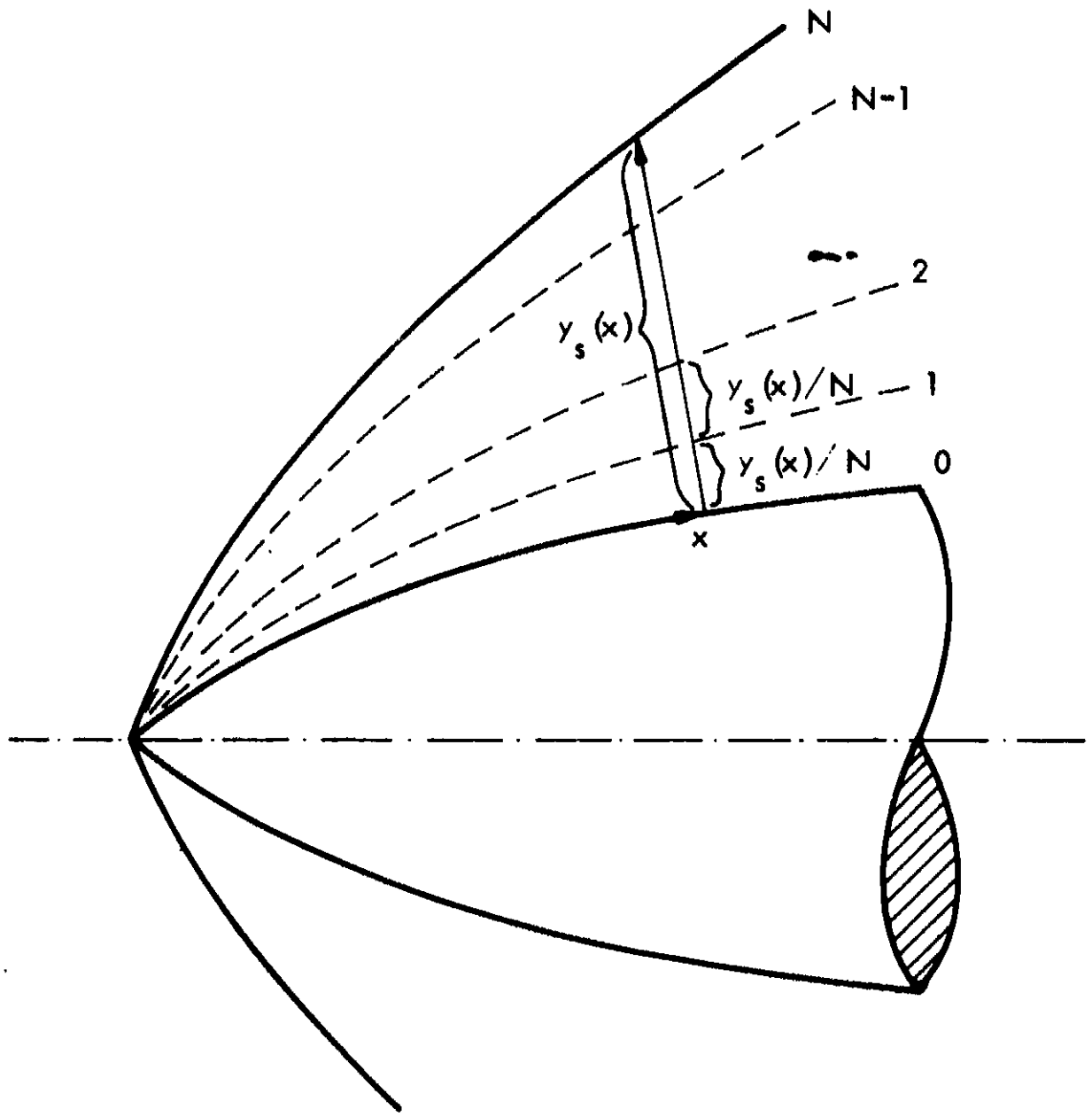

Fig. 6 Strip arrangement in shock layer.

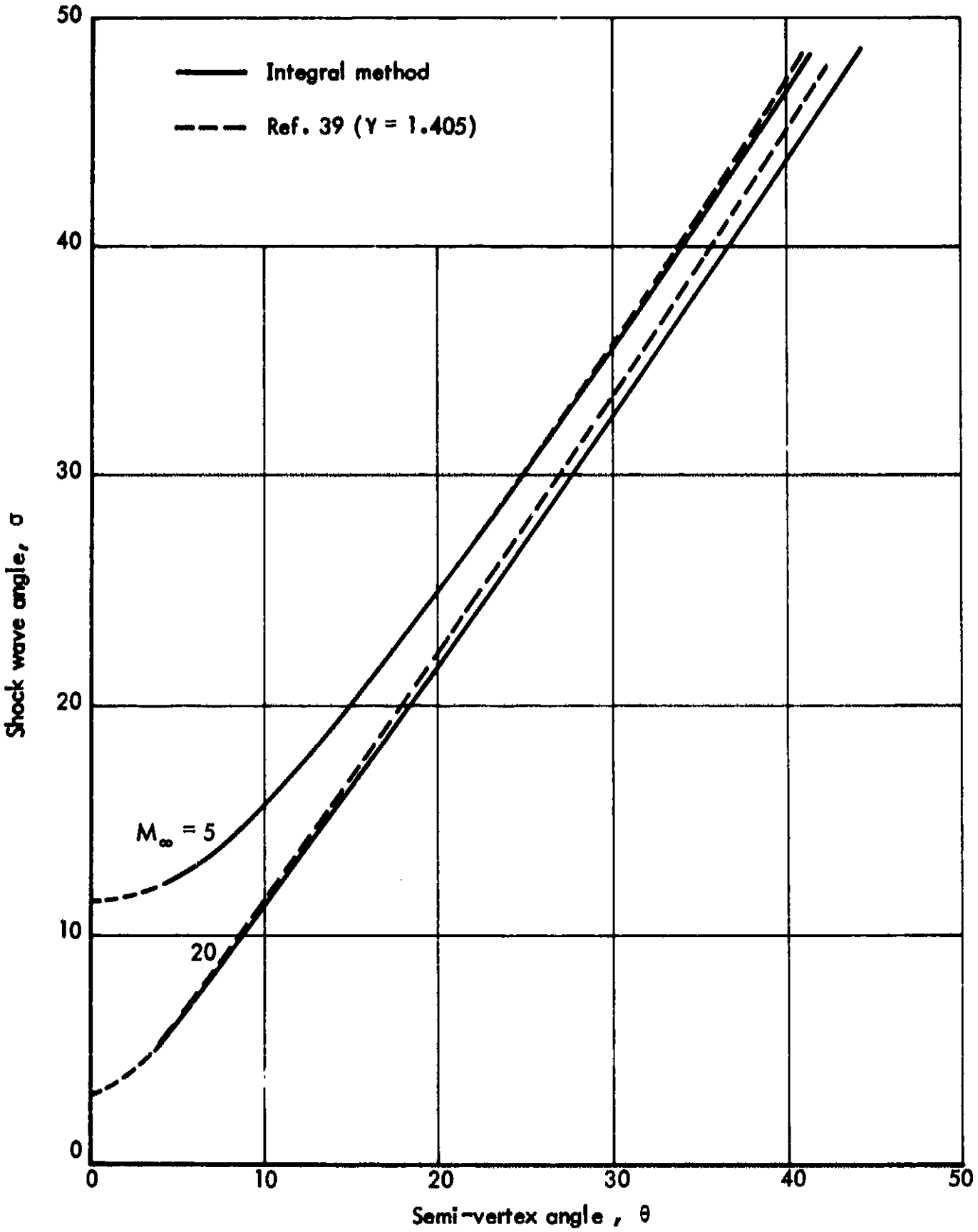

Fig. 7 Variation of shock wave angle σ with cone semi-vertex angle θ (chem. frozen, vibr. equil., $T_\infty = 250\ ^\circ K$).

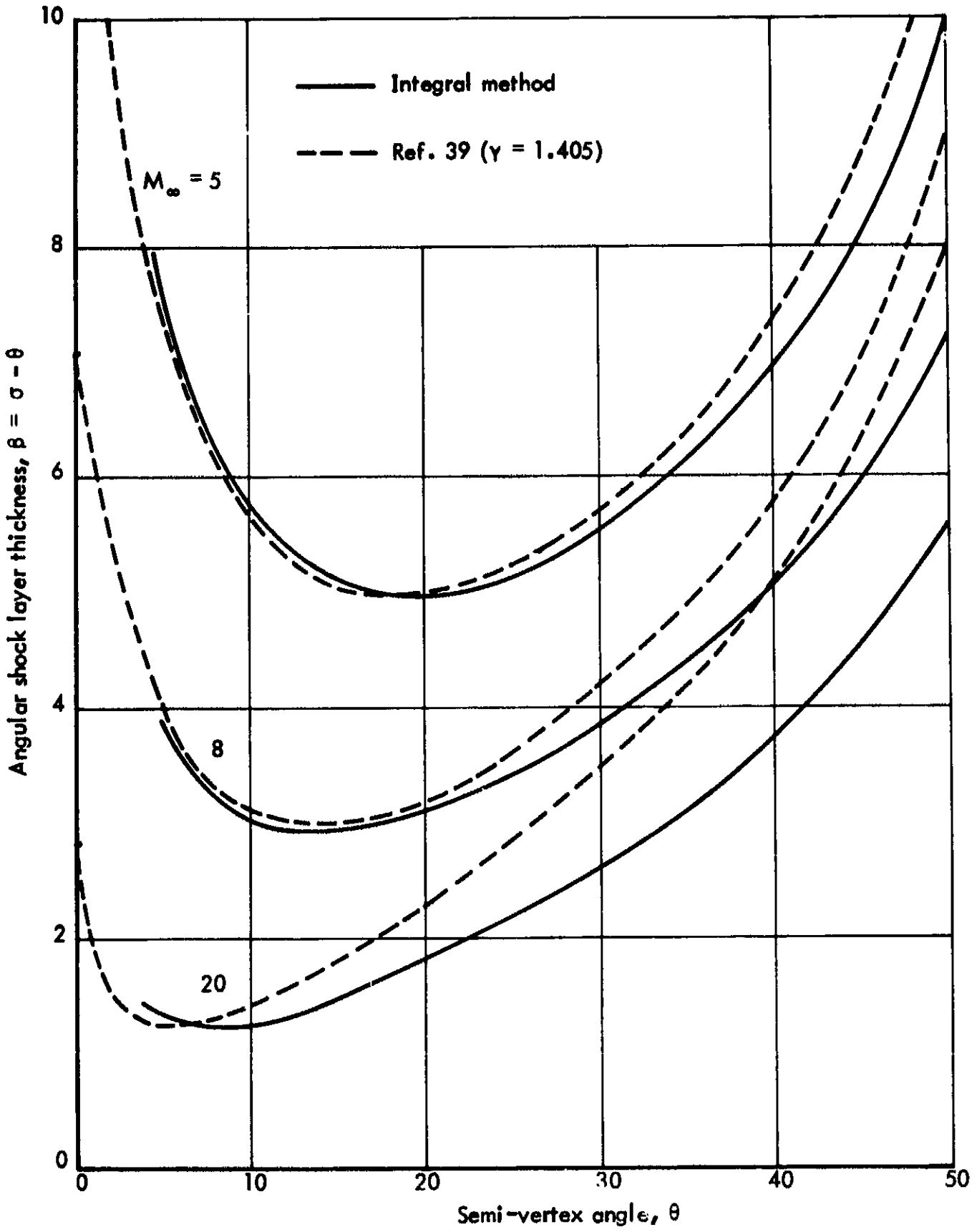

Fig. 8 Variation of angular shock layer thickness β with cone semi-vertex angle θ (chem. frozen, vibr. equil., $T_\infty = 250\ ^\circ K$).

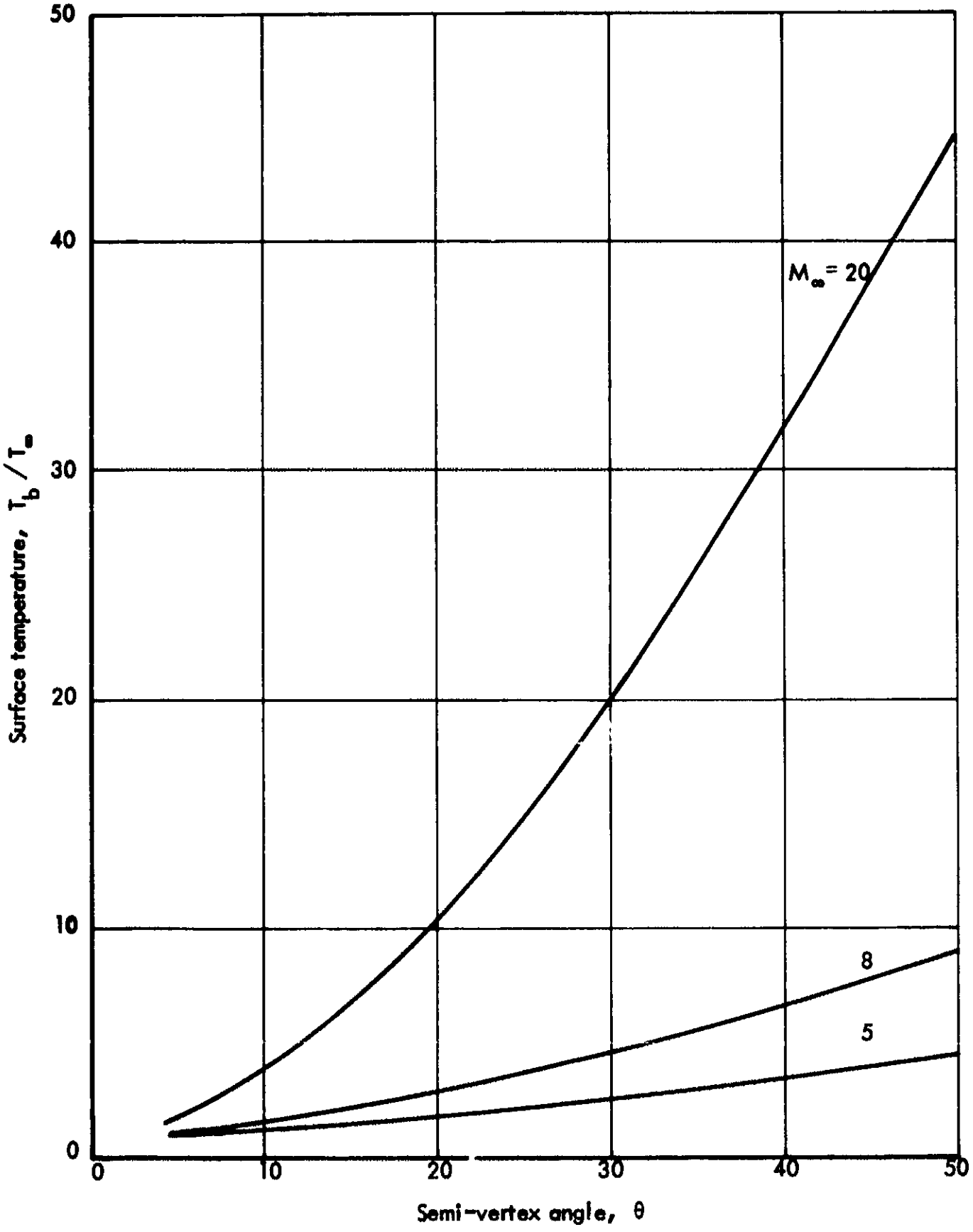

Fig. 9 Variation of cone surface temperature with semi-vertex angle (chem. frozen, vibr. equil., $T_\infty = 250\ ^\circ K$).

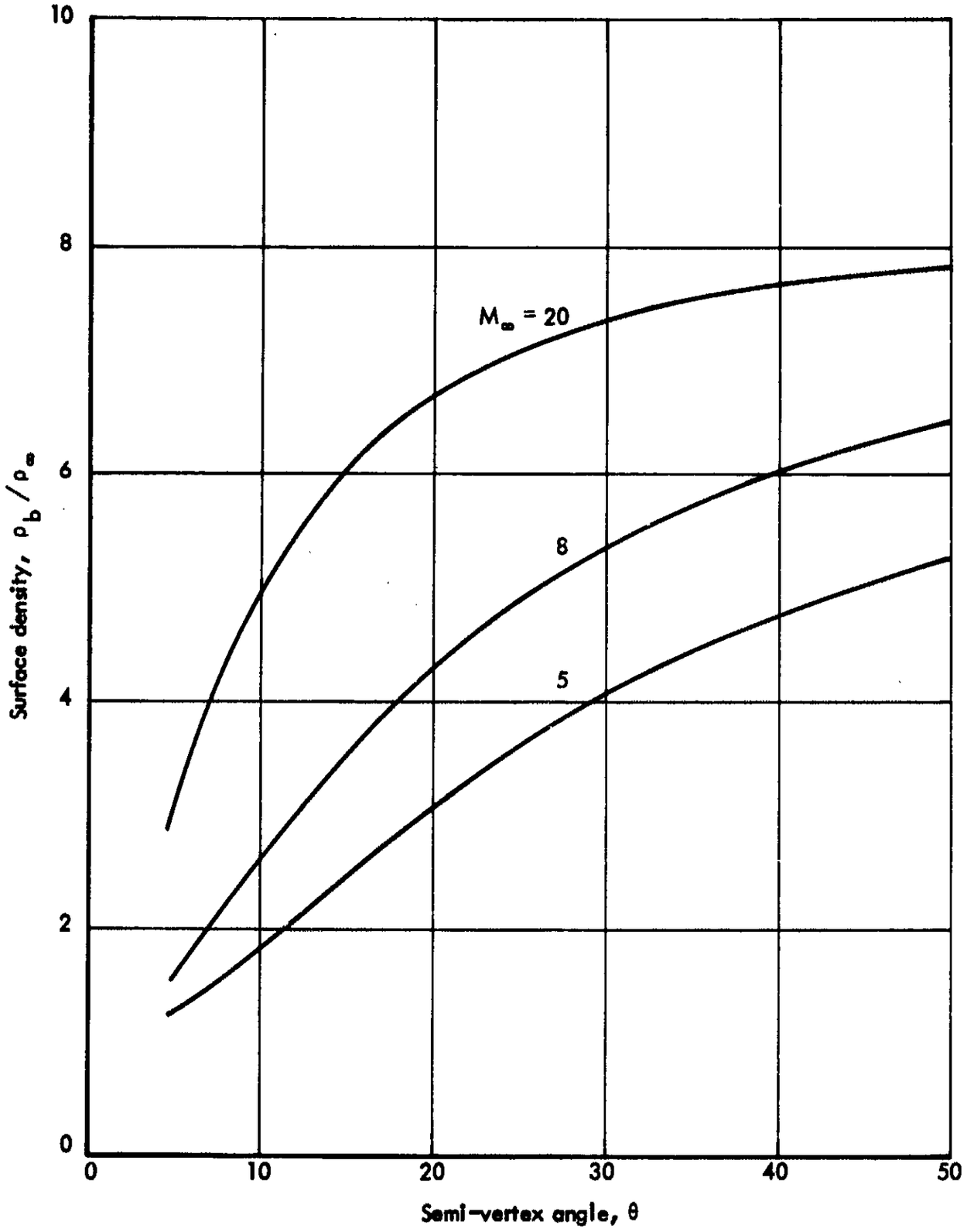

Fig. 10 Variation of cone surface density with semi-vertex angle (chem. frozen, vibr. equil., $T_\infty = 250\ ^\circ K$).

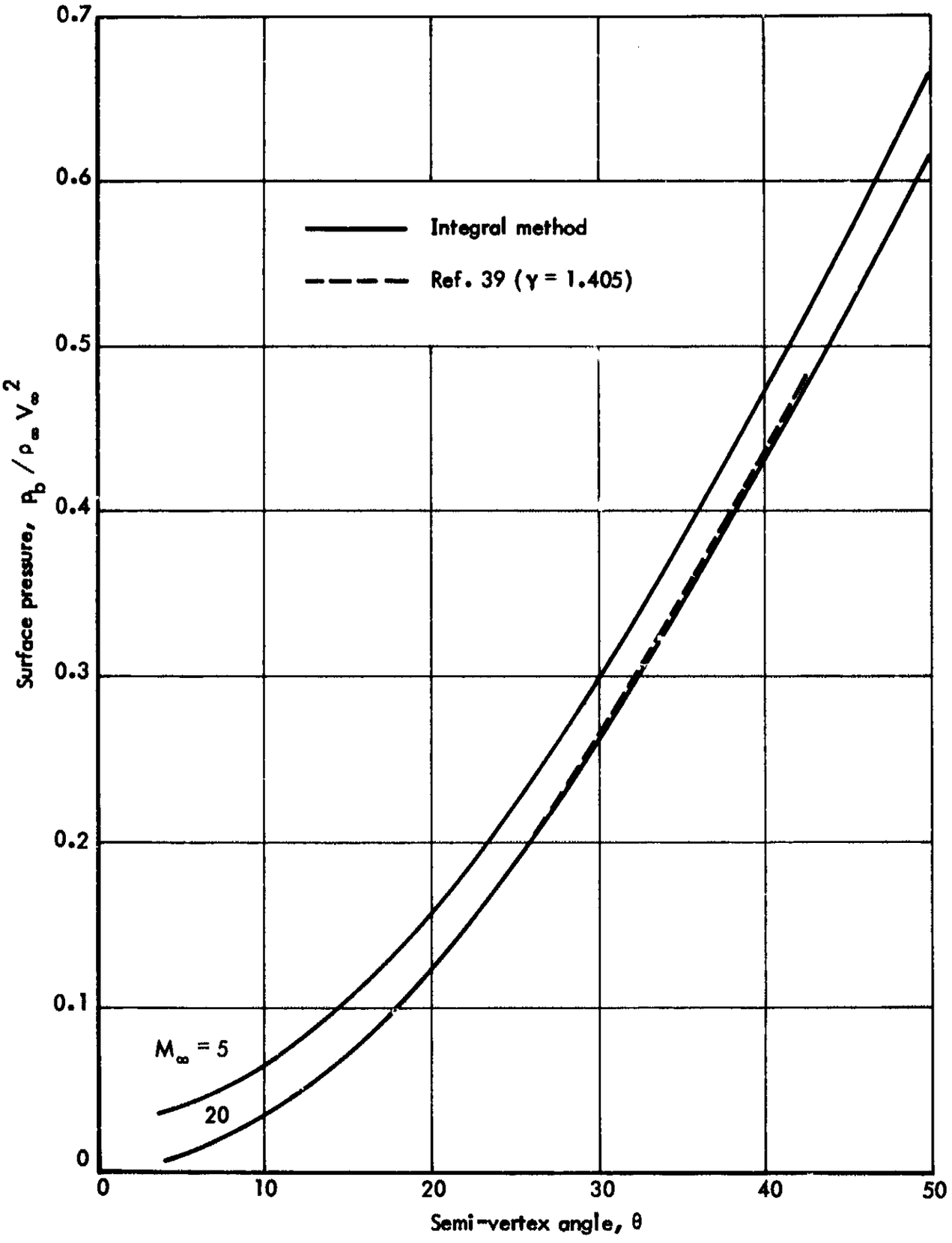

Fig. 11 Variation of cone surface pressure with semi-vertex angle (chem. frozen, vibr. equil., $T_\infty = 250\ ^\circ K$).

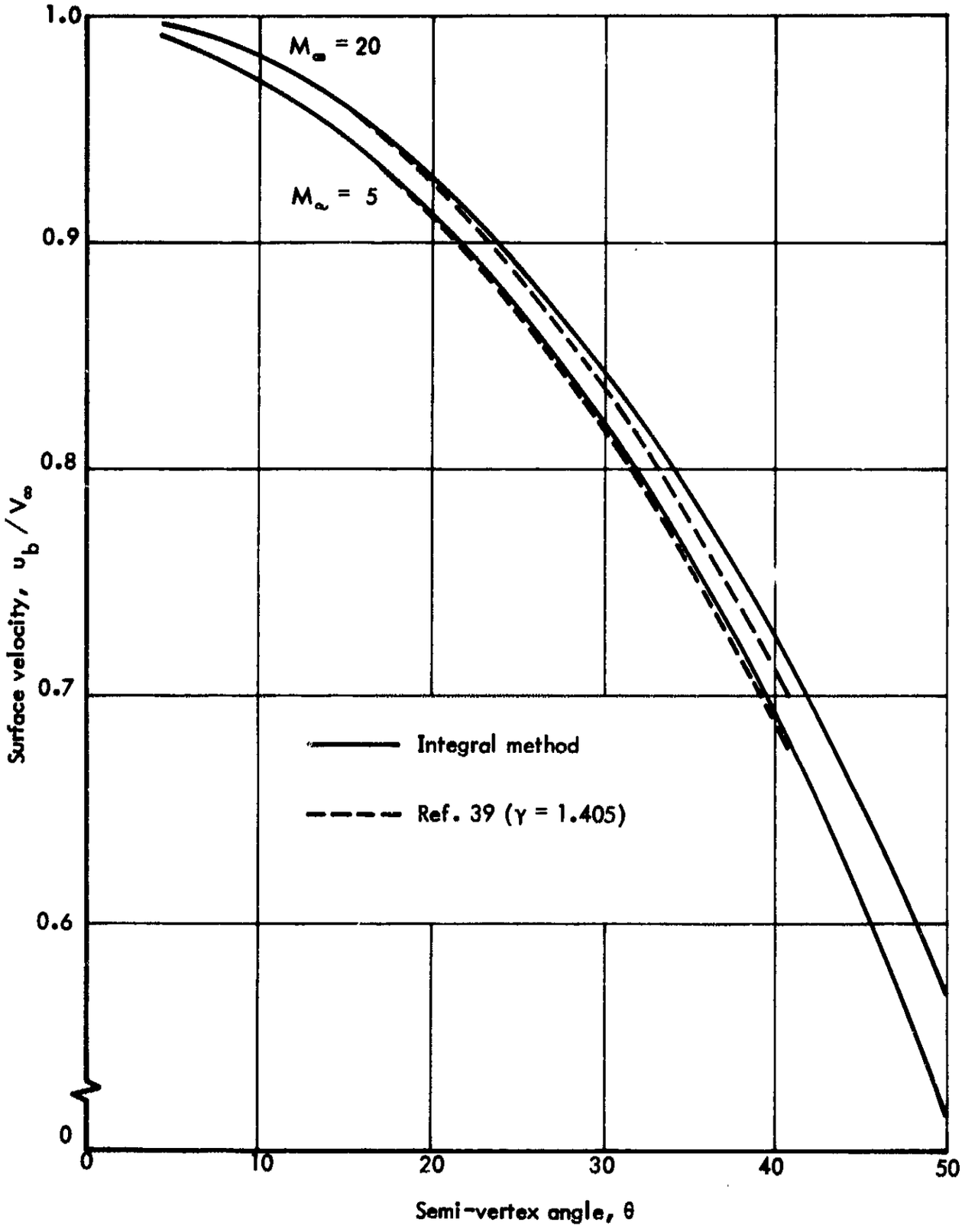

Fig. 12 Variation of cone surface velocity with semi-vertex angle (chem. frozen, vibr. equil., $T_\infty = 250\ ^\circ K$).

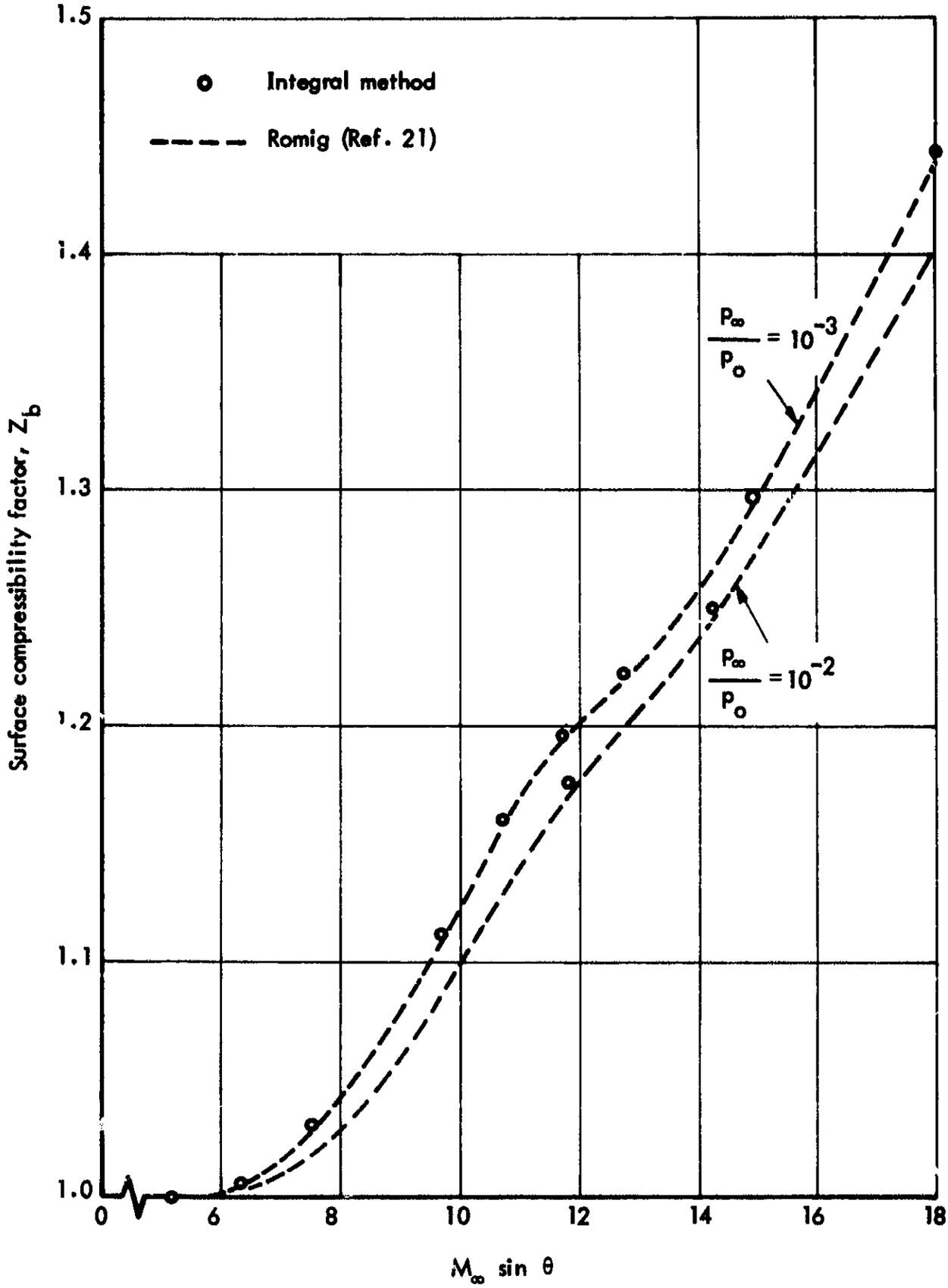

Fig. 13 Surface compressibility factor for equilibrium cone flow ($T_\infty = 273.16^\circ K$, $p_o = 1.0$ atm).

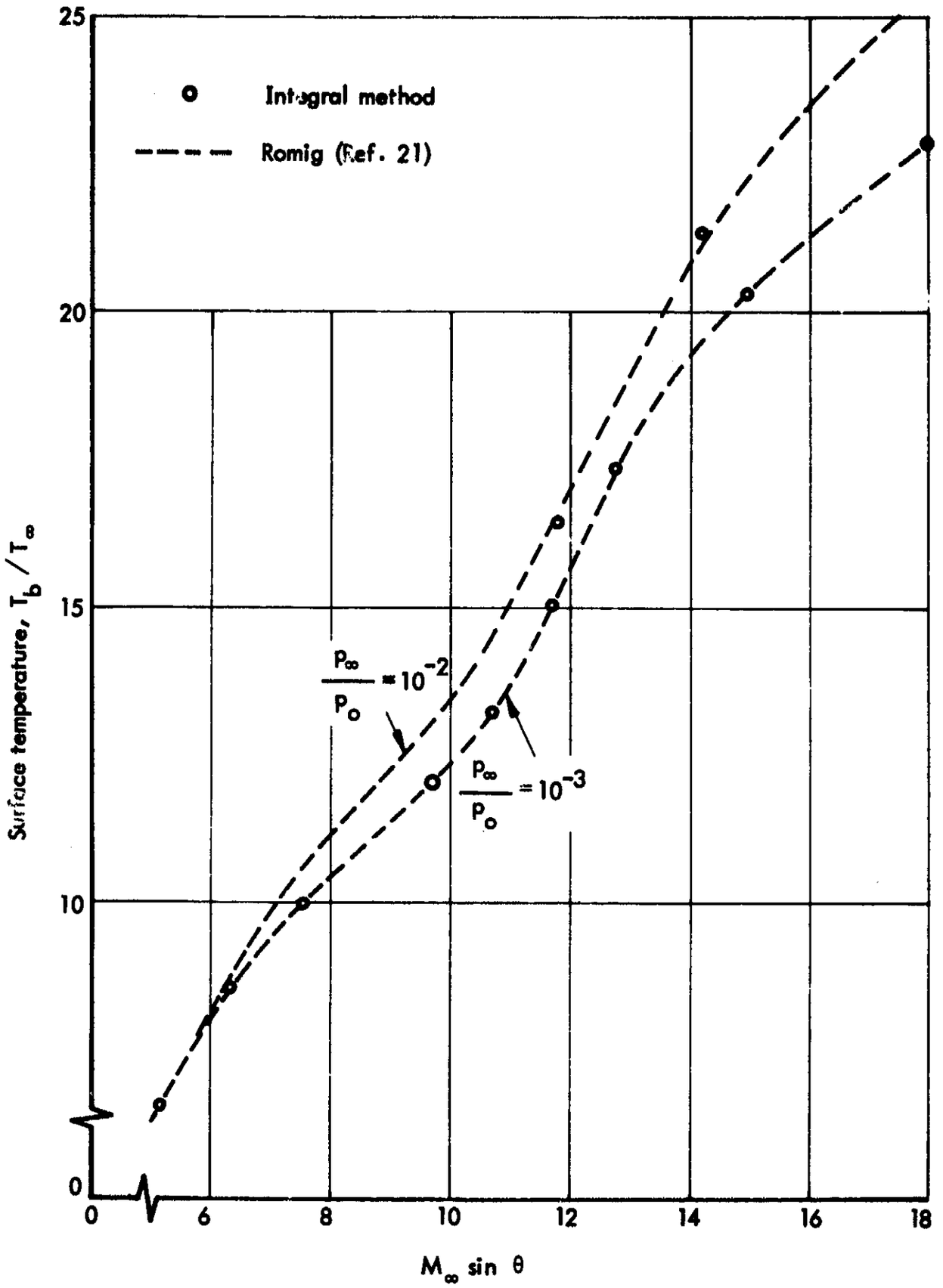

Fig. 14 Surface temperature for equilibrium cone flow ($T_\infty = 273.16\,^{\circ}K$, $p_o = 1.0$ atm).

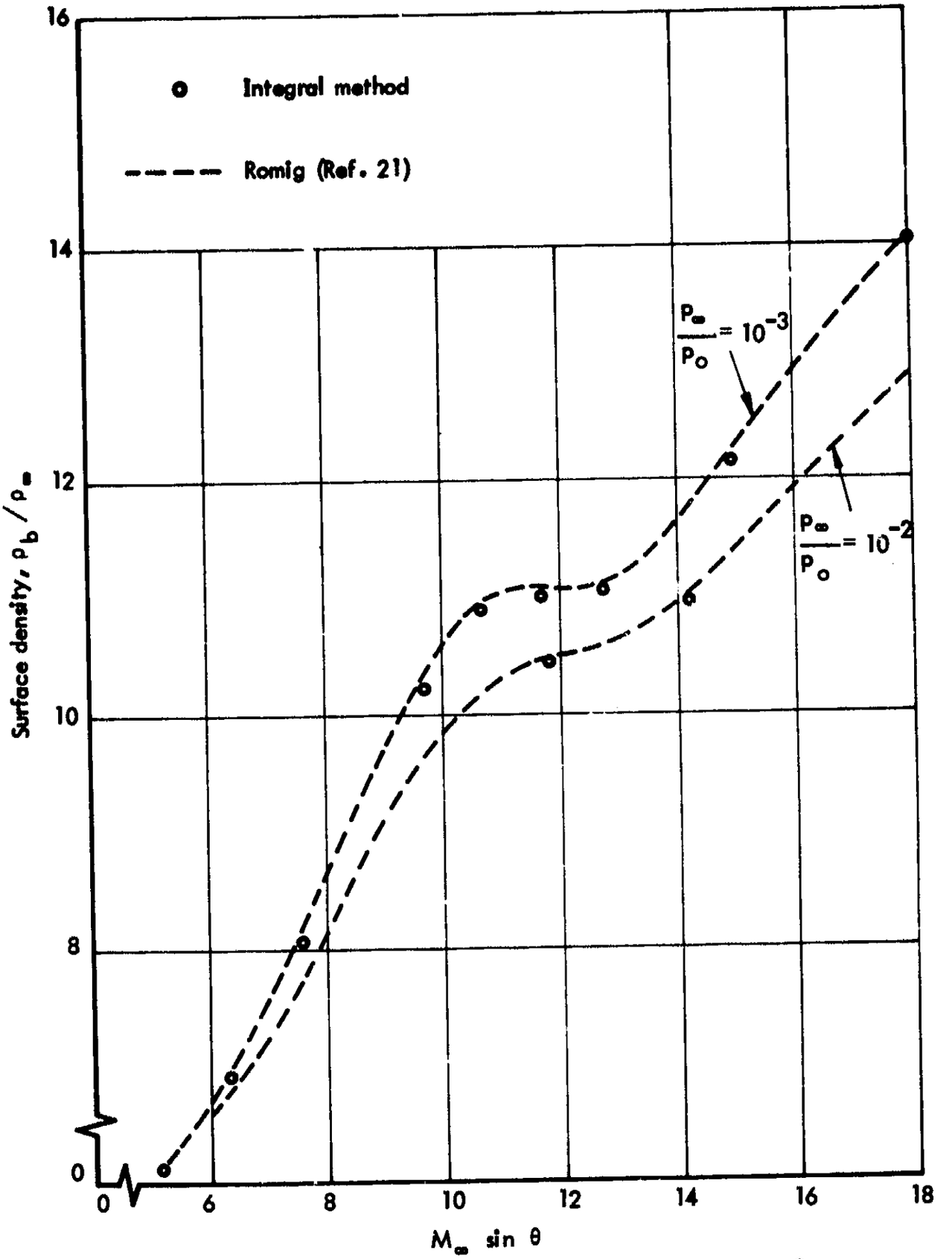

Fig. 15 Surface density for equilibrium cone flow ($T_\infty = 273.16\ ^\circ K$, $P_o = 1.0$ atm).

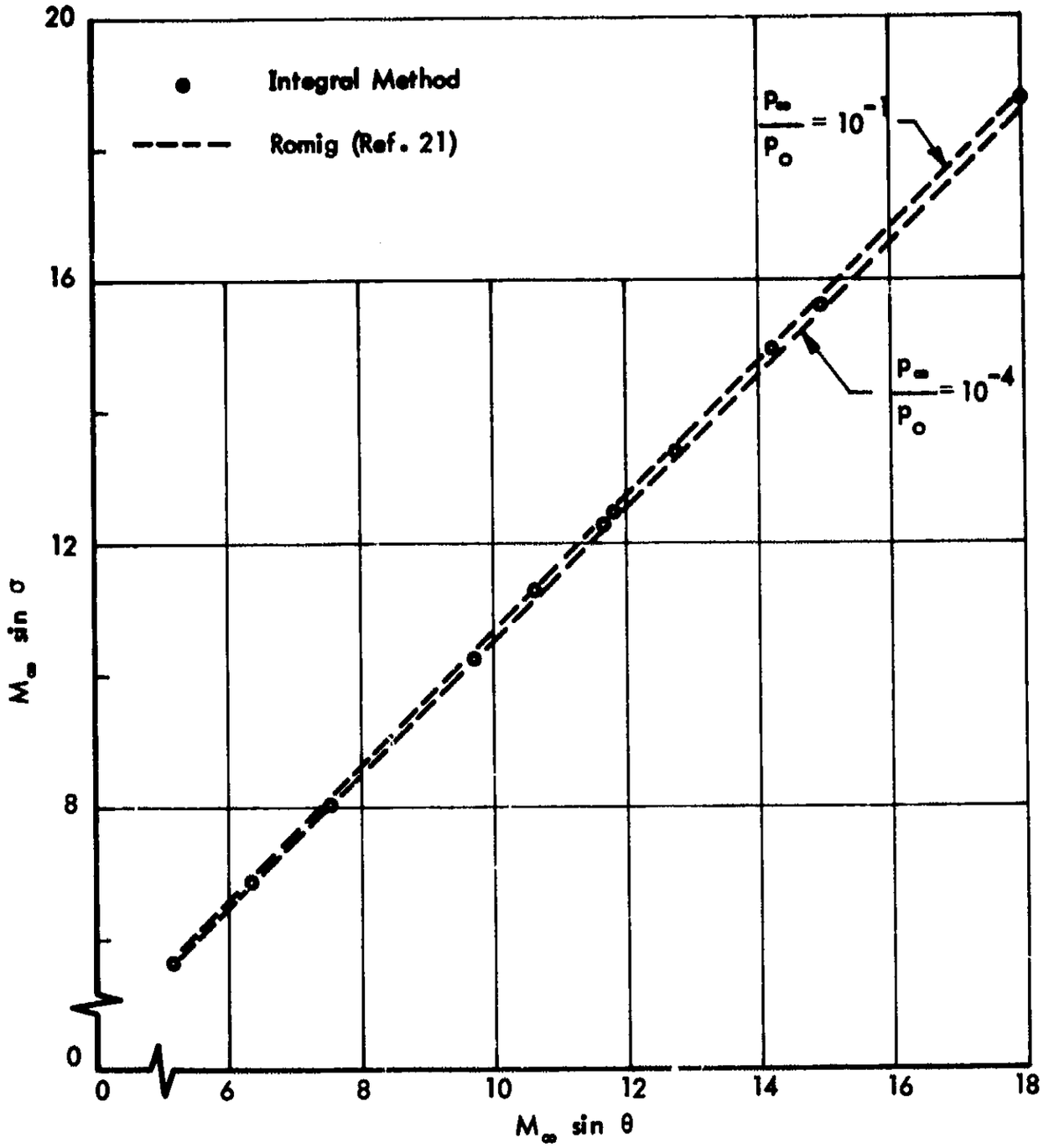

Fig. 16 Shock wave angle σ for equilibrium cone flow ($T_\infty = 273.16^\circ K$, $p_o = 1.0$ atm).

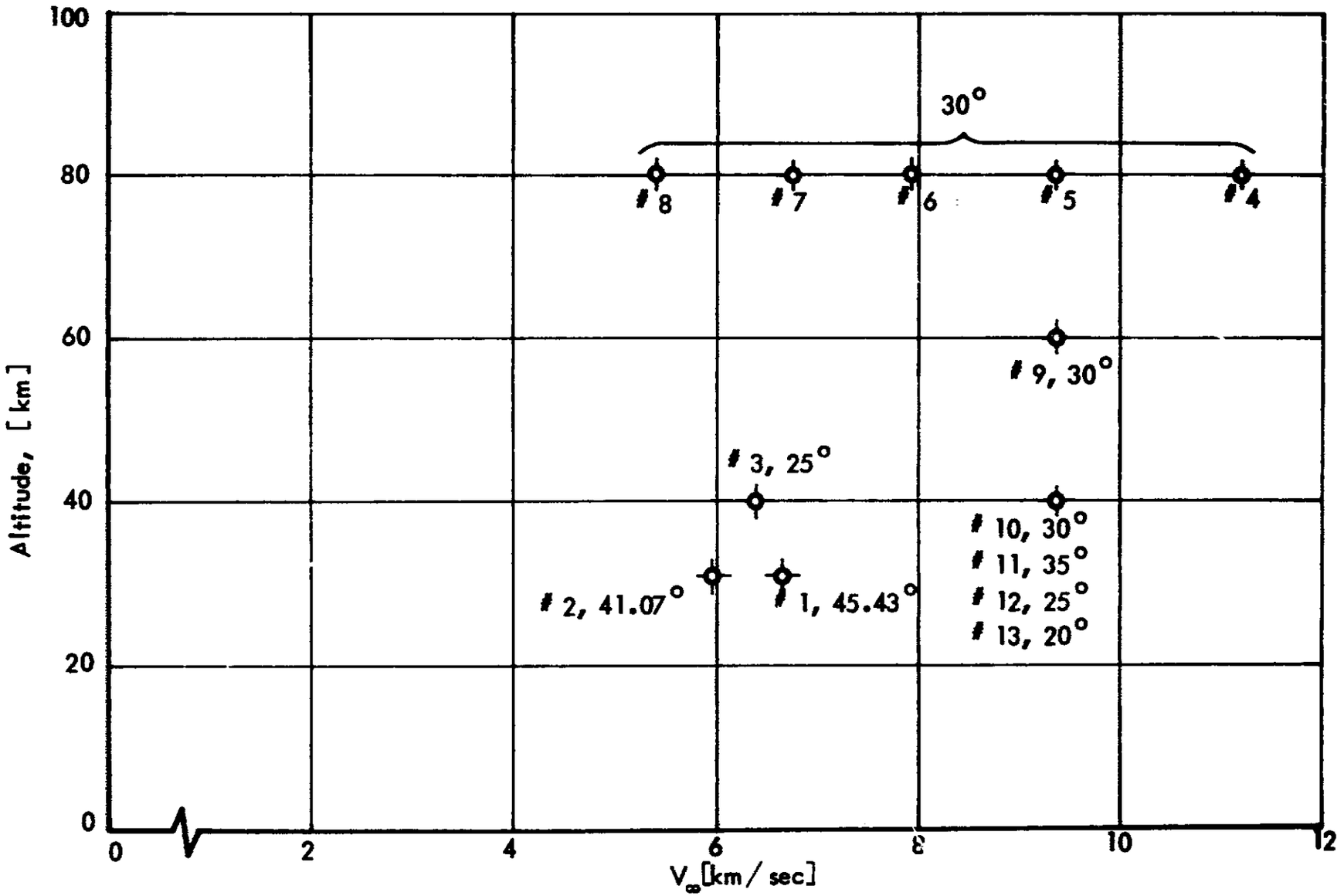

Fig. 17 Survey of investigated nonequilibrium flow cases.

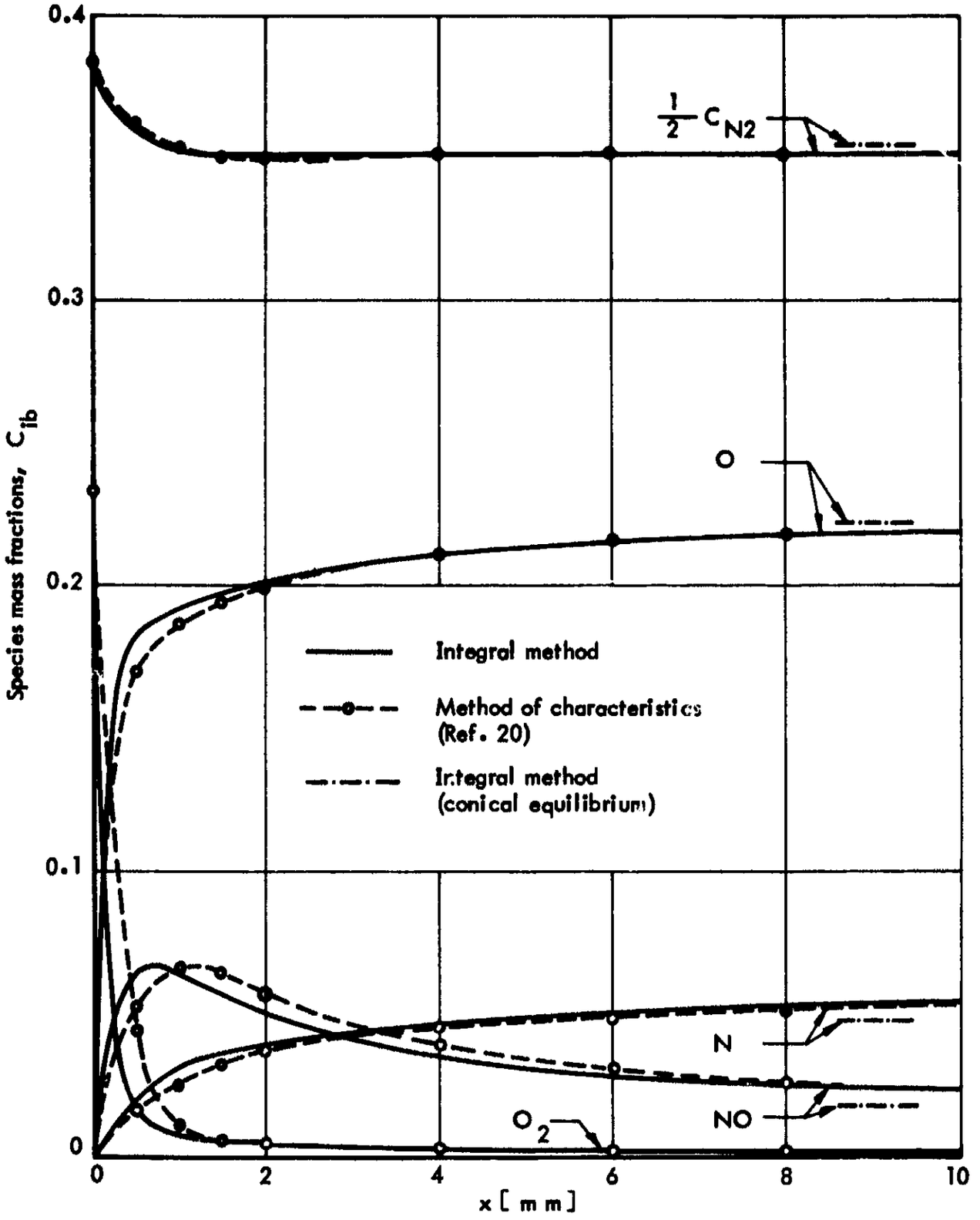

Fig. 18 Cone surface species mass fractions for case 1 (θ = 45.43 °, V_∞ = 6638.0 m/sec, T_∞ = 273.16 °K, p_∞ = 0.01 atm).

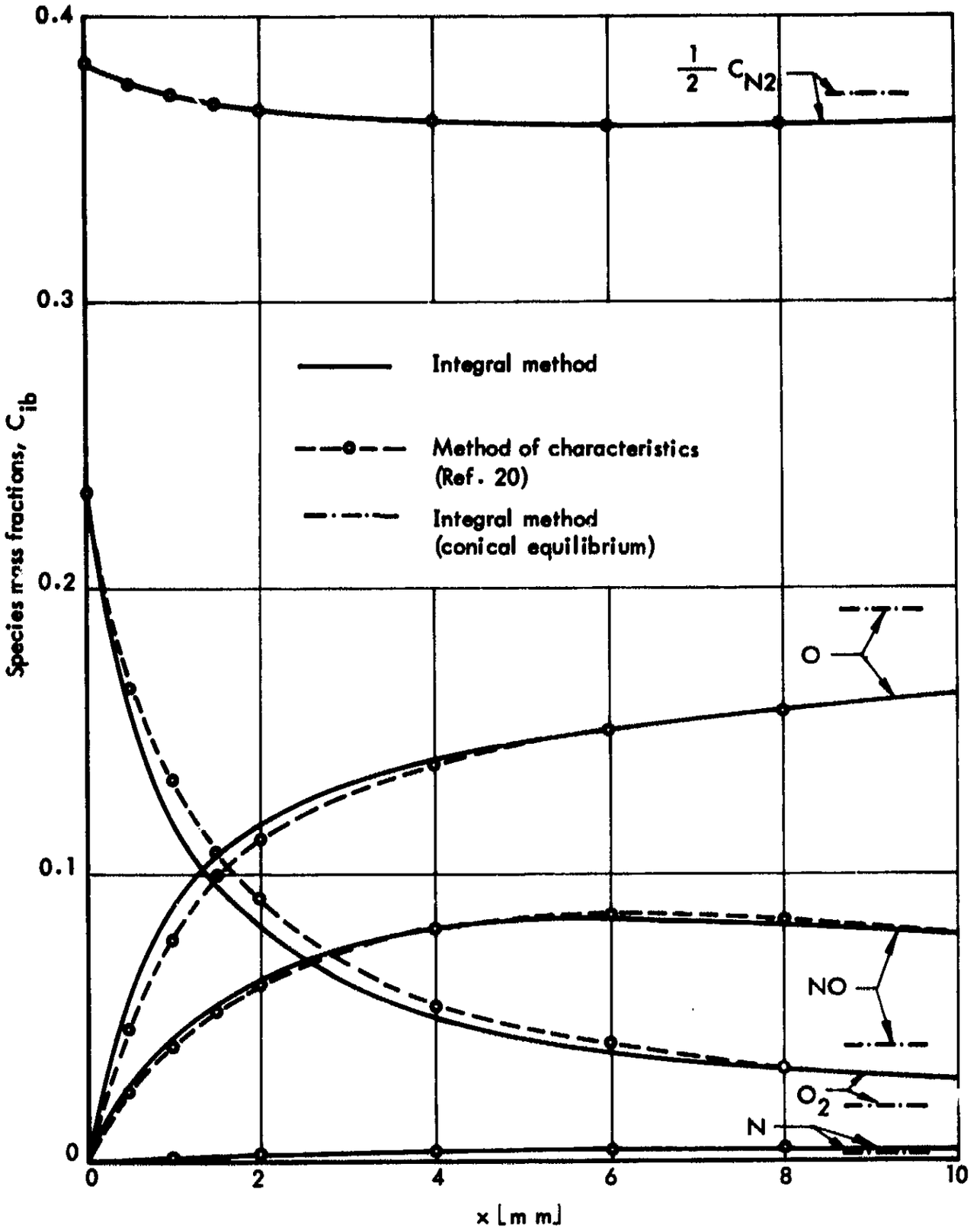

Fig. 19 Cone surface species mass fractions for case 2 ($\theta = 41.07^{\circ}$, $V_{\infty} = 5974.0$ m/sec, $T_{\infty} = 273.16\ ^{\circ}K$, $p_{\infty} = 0.01$ atm).

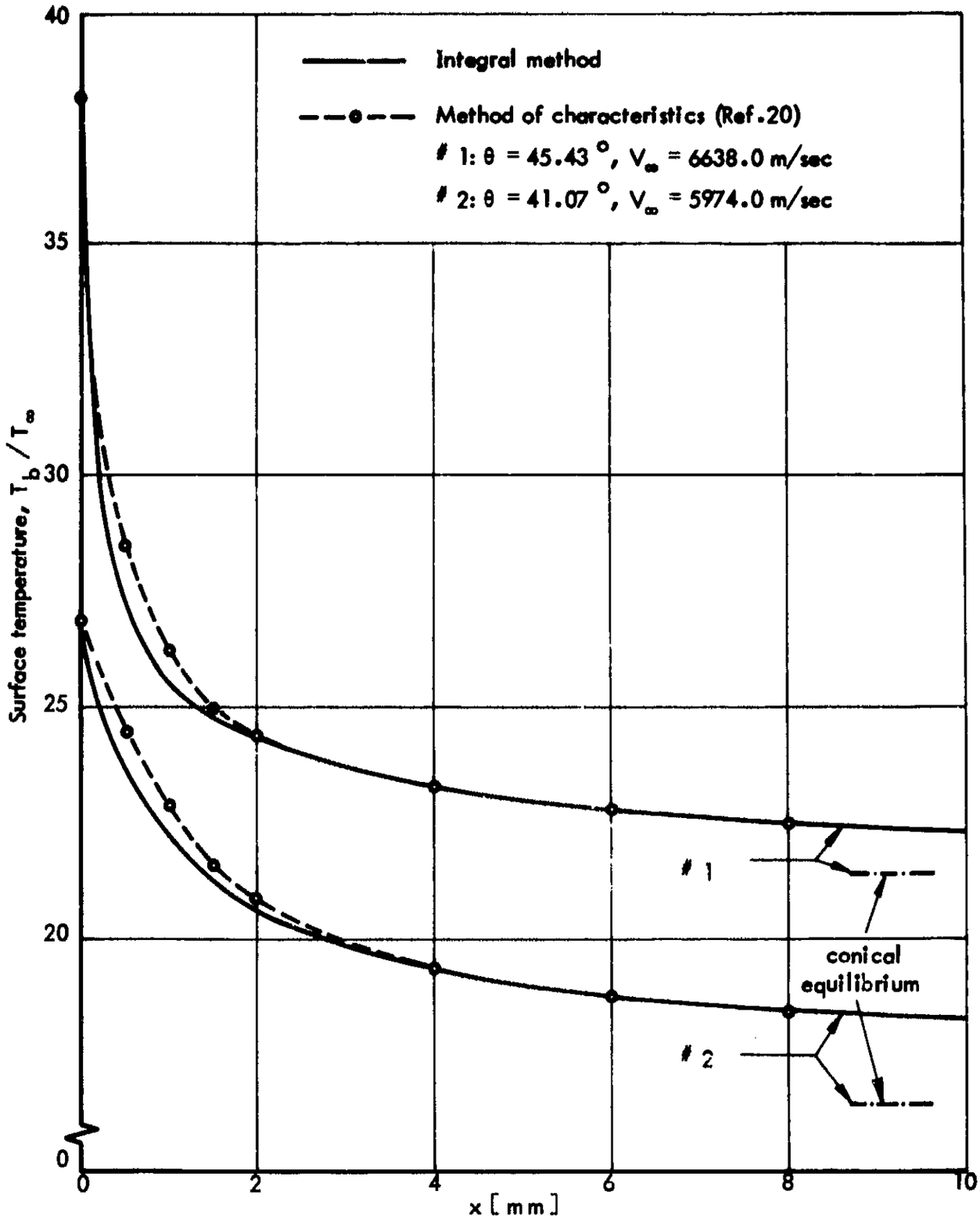

Fig. 20 Cone surface temperatures for cases 1 and 2 (T_∞ = 273.16 °K, p_∞ = 0.01 atm).

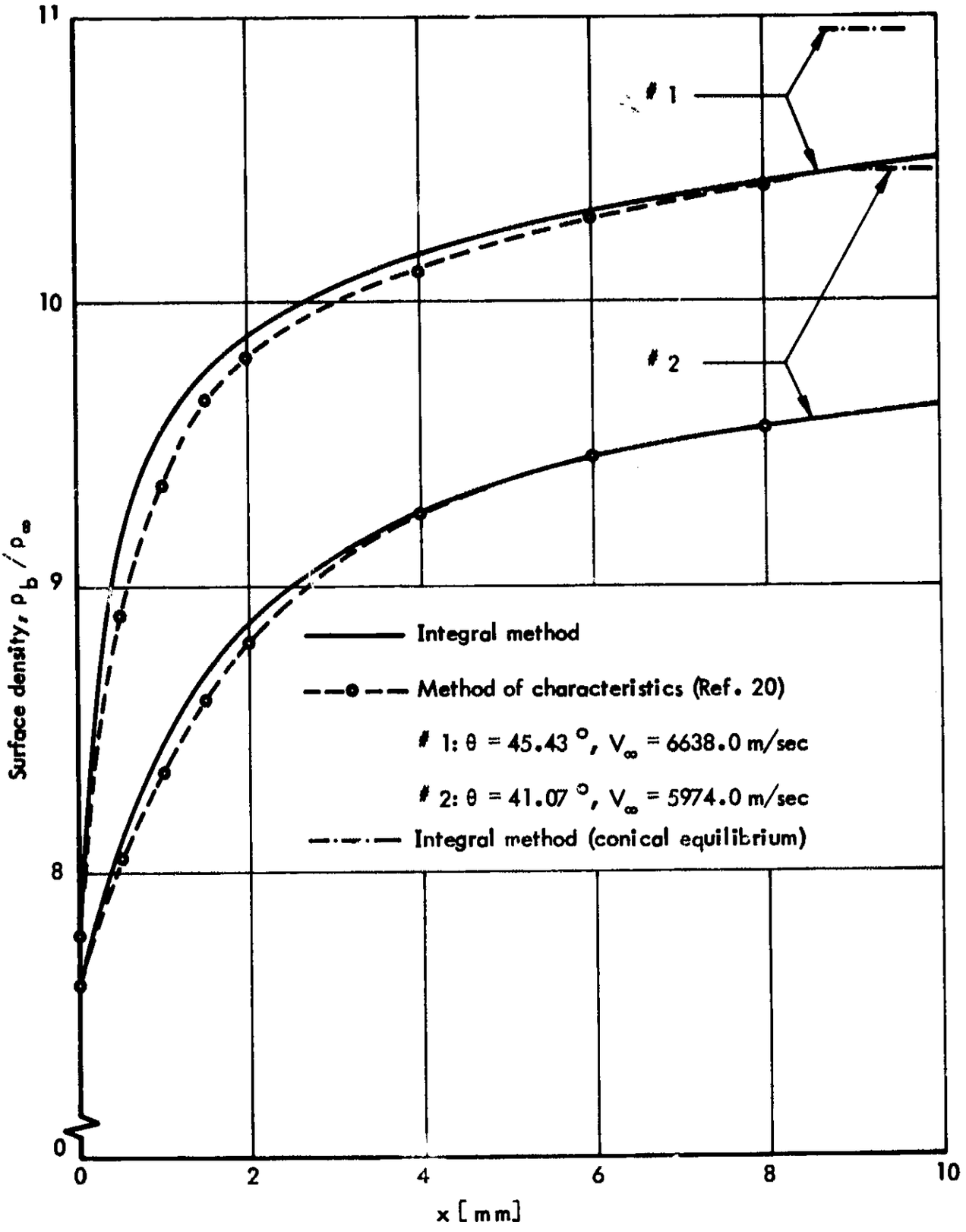

Fig. 21 Cone surface densities for cases 1 and 2 (T_∞ = 273.16 °K, p_∞ = 0.01 atm).

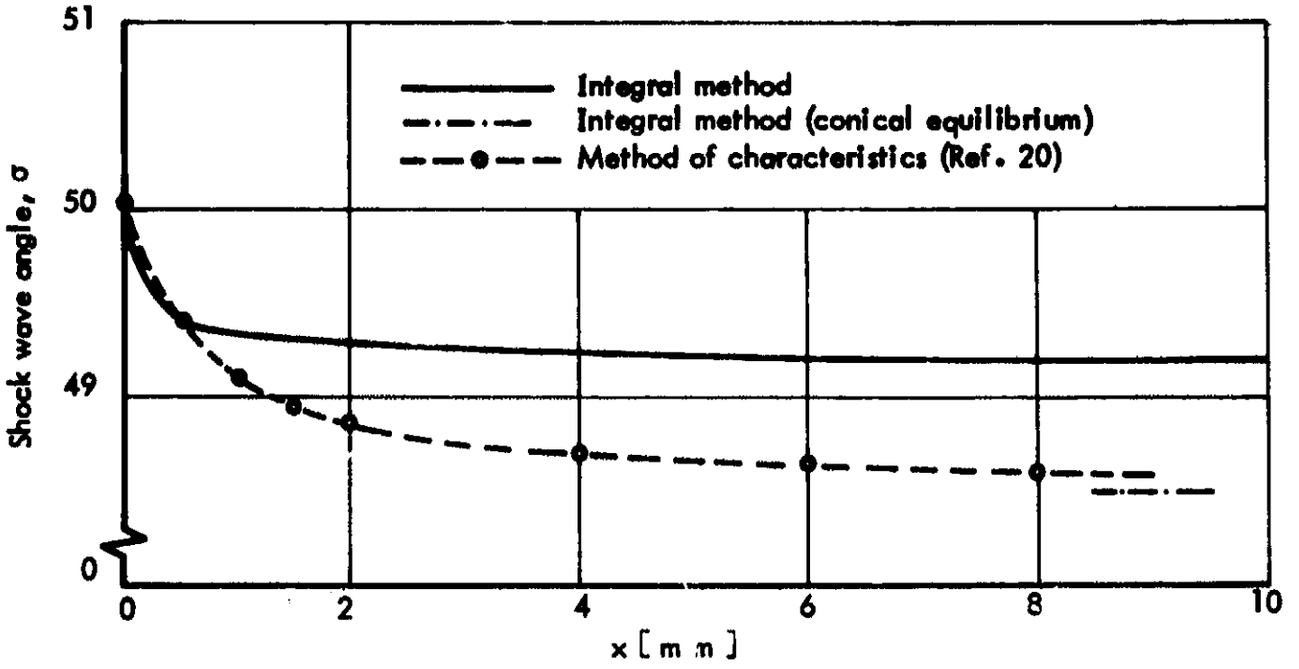

a) case 1: $\theta = 45.43^{\circ}$, $V_{\infty} = 6638.0$ m/sec.

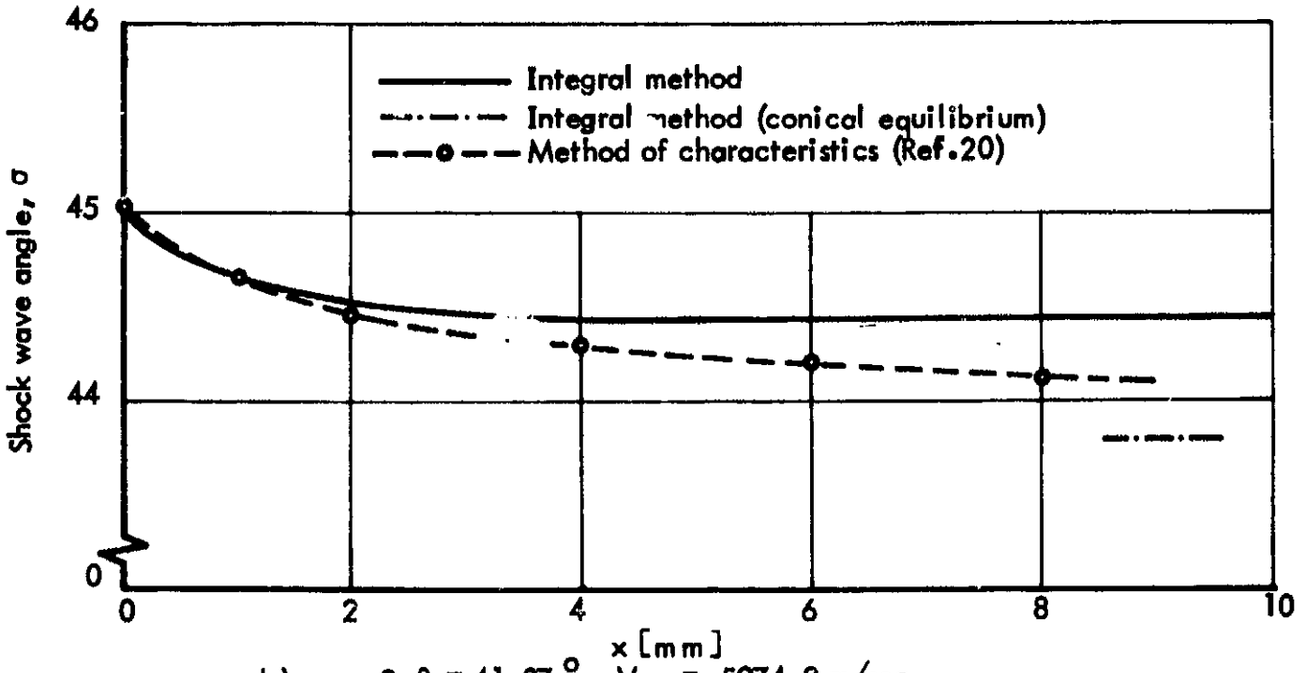

b) case 2: $\theta = 41.07^{\circ}$, $V_{\infty} = 5974.0$ m/sec.

Fig. 22 Shock wave angles for cases 1 and 2 ($T_{\infty} = 273.16\ ^{\circ}K$, $p_{\infty} = 0.01$ atm).

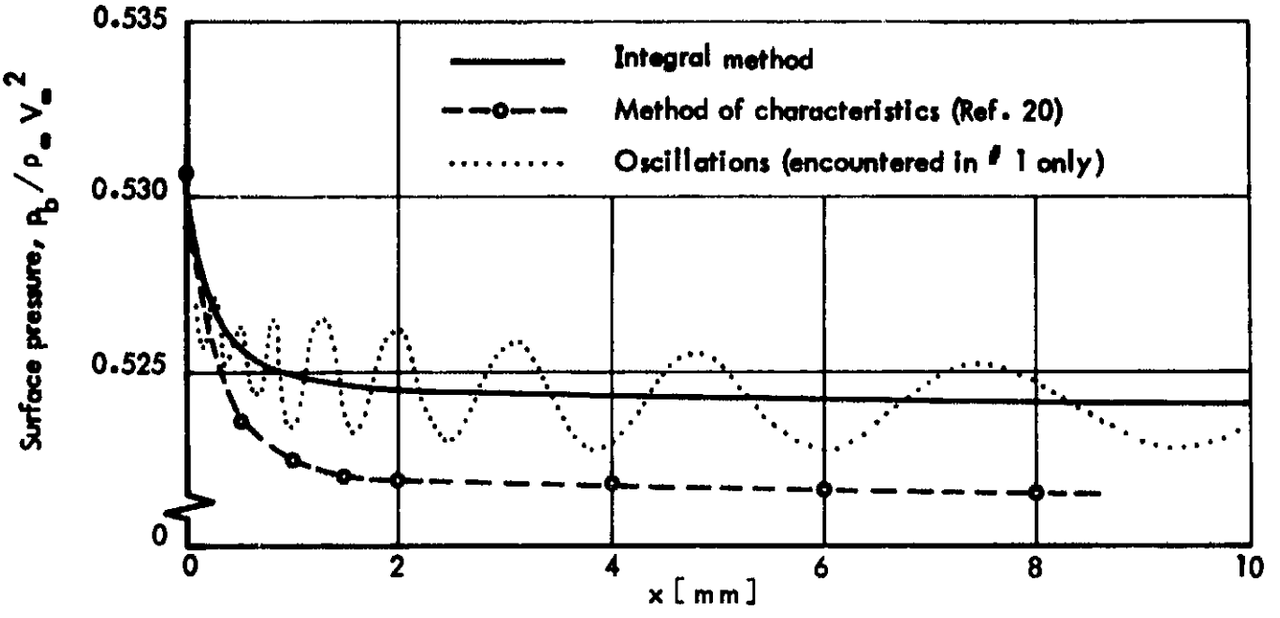

a) case 1: $\theta = 45.43^\circ$, $V_\infty = 6638.0$ m/sec.

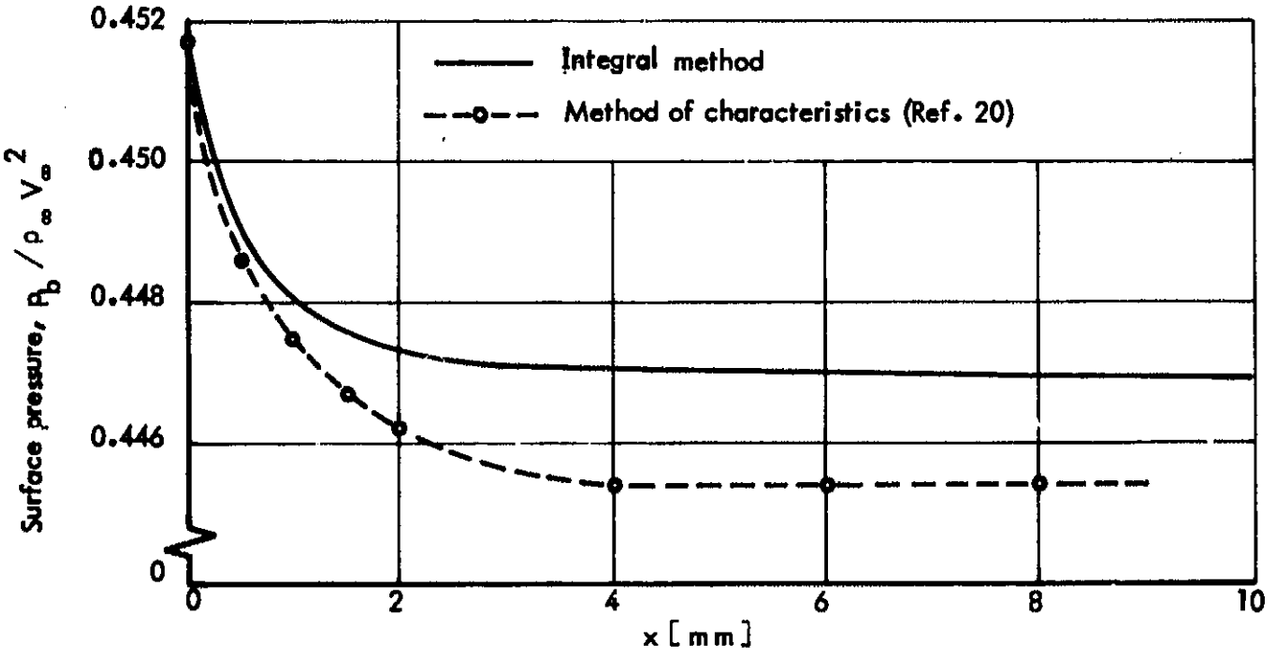

b) case 2: $\theta = 41.07^\circ$, $V_\infty = 5974.0$ m/sec.

Fig. 23 Cone surface pressures for cases 1 and 2 ($T_\infty = 273.16^\circ$K, $p_\infty = 0.01$ atm).

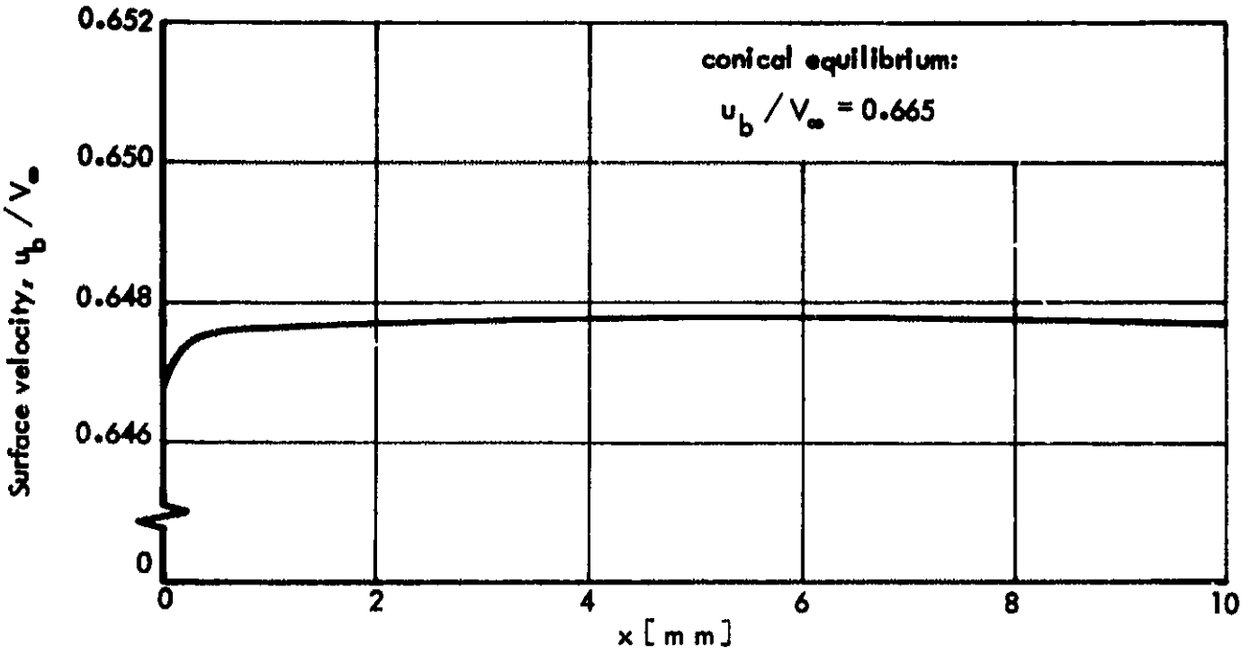

a) case 1: $\theta = 45.43^\circ$, $V_\infty = 6638.0$ m/sec.

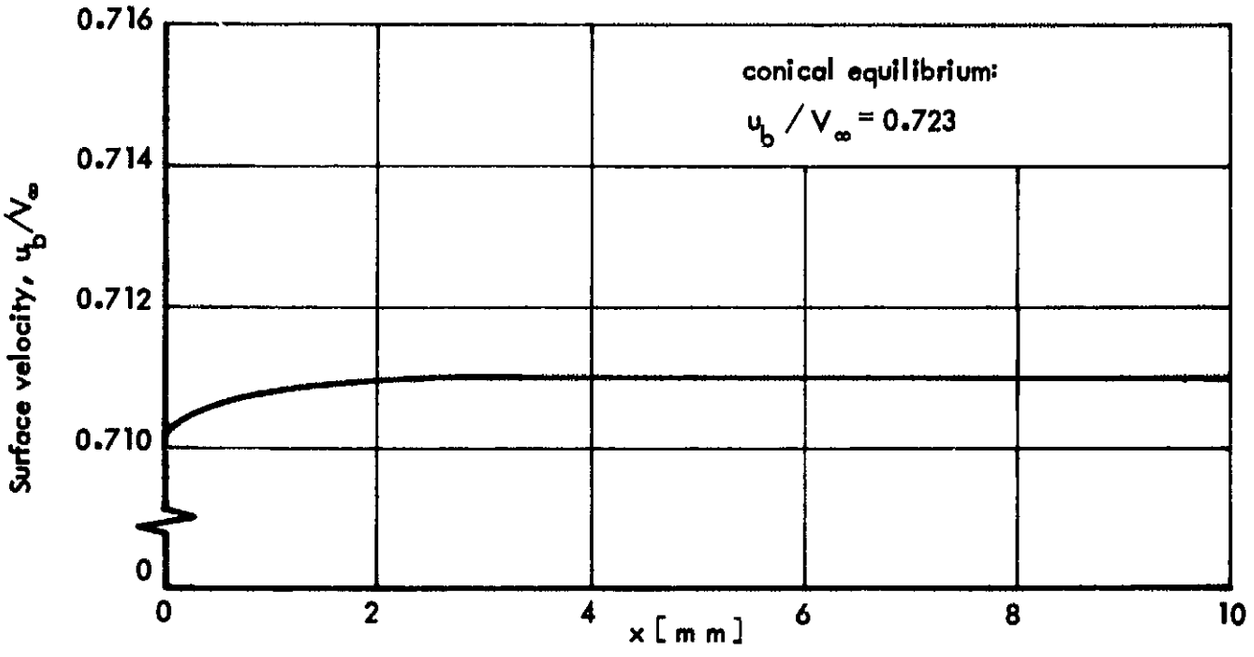

b) case 2: $\theta = 41.07^\circ$, $V_\infty = 5974.0$ m/sec.

Fig. 24 Cone surface velocities for cases 1 and 2 ($T_\infty = 273.16\ ^\circ K$, $p_\infty = 0.01$ atm).

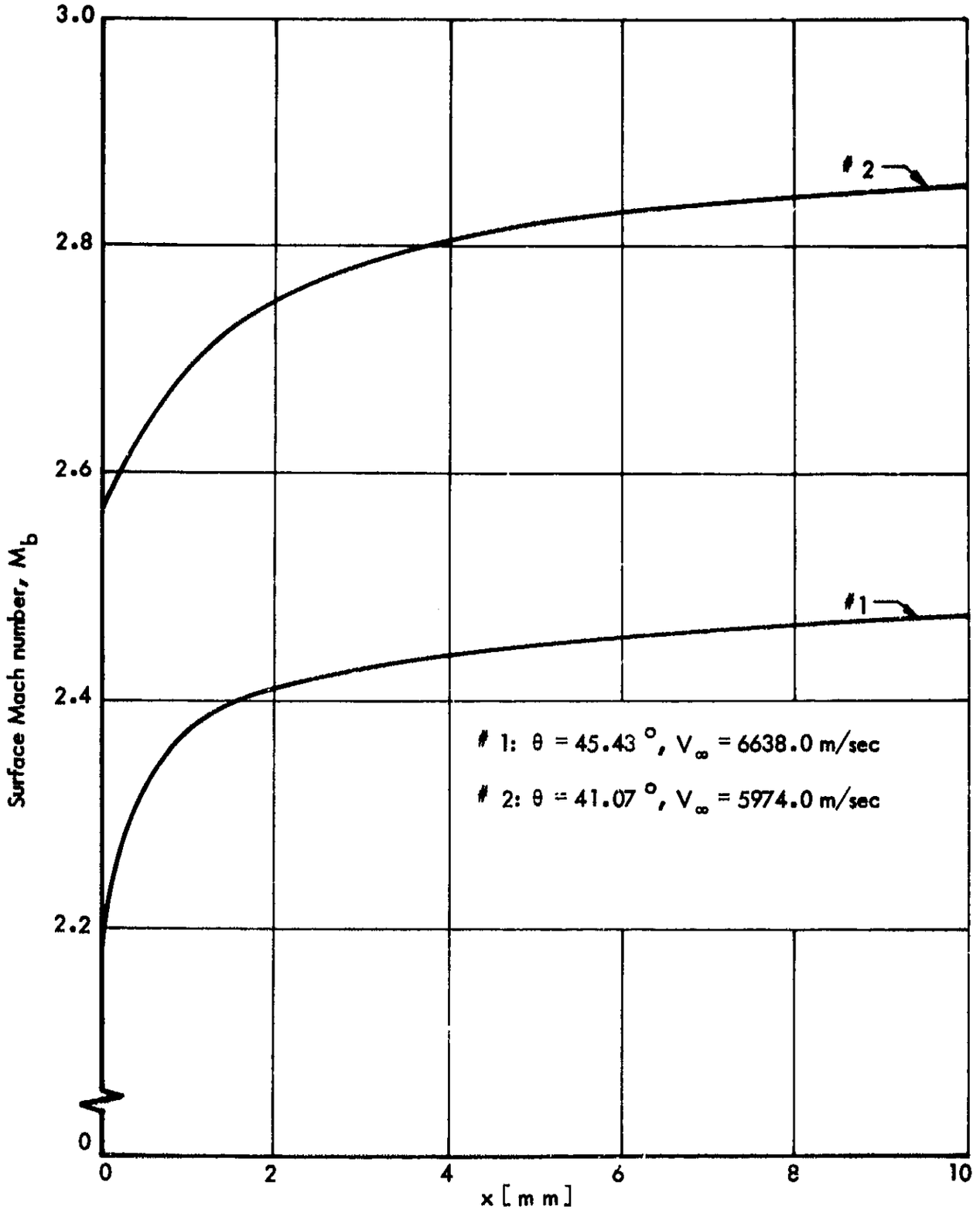

Fig. 25 Cone surface Mach numbers for cases 1 and 2 (T_∞ = 273.16 °K, p_∞ = 0.01 atm).

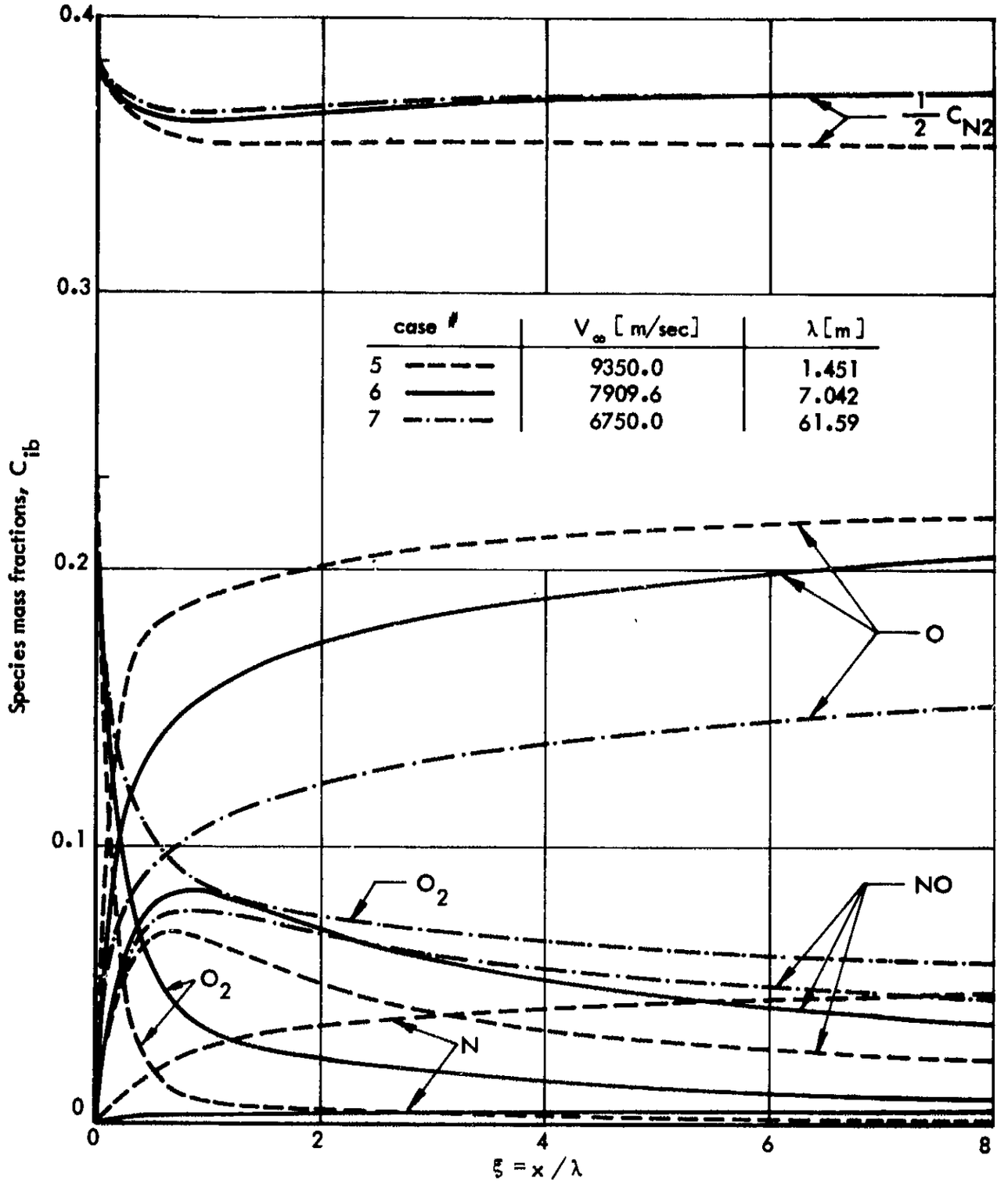

Fig. 26 Influence of free stream velocity on cone surface species mass fractions ($\theta = 30^\circ$, altitude 80 km).

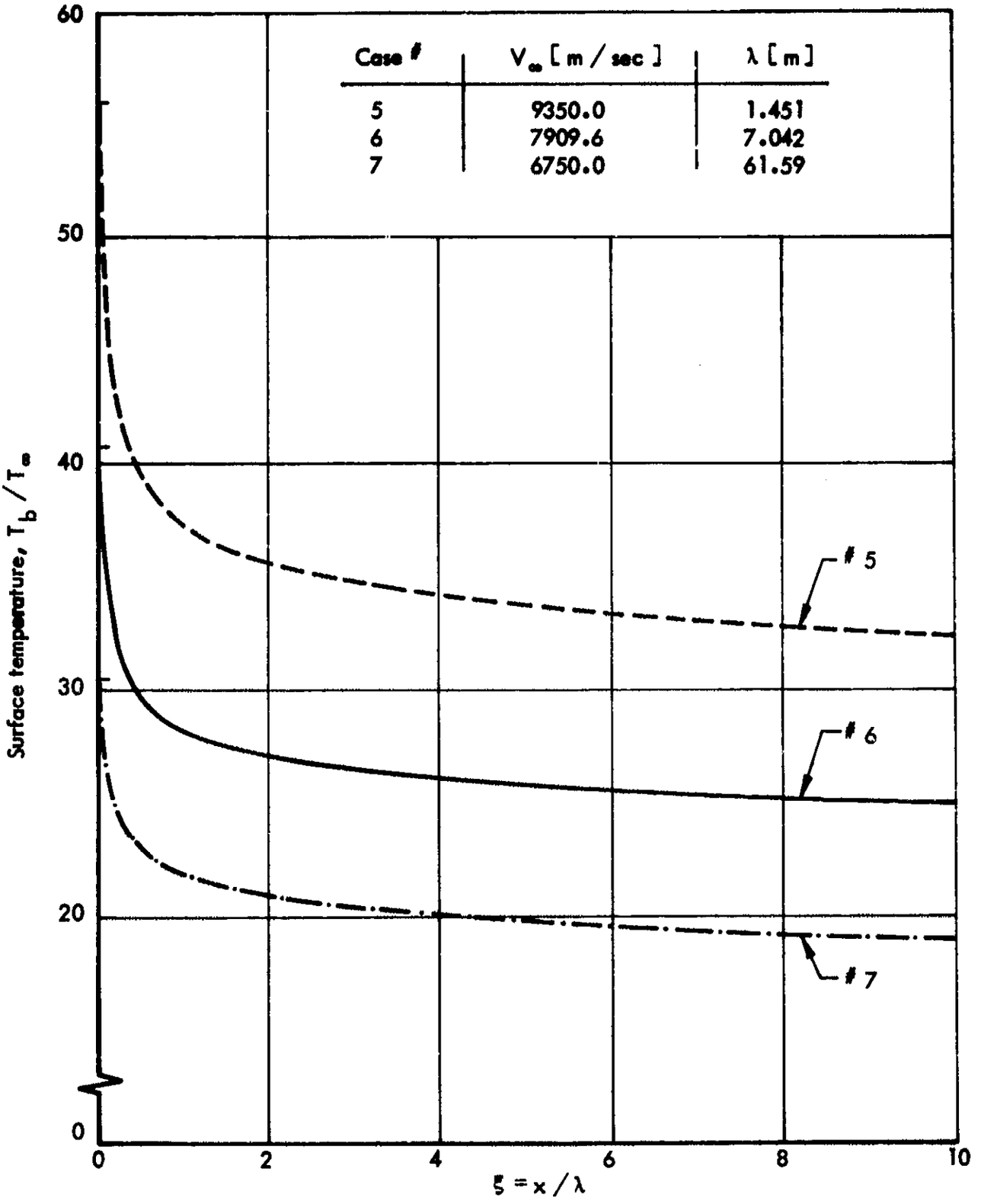

Fig. 27 Influence of free stream velocity on cone surface temperature ($\theta = 30^\circ$, altitude 80 km).

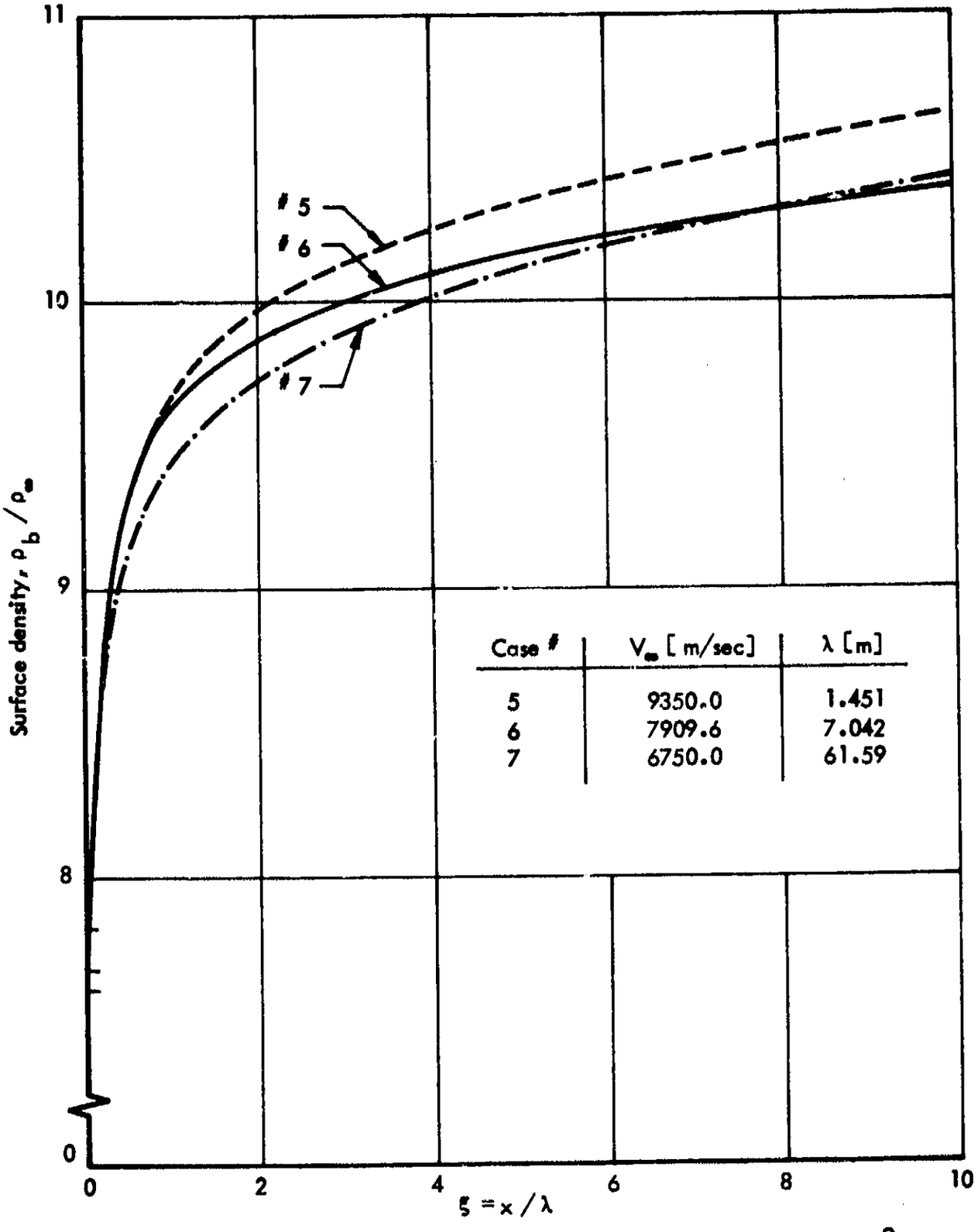

Fig. 28 Influence of free stream velocity on cone surface density ($\theta = 30^\circ$, altitude 80 km).

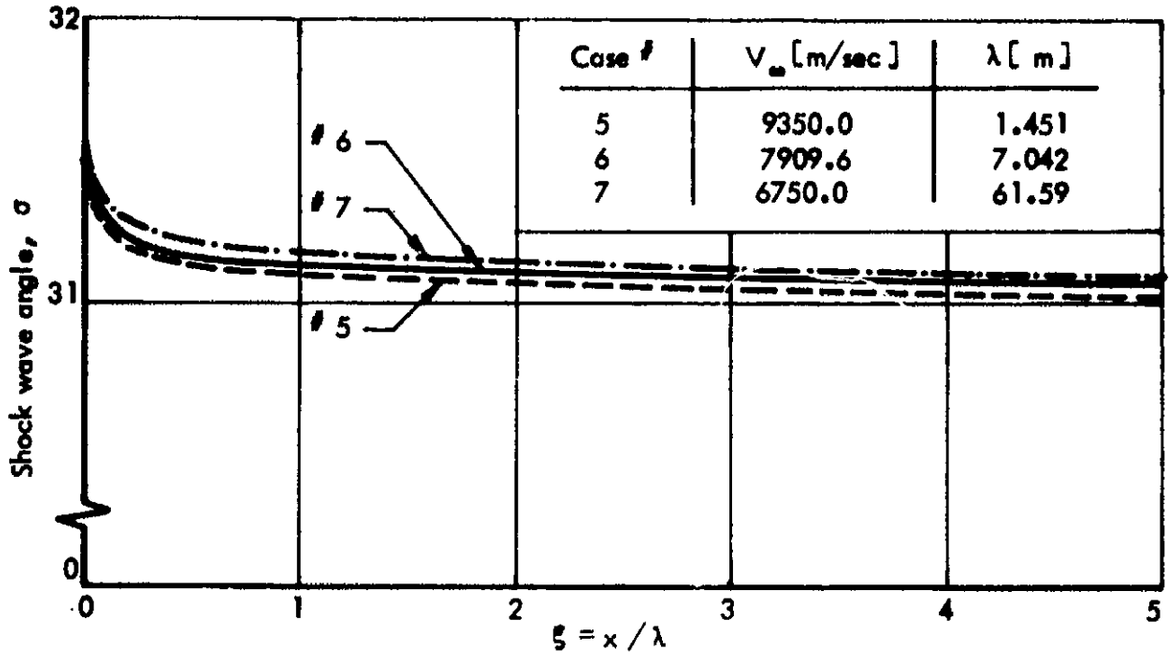

Fig. 29 Influence of free stream velocity on shock wave angle ($\theta = 30^\circ$, altitude 80 km).

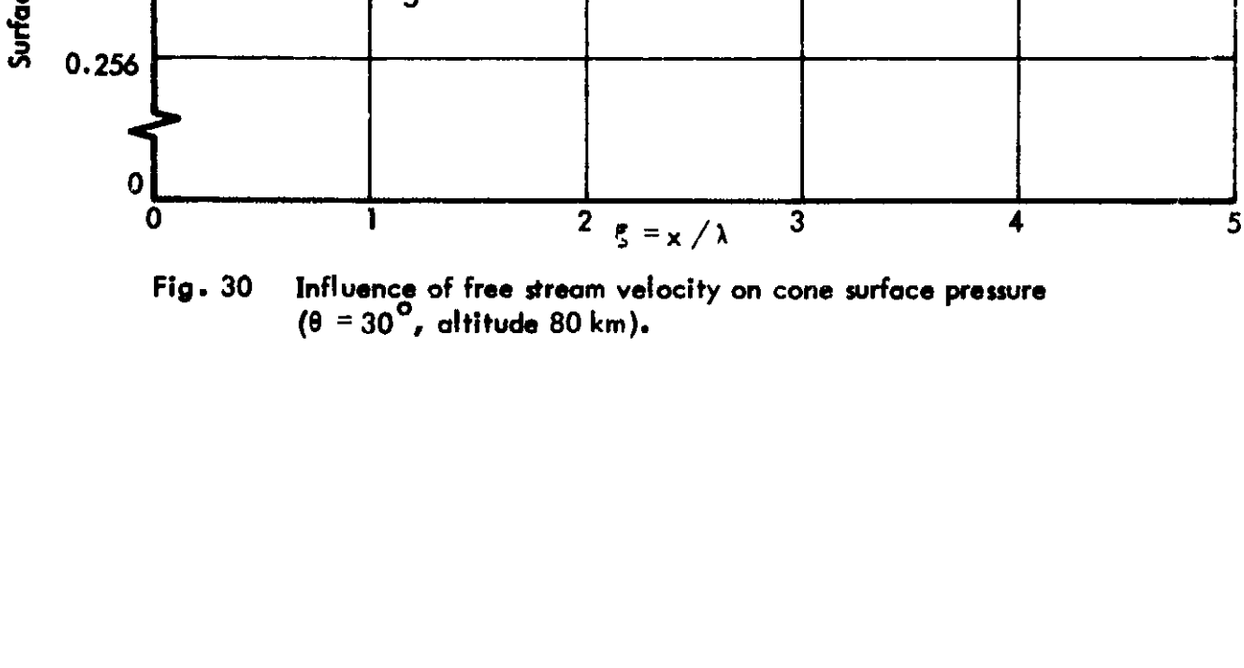

Fig. 30 Influence of free stream velocity on cone surface pressure ($\theta = 30^\circ$, altitude 80 km).

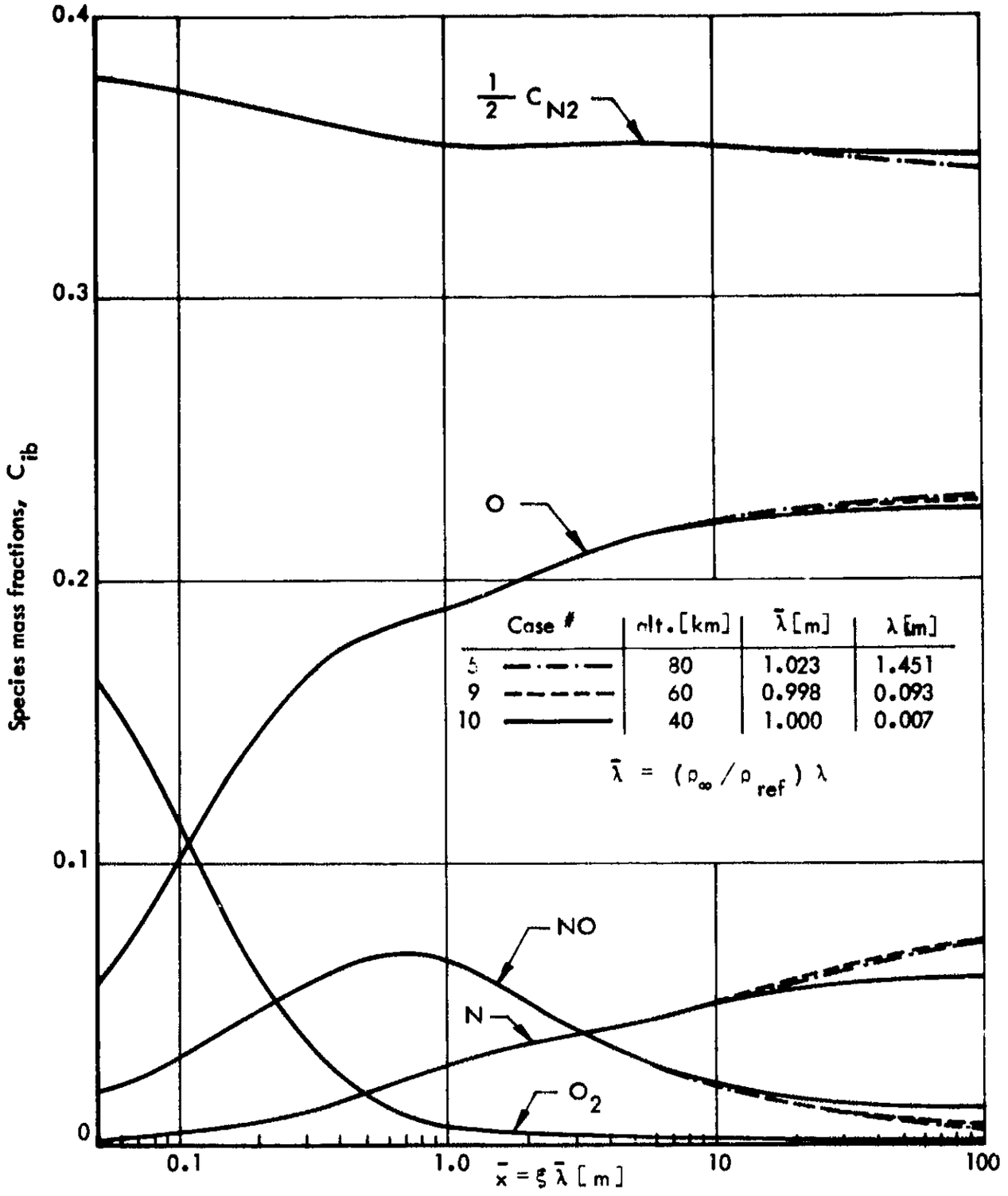

Fig. 31 Species mass fractions on cone surfaces for different altitudes ($\theta = 30^\circ$, $V_\infty = 9350.0$ m/sec).

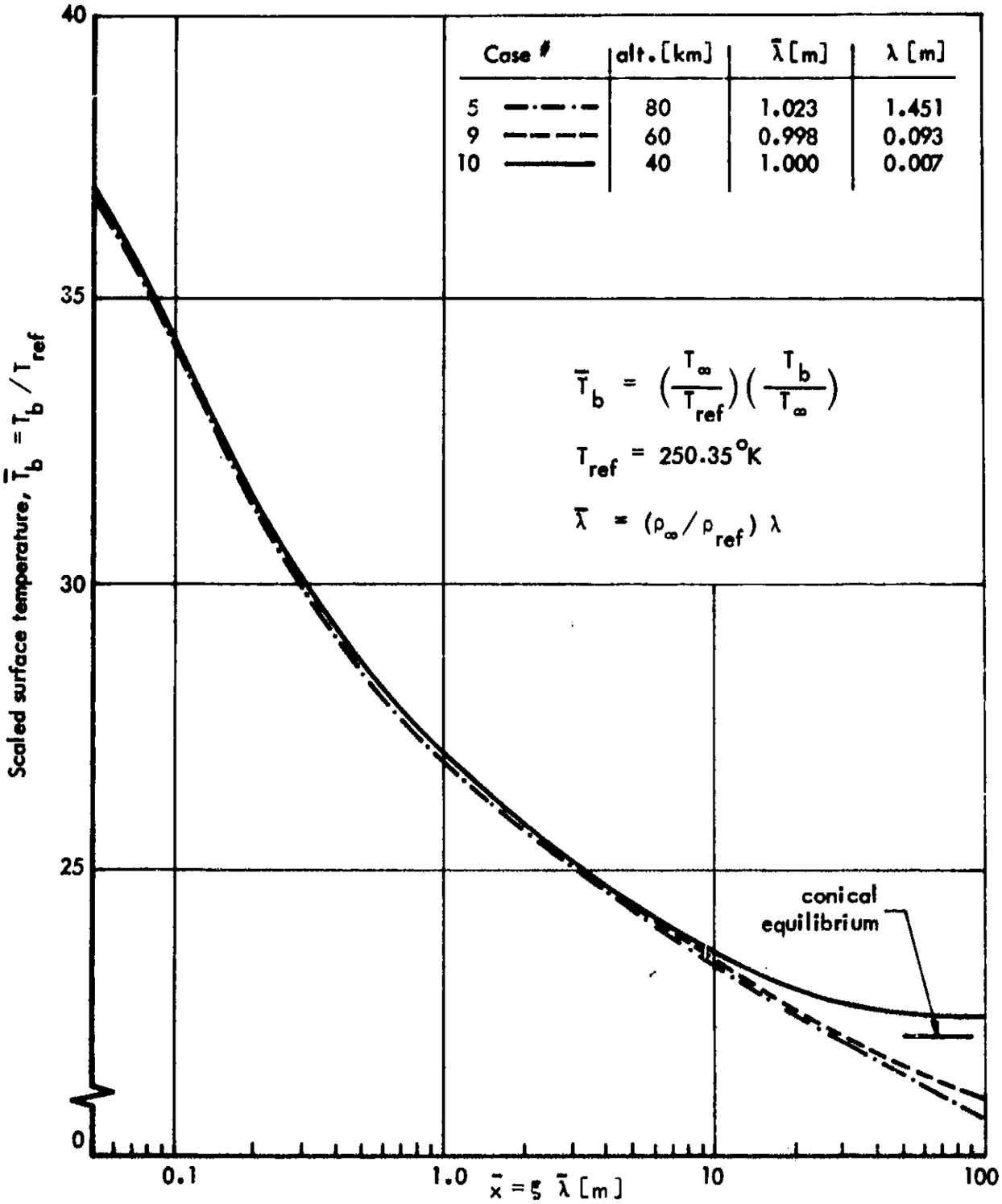

Fig. 32 Scaled temperature on cone surfaces for different altitudes ($\theta = 30^\circ$, $V_\infty = 9350.0$ m/sec).

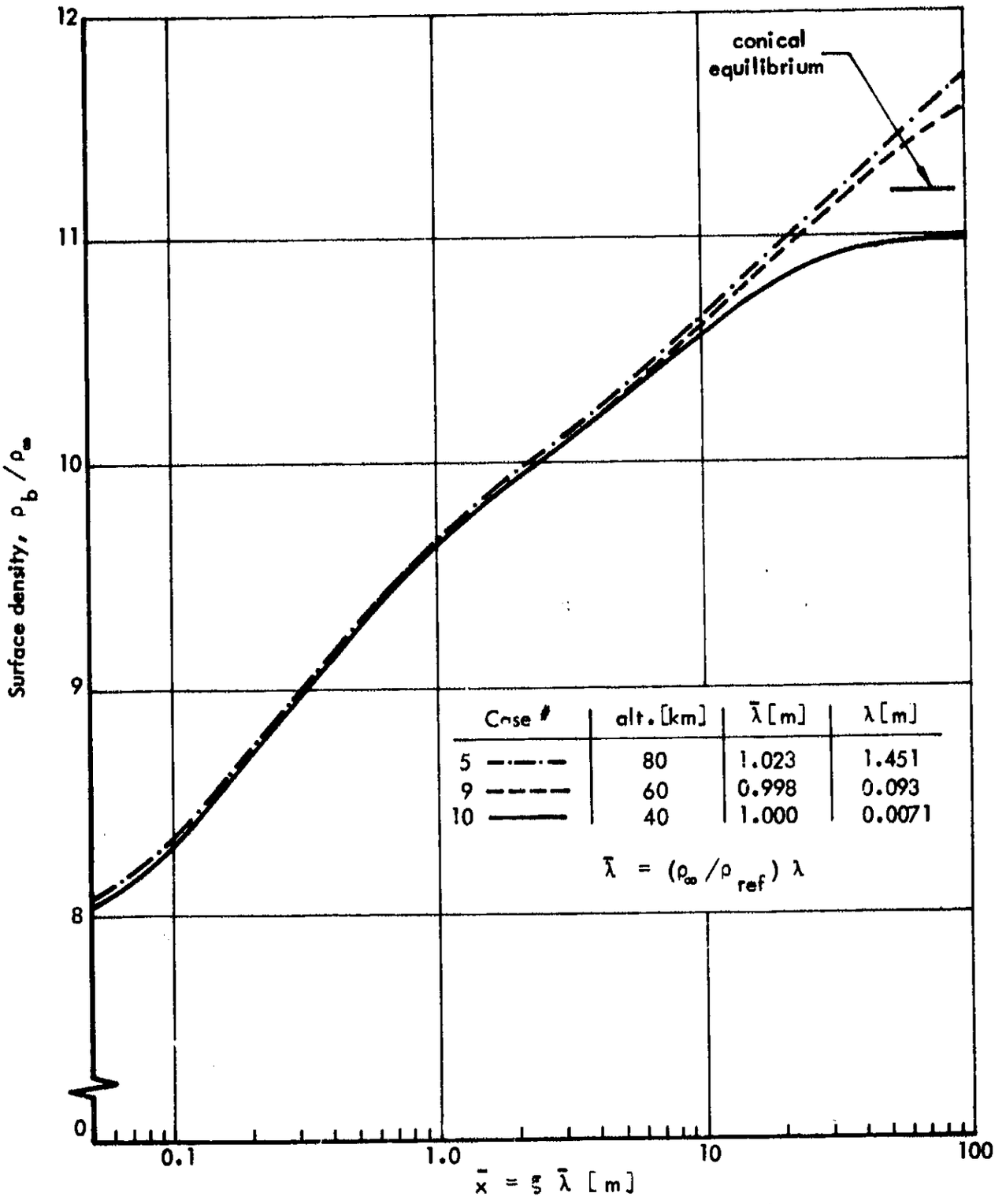

Fig. 33 Density on cone surfaces for different altitudes ($\theta = 30^\circ$, $V_\infty = 9350.0$m/sec).

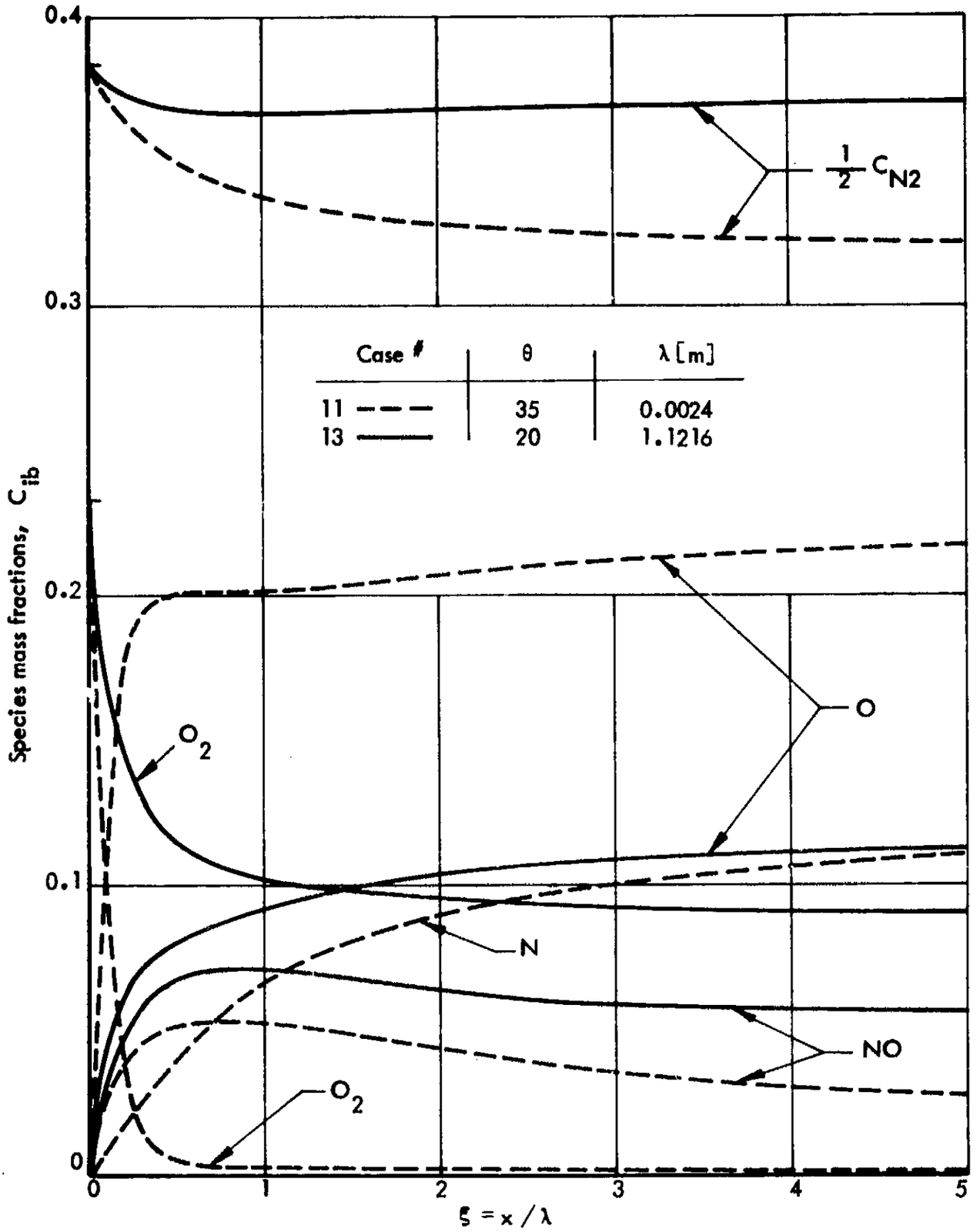

Fig. 34 Influence of cone semi-vertex angle on surface species mass fractions (V_∞ = 9350.0 m/sec, altitude 40 km).

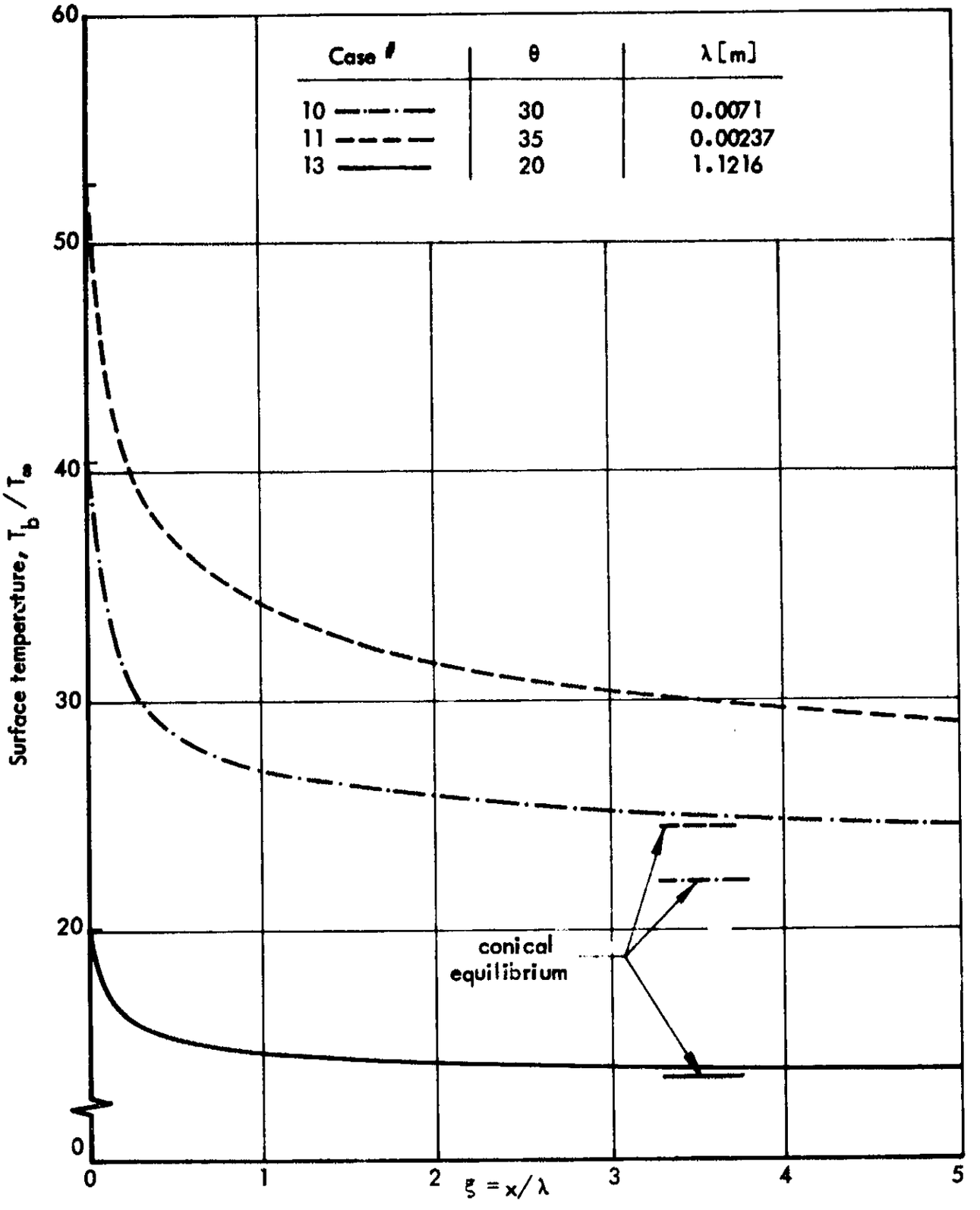

Fig. 35 Influence of cone semi-vertex angle on surface temperature (V_∞ = 9350.0 m/sec, altitude 40 km).

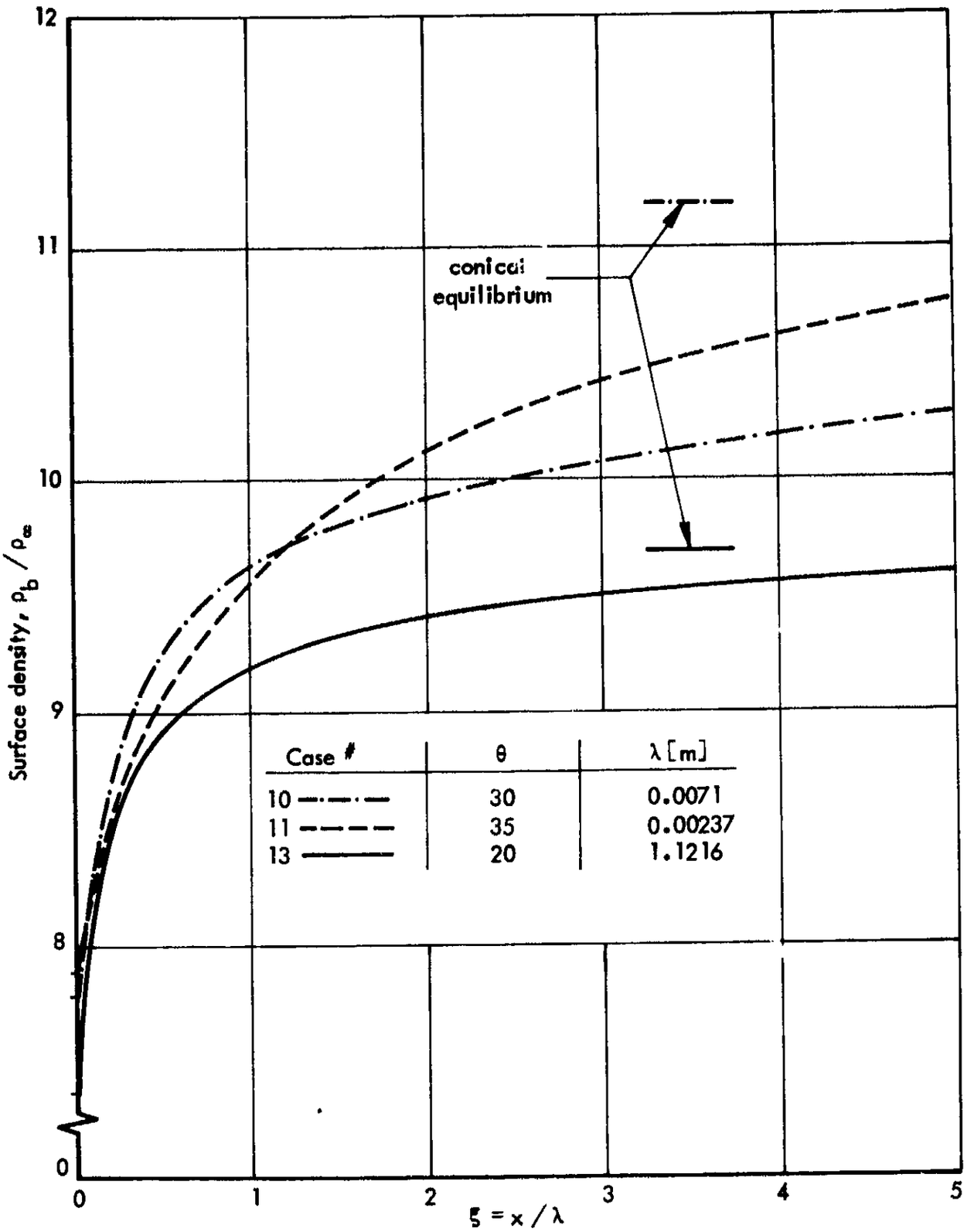

Fig. 36 Influence of cone semi-vertex angle on surface density (V_∞ = 9350.0 m/sec, altitude 40 km).

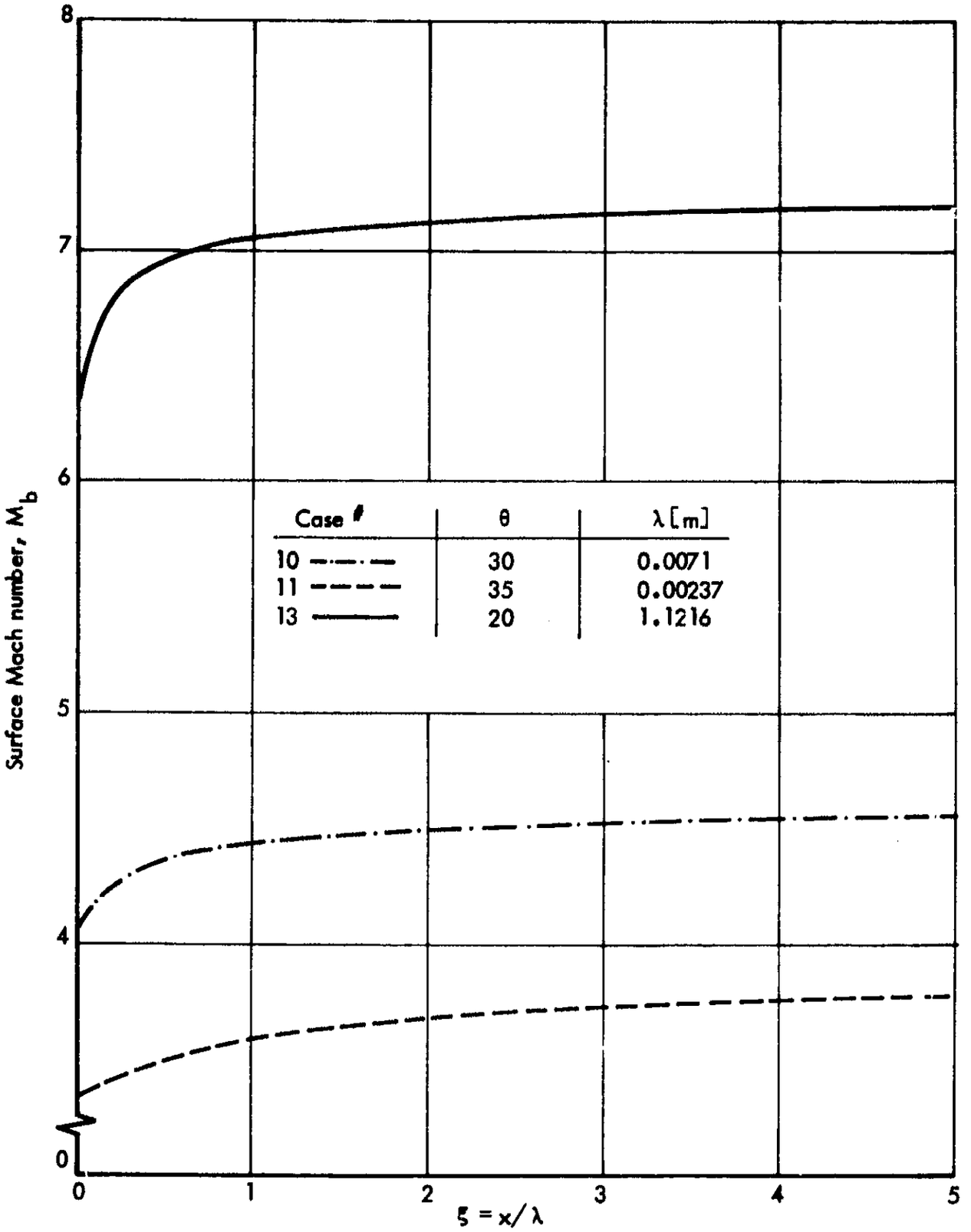

Fig. 37 Influence of cone semi-vertex angle on surface Mach number (V_∞ = 9350.0 m/sec, altitude 40 km).

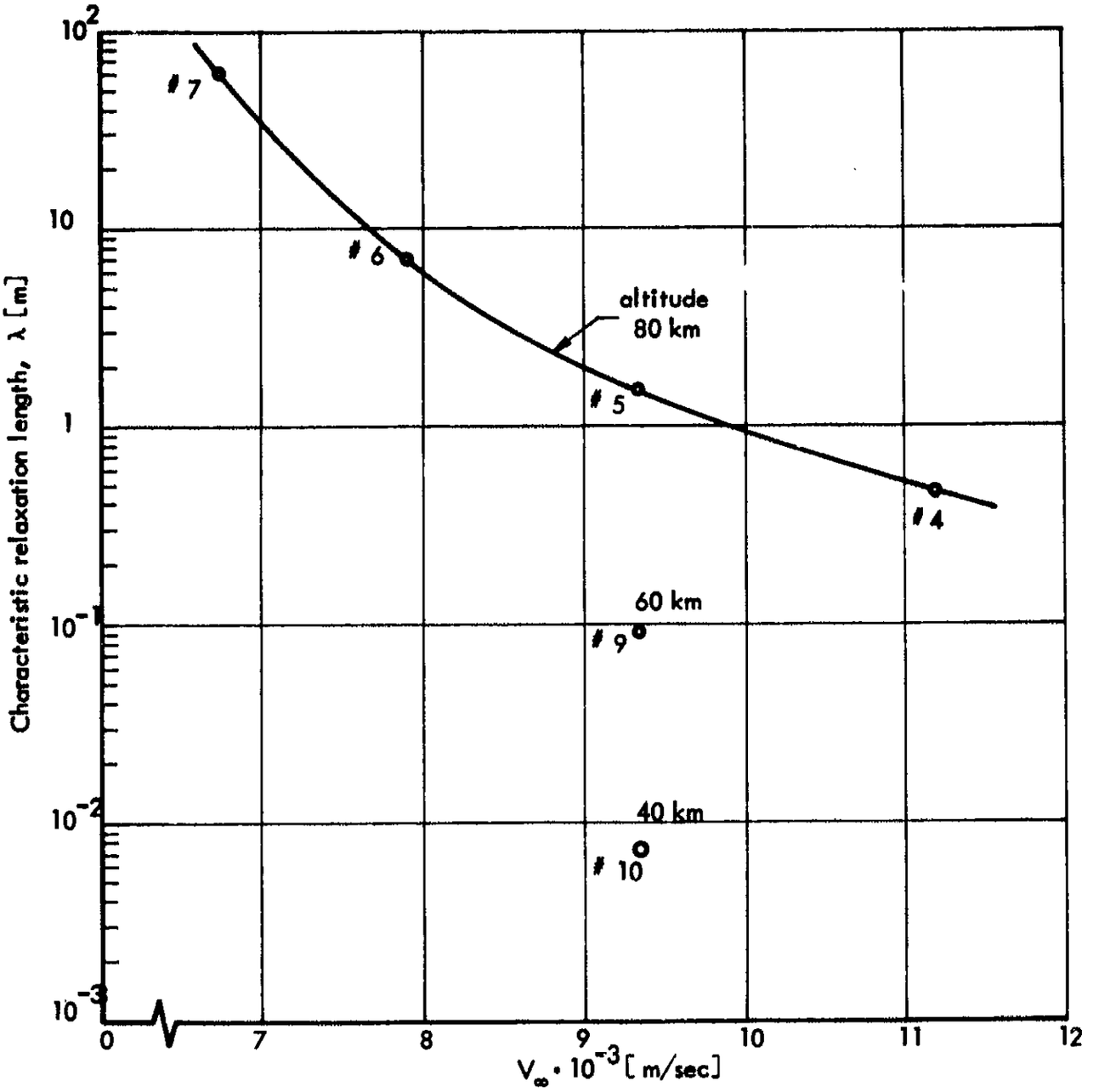

Fig. 38 Influence of free stream velocity (and altitude) on characteristic relaxation length ($\theta = 30^\circ$).

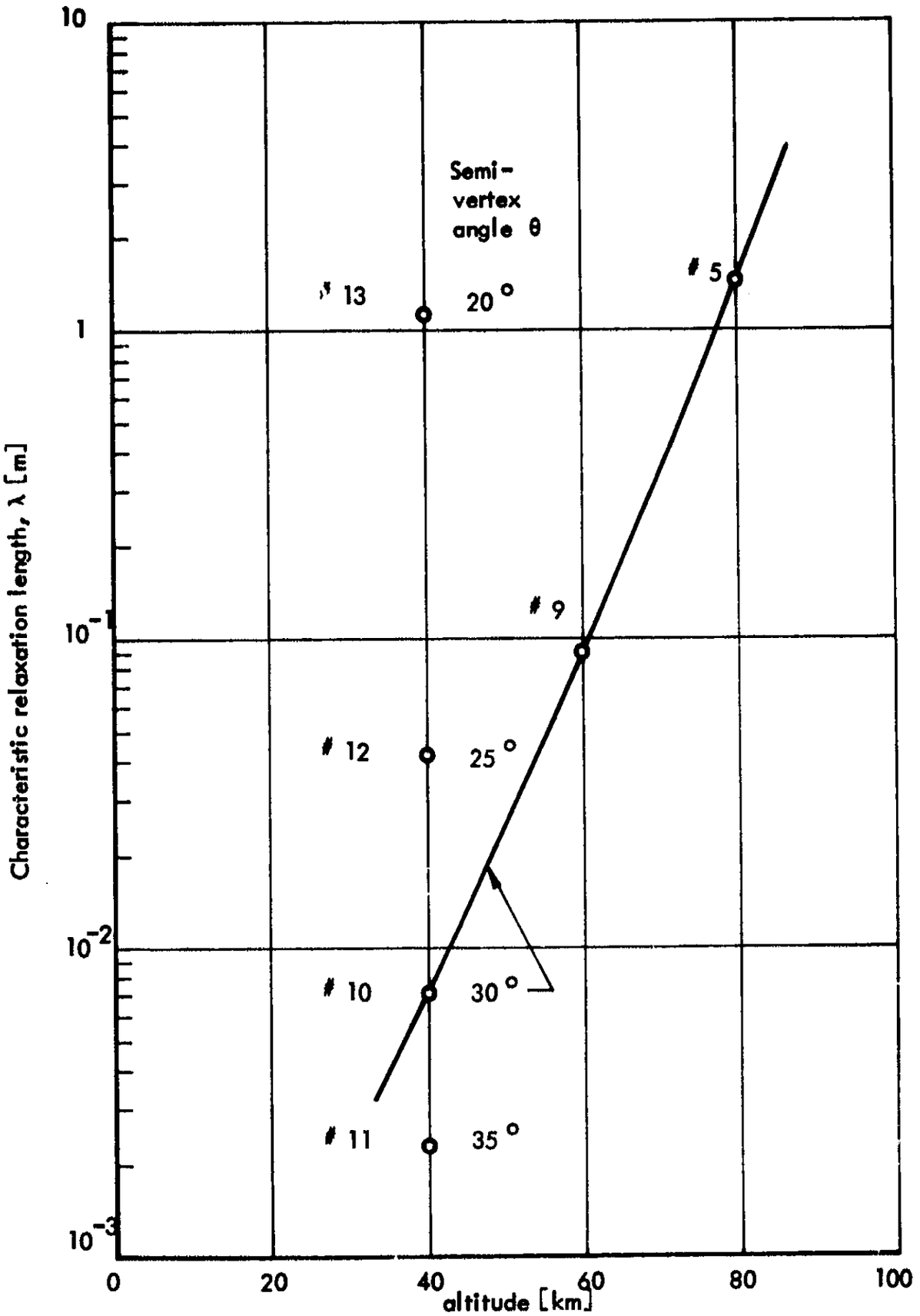

Fig. 39 Influence of altitude (and θ) on characteristic relaxation length (V_∞ = 9350.0 m/sec).

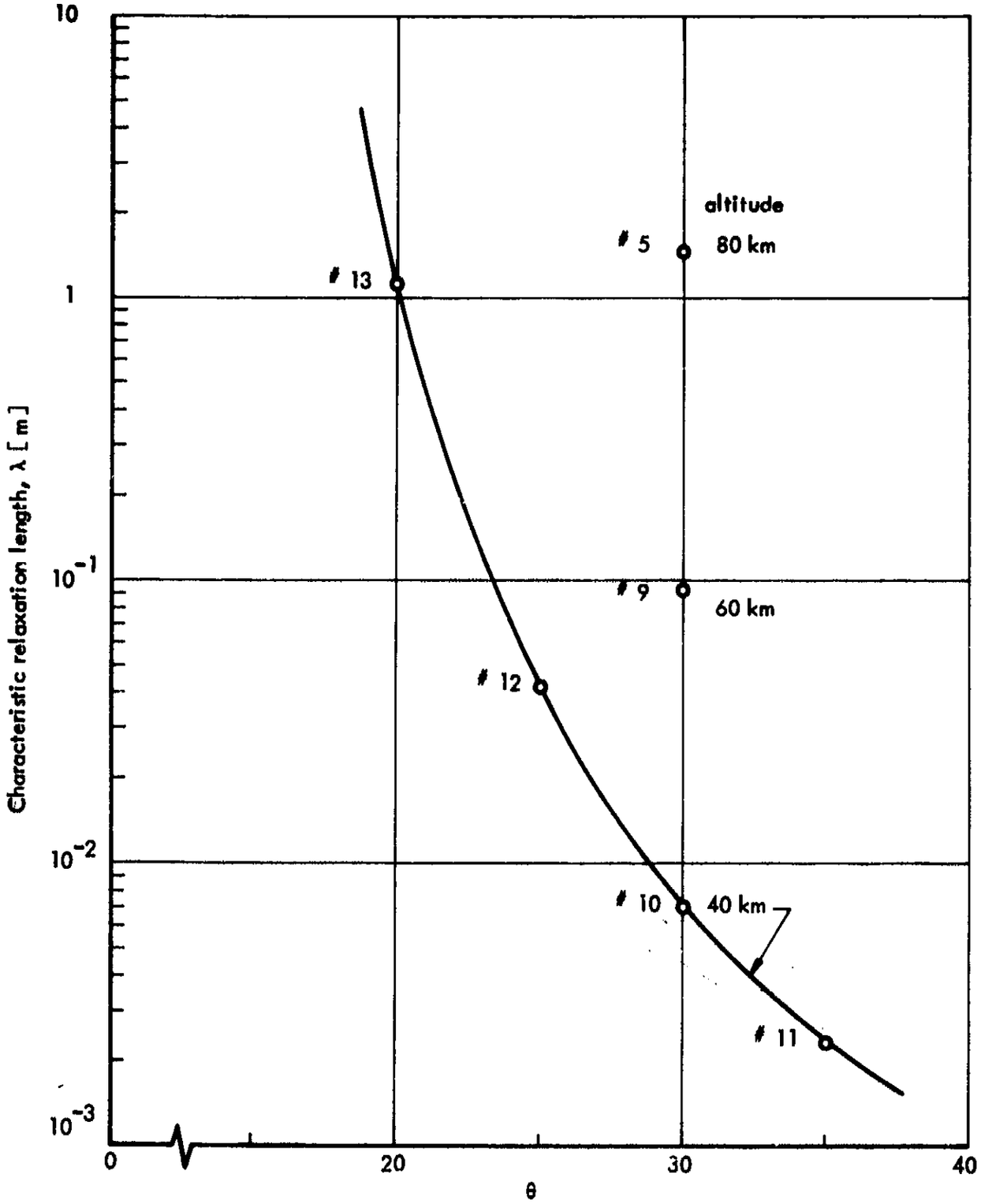

Fig. 40 Influence of cone semi-vertex angle (and altitude) on characteristic relaxation length (V_∞ = 9350.0 m/sec).

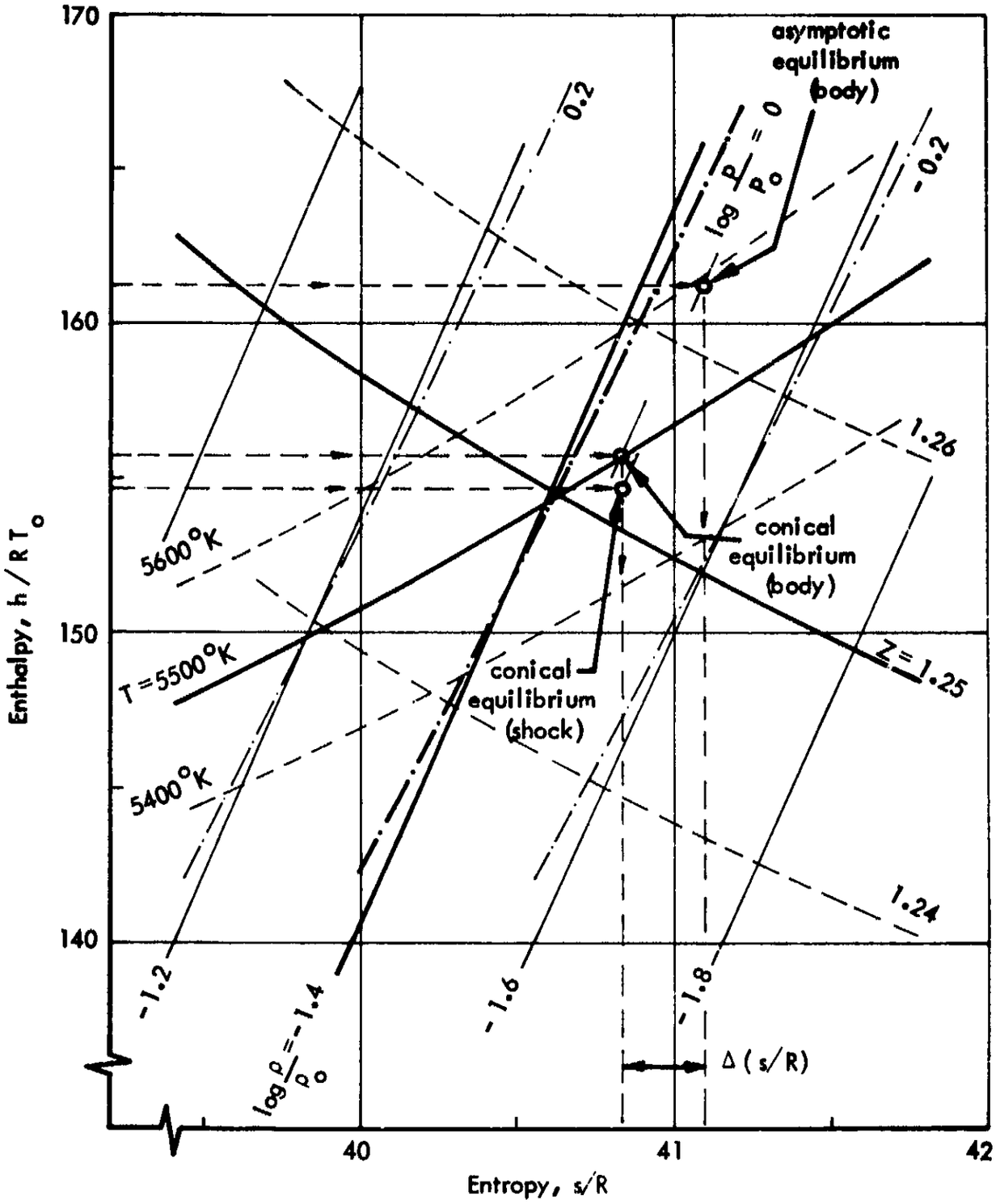

Fig. 41 Comparison of conical and asymptotic equilibrium for case 10 ($\theta = 30^{\circ}$, $V_{\infty} = 9350.0$ m/sec, altitude 40 km) in a Mollier diagram (Ref. 41; $T_o = 273.16\ ^{\circ}K$, $p_o = 1.0$ atm, $\rho_o = 1.288\ kg/m^3$, $R = 288.188\ J/kg\ ^{\circ}K$).

APPENDIX A

SOME EXPRESSIONS RELATED TO THERMODYNAMICS

Frozen specific heat c_p :

$$c_p = R^* \left\{ Y_{O2} \left[3.5 + \left(\frac{\theta^v_{O2}}{T} \right)^2 \frac{e^{\theta^v_{O2}/T}}{\left(e^{\theta^v_{O2}/T} - 1 \right)^2} \right] \right.$$

$$+ Y_{N2} \left[3.5 + \left(\frac{\theta^v_{N2}}{T} \right)^2 \frac{e^{\theta^v_{N2}/T}}{\left(e^{\theta^v_{N2}/T} - 1 \right)^2} \right]$$

$$+ Y_{NO} \left[3.5 + \left(\frac{\theta^v_{NO}}{T} \right)^2 \frac{e^{\theta^v_{NO}/T}}{\left(e^{\theta^v_{NO}/T} - 1 \right)^2} \right]$$

$$\left. + 2.5 \left(Y_O + Y_N \right) \right\} \qquad \text{(A-1)}$$

Frozen speed of sound, a_f :

$$a_f^2 = \frac{c_p \, R \, Z \, T}{c_p - R \, Z} \qquad \text{(A-2)}$$

Dimensionless functions L, S :

$$L = \frac{\lambda}{V_\infty^2} \sum_i h_i \frac{d C_i}{d x} \qquad \text{(A-3)}$$

$$S = \lambda \frac{R^* T_\infty}{V_\infty^2} \sum_i \frac{1}{M_i} \frac{d C_i}{d x} \qquad \text{(A-4)}$$

APPENDIX B

DIMENSIONLESS FUNCTIONS Ω_i FOR DIFFERENTIAL SHOCK RELATIONS AND INITIAL DERIVATIVES

$$\Omega_1 = \frac{2 V_\infty \cos\sigma \left[V_\infty \sin\sigma (V_\infty \sin\sigma - B) - (2 - b)(h_s - h_\infty) \right]}{T_\infty \left[(R Z_\infty - 2 c_{ps}) B + (V_\infty \sin\sigma) b c_{ps} \right]} \tag{B-1}$$

$$\Omega_2 = \frac{V_\infty \cos\sigma}{B} \left[1 + \frac{\tan\sigma}{B^2} (T_\infty c_{ps} \Omega_1 - V_\infty^2 \sin\sigma \cos\sigma) \right] \tag{B-2}$$

where

$$b = 1 + \frac{R Z_\infty T_\infty}{(V_\infty \sin\sigma)^2} \tag{B-3}$$

$$B = \sqrt{(V_\infty \sin\sigma)^2 - 2 (h_s - h_\infty)} \tag{B-4}$$

$$\Omega_3 = \left(\frac{\rho_\infty}{\rho_s} - 1 \right) (\sin\sigma \cos\beta + \cos\sigma \sin\beta) - \left(\frac{\rho_\infty}{\rho_s} \right)^2 \sin\sigma \sin\beta \, \Omega_2 \tag{B-5}$$

$$\Omega_4 = \left(\frac{\rho_\infty}{\rho_s} - 1 \right) (\sin\sigma \sin\beta - \cos\sigma \cos\beta) - \left(\frac{\rho_\infty}{\rho_s} \right)^2 \sin\sigma \cos\beta \, \Omega_2 \tag{B-6}$$

The following expressions are valid only at $x = 0$ for $K = 0$:

$$\Omega_5 = \frac{1}{\rho_\infty V_\infty (2+j)} \left\{ \frac{\rho_s u_s - \rho_b u_b}{\sin 2\beta} + \frac{\rho_s v_s}{\sin^2 \beta} \right.$$

$$+ 2(\cot\beta + j\cot\theta)(\rho_\infty v_s \Omega_2 + \rho_s V_\infty \Omega_4) \qquad \text{(B-7)}$$

$$\left. + j(1 + \tan\beta \cot\theta)(\rho_\infty u_s \Omega_2 + \rho_s V_\infty \Omega_3) \right\}$$

$$\Omega_6 = \frac{1}{\rho_\infty V_\infty^2} \left\{ \frac{(p_b + \rho_b u_b^2) - (p_s + \rho_s u_s^2)}{\sin 2\beta} - \frac{\rho_s u_s v_s}{\sin^2 \beta} \right.$$

$$+ j(1 + \tan\beta \cot\theta)(\rho_\infty u_s^2 \Omega_2 + 2\rho_s V_\infty u_s \Omega_3)$$

$$\text{(B-8)}$$

$$+ 2(\cot\beta + j\cot\theta)(\rho_\infty u_s v_s \Omega_2 + \rho_s V_\infty v_s \Omega_3 + \rho_s V_\infty u_s \Omega_4)$$

$$\left. + j\tan\beta\cot\theta(\rho_s T_\infty \Omega_1 + \rho_\infty T_s \Omega_2) R Z_s \right\}$$

$$\Omega_7 = \frac{1}{\rho_\infty V_\infty^2} \left\{ \left[\frac{\rho_s u_s v_s}{\sin 2\beta} + \frac{p_s + \rho_s v_s^2 - p_b}{\sin^2 \beta} \right.\right.$$

$$- j(1 + \tan\beta\cot\theta)(\rho_\infty u_s v_s \Omega_2 + \rho_s V_\infty v_s \Omega_3 + \rho_s V_\infty u_s \Omega_4)$$

$$\left.\left. - 2(\cot\beta + j\cot\theta)(\rho_\infty v_s^2 \Omega_2 + 2\rho_s V_\infty v_s \Omega_4) \right] (2\cot\beta + j\cot\theta)^{-1} \right.$$

$$\left. - R Z_s (\rho_s T_\infty \Omega_1 + \rho_\infty T_s \Omega_2) \right\} \qquad \text{(B-9)}$$

APPENDIX C

FUNCTIONS a_{ij} AND A_i IN EQUATIONS (4.30) THROUGH (4.33)

$$a_{11} = u_b^2 \tag{C-1}$$

$$a_{12} = - \rho_b c_{pb} \tag{C-2}$$

$$a_{21} = R Z_b T_b + \epsilon u_b^2 \tag{C-3}$$

$$a_{22} = \rho_b \left[R Z_b - (1+\epsilon) c_{pb} \right] \tag{C-4}$$

$$a_{33} = (1+j \bar{\delta} \cos\theta)(\rho_\infty u_s v_s \Omega_2 + \rho_s V_\infty v_s \Omega_3 + \rho_s V_\infty u_s \Omega_4) \tag{C-5}$$

$$a_{44} = \rho_b u_b \tag{C-6}$$

$$\begin{aligned} A_1 = \frac{u_b}{y_s} \Big\{ & \rho_s u_s \left[(1+K y_s) \tan\beta - (1-K y_s) j \bar{\delta} \sin\theta \right] \\ & - \rho_b u_b \left[(1+K y_s) \tan\beta + j \bar{\delta} \sin\theta \right] \\ & - \rho_s v_s (1 + j \bar{\delta} \cos\theta)(2 + 3 K y_s) \Big\} \\ & - u_b (\rho_\infty u_s \Omega_2 + \rho_s V_\infty \Omega_3)(1 + j \bar{\delta} \cos\theta) \frac{A_3}{a_{33}} \\ & + \frac{1}{\lambda} \rho_b V_\infty^2 L_b \end{aligned} \tag{C-7}$$

$$A_2 = \frac{\rho_b V_\infty^2}{\lambda}\left[(1+\epsilon)L_b - \left(\frac{T_b}{T_\infty}\right) S_b\right]$$

$$+ \frac{\epsilon}{y_s}\Big\{(p_s + \rho_s u_s^2)\left[(1+Ky_s)\tan\beta - (1-Ky_s)\,j\bar{\delta}\sin\theta\right]$$

$$-(p_b + \rho_b u_b^2)\left[(1+Ky_s)\tan\beta + j\bar{\delta}\sin\theta\right]$$

$$-\rho_s u_s v_s (1+j\bar{\delta}\cos\theta)(2+5Ky_s)$$

$$+j\bar{\delta}\sin\theta\left[p_b + p_s(1+Ky_s)\right]\Big\}$$

$$-\epsilon(1+j\bar{\delta}\cos\theta)\Big[RZ_s(\rho_s T_\infty \Omega_1 + \rho_\infty T_s \Omega_2)$$

$$+\rho_\infty u_s^2 \Omega_2 + 2\rho_s V_\infty u_s \Omega_3\Big]\frac{A_3}{a_{33}} \qquad \text{(C-8)}$$

$$A_3 = \frac{1}{y_s}\Big\{\rho_s u_s v_s\left[(1+Ky_s)\tan\beta - (1-Ky_s)\,j\bar{\delta}\sin\theta\right]$$

$$+(p_b - p_s)(2+j\bar{\delta}\cos\theta) - \rho_s v_s^2 (1+j\bar{\delta}\cos\theta)(2+3Ky_s)$$

$$+\left[p_b - p_s + \rho_b u_b^2 + 2\rho_s u_s^2 (1+j\bar{\delta}\cos\theta)\right]Ky_s\Big\} \qquad \text{(C-9)}$$

$$A_4 = \dot{W}_{ib} + \alpha(1+Ky_s)(1+j\bar{\delta}\cos\theta)\,\dot{W}_{is}$$

$$-\frac{\alpha(C_{ib} - C_{is})}{y_s}\Big\{\rho_s u_s\left[(1+Ky_s)\tan\beta - (1-Ky_s)\,j\bar{\delta}\sin\theta\right]$$

$$-\rho_s v_s (1+j\bar{\delta}\cos\theta)(2+3Ky_s)\Big\}$$

$$+\alpha(C_{ib} - C_{is})(1+j\bar{\delta}\cos\theta)(\rho_\infty u_s \Omega_2 + \rho_s V_\infty \Omega_3)\frac{A_3}{a_{33}} \qquad \text{(C-10)}$$